FINITE ELEMENT MODELS FOR THE THERMO-CHEMO-MECHANICAL ANALYSIS OF CONCRETE STRUCTURES REGARDING AGEING AND DAMAGE

Gustavo Luz Xavier da Costa

Dissertação de Mestrado apresentada ao Programa de Pós-graduação em Engenharia Civil, COPPE, da Universidade Federal do Rio de Janeiro, como parte dos requisitos necessários à obtenção do título de Mestre em Engenharia Civil.

Orientadores: Fernando Luiz Bastos Ribeiro
José Claudio de Faria Telles

Rio de Janeiro
Junho de 2020

FINITE ELEMENT MODELS FOR THE THERMO-CHEMO-MECHANICAL ANALYSIS OF CONCRETE STRUCTURES REGARDING AGEING AND DAMAGE

Gustavo Luz Xavier da Costa

DISSERTAÇÃO SUBMETIDA AO CORPO DOCENTE DO INSTITUTO ALBERTO LUIZ COIMBRA DE PÓS-GRADUAÇÃO E PESQUISA DE ENGENHARIA DA UNIVERSIDADE FEDERAL DO RIO DE JANEIRO COMO PARTE DOS REQUISITOS NECESSÁRIOS PARA A OBTENÇÃO DO GRAU DE MESTRE EM CIÊNCIAS EM ENGENHARIA CIVIL.

Orientadores: Fernando Luiz Bastos Ribeiro
José Claudio de Faria Telles

Aprovada por: Prof. Fernando Luiz Bastos Ribeiro
Prof. José Claudio de Faria Telles
Prof. Samir Maghous
Prof. Pierre Rossi

RIO DE JANEIRO, RJ – BRASIL
JUNHO DE 2020

Costa, Gustavo Luz Xavier da

Finite Element models for the thermo-chemo-mechanical analysis of concrete structures regarding ageing and damage / Gustavo Luz Xavier da Costa. – Rio de Janeiro: UFRJ/COPPE, 2020.

XII, 94 p.: il.; 29,7 cm.

Orientadores: Fernando Luiz Bastos Ribeiro

José Claudio de Faria Telles

Dissertação (mestrado) – UFRJ / COPPE / Programa de Engenharia Civil, 2020.

Referências Bibliográficas: p. 90 – 94.

1. Thermo-chemo-mechanical. 2. Concrete. 3. Damage. 4. Ageing. 5. Finite Element. I. Ribeiro, Fernando Luiz Bastos *et al.* II. Universidade Federal do Rio de Janeiro, COPPE, Programa de Engenharia Civil. III. Título.

“If I have seen further it is by standing on the shoulder of giants.”

Isaac Newton (1676)

Agradecimentos

Gostaria de reconhecer aqueles que contribuíram ao desenvolvimento deste trabalho. Portanto, agradeço

Aos meus pais, Glaucia e Carlos, que sempre me deram todo apoio necessário em todas as etapas da minha vida.

Aos meus orientadores, pelo auxílio na condução dessa pesquisa.

Aos meus amigos e colegas de mestrado.

Ao Conselho Nacional de Desenvolvimento Científico e Tecnológico (CNPq) pelo apoio financeiro.

A todos que direta ou indiretamente ajudaram na elaboração desse estudo.

Resumo da Dissertação apresentada à COPPE/UFRJ como parte dos requisitos necessários para a obtenção do grau de Mestre em Ciências (M.Sc.)

MODELOS EM ELEMENTOS FINITOS PARA A ANÁLISE TERMO-QUÍMICO-MECÂNICA DE ESTRUTURAS DE CONCRETO CONSIDERANDO ENVELHECIMENTO E DANO

Gustavo Luz Xavier da Costa

Junho/2020

Orientadores: Fernando Luiz Bastos Ribeiro
José Claudio de Faria Telles

Programa: Engenharia Civil

Este estudo abordará o comportamento termo-químico-mecânico do concreto considerando envelhecimento e dano. Para tanto, modelos matemáticos serão desenvolvidos e resolvidos por meio do Método dos Elementos Finitos. A análise será composta por dois modelos, a saber: termo-químico e termo-mecânico. Primeiro, o modelo termo-químico será deduzido usando a termodinâmica aplicada a meios porosos quimicamente reativos. Um dos exemplos usados para validar o modelo termo-químico consiste em uma estrutura de concreto construída em camadas. Para esse caso, foi desenvolvida uma estratégia de renumeração dos nós da malha. Depois, o modelo termo-mecânico será apresentado bem como uma discussão sobre a necessidade de usar uma equação constitutiva incremental para modelar o envelhecimento do concreto. O envelhecimento é traduzido pelo aumento do modulo de Young com o tempo, isto é, pela hidratação do cimento. Em seguida, um modelo de dano isotrópico será incorporado ao modelo termo-mecânico com envelhecimento e uma estratégia de integração Não-local será adotada para evitar a falta de objetividade devido a localização de deformações. Finalmente, o modelo termo-químico-mecânico será apresentado por meio de dois exemplos teóricos: um corpo-de-prova de concreto e um muro de concreto genérico. Os resultados mostrarão que microfissuras e tensões residuais podem aparecer devido a hidratação do cimento. Isso, por sua vez, pode levar ao colapso prematuro da estrutura.

Abstract of Dissertation presented to COPPE/UFRJ as a partial fulfillment of the requirements for the degree of Master of Science (M.Sc.)

FINITE ELEMENT MODELS FOR THE THERMO-CHEMO-MECHANICAL ANALYSIS OF CONCRETE STRUCTURES REGARDING AGEING AND DAMAGE

Gustavo Luz Xavier da Costa

June/2020

Advisors: Fernando Luiz Bastos Ribeiro
José Claudio de Faria Telles

Department: Civil Engineering

This study will address the thermo-chemo-mechanical behaviour of concrete considering ageing and damage. To this end, mathematical models will be developed and worked out through the Finite Element Method. The analysis will be composed of two models, namely: thermo-chemical and thermo-mechanical. First, the thermo-chemical model will be deduced using thermodynamics applied to chemically reactive porous media. One of the examples used to validate the thermo-chemical model consists of a concrete structure built by layers. For this case, it was developed a renumbering strategy for the nodes of the mesh. Then, the thermo-mechanical model will be presented as well as the necessity for an incremental constitutive equation for modelling concrete ageing. The ageing is translated by the increase of Young's modulus, that is, by the cement hydration. Next, an isotropic damage model will be incorporated to the thermo-mechanical model with ageing and a Nonlocal integral-type strategy will be adopted to avoid lack of objectivity due to strain localization. Finally, the thermo-chemo-mechanical model will be presented by means of two theoretical examples: a concrete specimen and a generic concrete wall. The results will show that microcracks and residual stresses might take place due to hydration of cement. This in turn might lead to the premature collapse of the structure.

Contents

LIST OF ABBREVIATIONS

FEM	Finite Element Method
ITZ	Interfacial Zone Transition
NGP	Number of Gauss Points
RVE	Representative Volume Element

LIST OF SYMBOLS

Lowercase Roman letters

b	Resulting right-hand side vector of the system of equations
c_p	Specific heat capacity
d	Interaction radius in the Nonlocal technique
f_t	Tensile strength
g	Chemical potential of free water
h	Convective heat transfer coefficient
k	Thermal conductivity, iteration pointer
m_{fw}	Mass of free water
m_{sk}	Mass of formed skeleton
n	Normal vector
$\bar{q}$	Prescribed external heat source
t	Time
$\bar{t}$	Prescribed traction vector
w	Weight factor for Gauss quadrature

Uppercase Roman letters

A	Resulting coefficient matrix of the system of equations
A_m	Chemical affinity
Ã	Normalized chemical affinity
B	Matrix of derivatives of the interpolation functions

C	Connectivity array
$\mathbb{C}$	Constitutive matrix (2^{nd} rank tensor)
C_{th}	Heat capacity
D	Isotropic damage variable
E	Young's modulus
E_a	Activation energy
F_{cd}	Vector of prescribed displacements
F_{chem}	Vector of hydration reaction
F_{conv}	Vector of convection on Robin boundary
F_{ct}	Vector of prescribed temperature
F_{dl}	Vector of dead load due to body forces
F_{hf}	Vector of prescribed heat transfer on Neumann boundary
F_{int}	Vector due to internal forces
F_{pd}	Vector of displacements' contribution from the previous time instant
F_{tf}	Vector due to temperature variation
G	Chemical potential of hydrated cement
H	Convection matrix
$\|J\|$	Determinant of the Jacobian matrix
K	Stiffness matrix
L_m	Latent heat
L	Latent heat per unit of hydration degree, length
M	Mass matrix
N	Matrix of interpolation functions
NL	Matrix for the Nonlocal technique
P	Residual vector
Q	External heat source
R	Universal gas constant
S	Entropy
T	Temperature vector, Temperature scalar
T_{ref}	Reference temperature
U	Displacement vector
X	Coordinates array

Lowercase Greek letters

α	Coefficient of thermal expansion
α_0	Weighting function for the Nonlocal technique
Δt	Time interval
ε	Strain matrix (2^{nd} rank tensor)
ε_{d0}	Equivalent strain related to the tensile strength
ε_{eq}	Equivalent strain
$\bar{\varepsilon}_{eq,k}$	Nonlocal equivalent strain for a given Gauss Point *k*
η	Viscosity
ξ	Hydration degree
ρ	Density
σ	Stress matrix (2^{nd} rank tensor)
$\tilde{\sigma}$	Effective stress matrix (2^{nd} rank tensor)
φ	Dissipation
ψ	Helmholtz Free Energy

Uppercase Greek letters

Γ_d	Boundary where Dirichlet conditions are applied
Γ_n	Boundary where Neumann conditions are applied
Γ_r	Boundary where Robin conditions are applied

1 Introduction

1.1 General background

Concrete's properties are one of the main concerns of civil engineering community since its first usage as a structural material. One of its principal features is the ability to harden with time accompanied by the increase of its strength. However, this happens at the expense of considerable amount of heat generation. For massive concrete structures without reinforcement, for instance, this is responsible for cracking in the early age. In this context, the process of concrete hydration has been under intensive research by the scientific community because it will generally dictate the future behaviour of the structure.

The interest in understanding the hydration process is not in vain. The first days after concrete starts setting and hardening are crucial because that's when concrete start developing cracks that might reduce to a great extent its strength during its service life. Besides, unlike other materials, concrete starts as a viscoplastic material when it's mixed with water and ends as a majorly elastic material after setting finishes. A mathematical model that encompasses all these features is not trivial because they are usually coupled, meaning that one cannot analyze separately. Although its simplifications, several models have been developed during the last decades. They take into account the main features during concrete setting such as ageing, creep, autogenous shrinkage, plasticity, etc. The wide spread of numerical methods in the last century allowed one to test these models which have been demonstrating a good agreement with experimental data.

As previously stated, the aforementioned attributes of concrete will govern the response of structure when it is already set because one of the most critical issues is the growth of cracks due to thermal strains. Superficial cracks are sometimes observable with unaided eye or, if smaller, measured with an appropriate apparatus. Interior cracks, on the other hand, are more difficult to assess and one usually must resort to non-destructive methods to determine the magnitude of the damage.

Another serious problem caused by the combination of thermal expansion due to hydration of cement paste and mechanical restraints is the phenomenon of residual stresses even without apparent strains. It might occur if the placing temperature is approximately

equal to that when concrete is already set and the restraints allow the structure to return to its original dimensions at the time it was placed (an illustrative example will be presented later). Residual stresses are undesirable because, as opposed to strains, stresses are not easily measurable. This, in turn, might make the structure collapses with lower strains than predicted in the design stage.

The hydration of the cement paste present in concrete as well as its thermal and mechanical effects is referred to its thermo-chemo-mechanical behaviour. The chemical reactions take place as soon as the cement paste is mixed with water which in turn lead to thermo-mechanical strains and vice versa. For concrete, in general, it can be assumed that temperature variations induce mechanical strains but not the other way around (it will be discussed later). Since one would like to evaluate the temperature evolution of concrete with time as well as its mechanical response, the differential equations that describe this behaviour are nonlinear and time-dependent. For this reason, it goes without saying that numerical methods are preferable for these models.

The widely known Finite Element Method, employed in the present study, is well suited when one wants to analyze the thermo-chemo-mechanical response of the structure when neglecting crack growth. Actually, it is appropriate even for crack propagation problems but it hinges on the methodology chosen to analyze it. Damage models, which are based on Continuum Damage Mechanics, suffer from an enormous drawback for softening problems. When one is modelling a problem by means of the FEM, it is usually expected that it converges as the mesh is refined. For damage models with softening, this is not the case and the results converge to a rupture with zero energy dissipation, which is completely unacceptable. This pathological behaviour including the remedies to circumvent it will be examined later. In any case, one can state in advance that it is a weakness of local numerical methods, that is, those for which equations are written at element level. In this context, Meshless methods have gained attention for crack propagation problems as they do not suffer from this deficiency.

Shortcomings aside, FEM is still adequate for the modelling of concrete if proper precautions are taken. Hence, the goal of the scientific community has been to develop mathematical models that more and more encompass a broad range of features. It is still challenging since engineers are usually interested in the macroscopic level of material description but important processes generally take place at lower scales.

1.2 Rationale and motivation

The development of this study aims at demonstrating the importance of the hydration of the cement paste present in concrete as well as its mechanical effects. The reason is because the chemical reaction of hydration usually takes place very rapidly, making the structure behave differently for each time instant. For massive concrete structures like dams or large foundations, for example, this is driving force behind crack growth in the early ages. Due to the importance of these structures and the difficulty to fix these pathologies one must resort to a methodology that consider all these phenomena. The most reasonable way to do this analysis is to resort to numerical methods. Thus, this research intends to work out the governing equations numerically by means of the Finite Element Method.

The methodology adopted to derive the thermo-chemical model is based on a consistent theoretical framework. The thermodynamics is the key theory behind this model which in turn guarantees the irreversibility of the hydration reaction. Besides, the resulting Finite Element formulation is easily implemented in an existing code. This methodology can be used to predict the temperature evolution for adiabatic, semi-adiabatic and isothermal conditions. Another important aspect is the node renumbering when simulating layered constructions. Hence, a strategy to reorder the labels of the nodes will be presented.

One of the reasons for using an isotropic damage model for crack modelling is the fact that it's vastly addressed in the literature. Consequently, it's easy to compare with existing experimental data. Besides, it's suitable for engineering purposes since an existing Finite Element code can incorporate it only by adding a new subroutine. This study will adopt an elastic damage model which is a simplification but shows a good agreement for quasi-static and cyclic loadings. It is also thermodynamically consistent which is translated by the fact that the damage variable always increases. Since the proposed damage model presents softening, a remedy must be adopted to avoid lack of objectivity. This research employed a nonlocal integral-type technique due to its feasibility.

In summary, the present study aims at contributing to the investigation of the thermo-chemo-mechanical behaviour of concrete in the early ages. Two important aspects that will be considered here are ageing and damage. Although both are widely known, mathematical models that comprise both aspects are not widespread yet. It must be demonstrated the importance of using an incremental constitutive equation when taking ageing

into consideration as well as its effects on the damage model. Thus, this research is also an endeavor with the purpose of filling this gap in the literature.

1.3 Methodology and objectives

In this dissertation, mathematical formulations will be presented to study the thermo-chemo-mechanical behaviour of concrete due to hydration of the cement paste. These models, represented by differential equations, will be obtained using the thermodynamics. The thermo-chemo-mechanical modelling will be divided into two analysis, namely: thermo-chemical and thermo-mechanical.

In the thermo-chemical model, concrete will be assumed as a closed system (*mass control*) which is composed of a deformable solid skeleton with micropore saturated with water. Then, the theory of chemically reactive porous media will be applied. The methodology will also consider the thermally activated nature of the hydration process, that is, the effect of the temperature on the chemical reaction. Once the governing equations are derived, the Galerkin method will be used to develop its Finite Element formulation which consists of a time-dependent and nonlinear system of equations. The Euler-backward scheme will be used to discretize the equations in time and the Newton's method will be implemented to solve the linearized system iteratively. In addition, it will be proposed a node renumbering strategy for the purpose of modelling layered placing of concrete.

Then, the thermo-mechanical model will be developed and the necessity of an incremental constitutive equation for modelling ageing materials will be discussed. Then, an isotropic damage model will be incorporated to it, using the concept of Effective Stress and the Principle of Strain-Equivalence. It will be possible to derive a constitutive equation that considers both ageing and damage. Then, a Finite Element formulation for it will be presented. The resulting system of equations is static and nonlinear because damage is a function of displacements and vice versa. The present study will use the Newton's method to solve the nonlinear system. In addition, a nonlocal integral-type technique will be presented in order to tackle the issue of lack of objectivity due to strain localization. This approach is quite attractive since the key idea of damage remains the same and only few changes are necessary for an existing Finite Element code.

Finally, the coupled thermo-chemo-mechanical analysis will be introduced. The hypothesis of weak coupling allows one to solve the thermo-chemical model first and the thermo-mechanical problem subsequently. This assumption means that temperature variations provoke mechanical strains and stresses but not the other way around. Finally, some numerical applications will be presented in order to demonstrate damage propagation due to thermal effects and the phenomenon of residual stresses without observable strains. It is expected that the obtained numerical results show the feasibility of the proposed methodology.

1.4 Dissertation organization

This first chapter gave a general overview of the problem that will be analyzed which is the thermo-chemo-mechanical analysis of concrete structures considering both ageing and damage.

The second chapter will briefly discuss some features of concrete. It will be exposed properties such as its main chemical components and its effects on the hydration reaction, factors influencing the concrete strength and a short description of the material at the microlevel.

The third chapter will develop the thermo-chemical model based on the thermodynamics of chemically reactive porous media. It will take into account the exothermic and thermally activated nature of the hydration of the cement paste. Some numerical applications will be presented in order to validate the model.

The fourth chapter will discuss the thermo-mechanical model regarding ageing and damage. It will also discuss the problem of lack of objectivity due to strain softening and a nonlocal technique as a remedy to circumvent it. The proposed formulation will be used in numerical applications and some of them compared with experimental data.

The fifth chapter will formulate the coupled thermo-chemo-mechanical model along with a flowchart with the view to demonstrate the logical scheme adopted. Two theoretical examples will be worked out in order to show the phenomena of microcracks and residual stresses on concrete structures due to hydration.

The sixth chapter will present concluding remarks of this research. It will summarize the key ideas exposed here and inferences that can be drawn from it.

Finally, the references used to develop this study will be given in chapter seven.

2 A brief overview of concrete

2.1 Main features

According to NEVILLE and BROOKS [1], the ancient Romans were perhaps the first to use concrete, from Latin *concretus*, a word that means "to grow together" (cf. LI [2] and MINDESS *et al.* [3]). The cement properties of water resistance and hardening with time made its use widespread. After some centuries in disuse, Roman cement was rediscovered and in the 19th century Joseph Aspdin coined the term *Portland cement*. Today, this word is employed to describe a broad range of cements that share some features in common but differ in its applications.

The production of Portland cement is made through the combination of raw materials. These are majorly composed by calcareous components such as limestone or chalk and argillaceous materials like clay or shale. They are grinded into powder, mixed in the right proportions and them placed inside a burning rotary kiln. The resulting material, known as *clinker*, is cooled, combined with gypsum and grinded once again. The outcome is what is known today as the Portland cement.

The major components that constitute cement are basically four oxides, namely: $3CaO.SiO_2$, $2CaO.SiO_2$, $3CaO.Al_2O_3$ and $4CaO.Al_2O_3.Fe_2O_3$ which are usually referred to as C_3S, C_2S, C_3A and C_4AF, respectively. In spite of the fact that they constitute the major part of the cement composition, it does not mean other minor components do not play a significant role in the concrete behaviour it just means that they constitute the majority of mass composition of the cement.

The oxides present in cement have its own particularities. Usually the reduction of one of them might improve some characteristics but worsen others. As will be seen, some of these components are responsible for a great amount of heat generation but also for its strength when concrete is set. Besides, the usage of cement in concrete is generally accompanied by the addition of admixtures because they enhance important properties such as strength and setting time. However, appropriate precautions must be taken when using it, otherwise it might lead to pathologies in the structure.

2.2 Hydration reaction

As soon as cement paste is mixed with water to compose concrete, a complex set of chemical and physical processes take place. For this research, the main concern regarding cement hydration is related to its capability of increasing its temperature due to heat generation. This section will deal with the mechanism behind the hydration process and which components of cement are responsible for this behaviour. A mathematical description of the problem will be presented in chapter 3.

When water reaches cement, all the four major components previously mentioned reacts with it to form hydrates. These reactions are not fully understood yet because they occur simultaneously which makes such analysis complex and an object under intensive research yet. For the sake of simplicity, one may consider these processes happening separately (cf. NEVILLE and BROOKS [1] and LI [2]) which correspond to assuming that they do not interact with each other.

The calcium silicates C_2S and C_3S produce quite similar compounds during the hydration reaction. Together they produce hydrates known as *tobermorite* gel or simply C-S-H gel (cf. MEHTA and MONTEIRO [4]). This poorly crystallized porous component (cf. POPOVICS [5]) is responsible for the strength of concrete and is one of the most important outcomes of the hydration reaction because it will influence the mechanical behaviour throughout the whole service life of concrete. However, the rate at which their reactions occur is completely different since C_3S reacts faster than C_2S which makes C_3S responsible for the early age strength of concrete while C_2S contributes to its long-term strength.

The chemical reaction of C_3A and water must be remarked as well. This compound sets very quickly when combined with water and that is why gypsum is added with clinker. In this context, the hydration of C_3A *per se* is not so important for practical engineering problems but rather its occurrence in the presence of gypsum. The outcome of the reaction is a component referred to as *ettringite* which may be either beneficial or malefic depending on how the process will develop. If ettringite is formed before the cement paste is set then it will act as a natural reinforcement and increase the concrete strength. If that does not happen, ettringite might grow to an extent that will break the hardened products already formed which might lead to cracking in the early age.

There are two compounds that are responsible for the majority of heat generated during concrete setting, namely: C_3A and C_3S. For engineers, though, the total amount of heat is not the most important aspect but rather the rate at which it takes place. Indeed, if temperature increase slower than the capacity of the structure to dissipate it then it will not become a problem. Massive structures, for instance, dissipate heat is very slowly. This in turn will lead to thermal cracks during setting. Something important to keep in mind is that heat generated due to hydration of cement paste is not always malefic. For concrete placing during winter in cold-weather places it might be beneficial since it will accelerate the setting time.

Considering that the rate of heat generation is the important feature to be analyzed then some observations can be made. The fineness of the cement, for instance, can change the velocity of hydration reaction but not the total amount of heat generated which is generally dictated by cement content present in concrete (cf. NEVILLE and BROOKS [1]). In addition, the usage of cold water is sometimes recommended because it may decrease the reaction velocity. This procedure is usually adopted in the construction of large dams where cold water or even ice is mixed with concrete during its preparation. More information about prevention of thermal cracks in concrete structures can be found in the reports presented by SPRINGENSCHMID [6].

Another interesting characteristic of hydration reaction is related to its exothermic and thermally activated behaviour. In summary, it means that temperature increase due to hydration reaction (exothermic) and the temperature rise itself hasten the kinetics of hydration (thermal activation). This property becomes more noticeable in massive structures but it might be an issue for daily structures as well. From a mathematical point of view, the thermal activation is regarded as a nonlinearity because the temperature will depend on the hydration extent and vice versa.

The process of hydration of cement paste is still under intensive research. The scientific community is not completely aware of the role played by each compound and how exactly they interact with each other during setting. So far, simplified models have been presented and demonstrated good agreement with experimental data but a more satisfactory understanding is still to be achieved.

2.3 Mechanical aspects

From the previous discussion one can conclude that thermal strains will take place as a result of temperature variations. Instead of focusing only on the mechanical effects in the structure due to hydration, this section will present mechanical features of concrete as a whole. However, one cannot separate it completely from hydration reaction because the mechanical response will be dictated by the components formed when concrete is still setting.

Concrete strength along with its durability and water resistance is usually considered as the most remarkable features of concrete. Its considerable capability to endure large compressive loads without failing is one of the reasons that makes it suitable for practical engineering situations. However, something interesting to note is that by analyzing the mechanical properties of coarse aggregate, cement paste, mortar and concrete separately one can conclude that their stress-strain curve behave quite differently as shown in Figure 1.

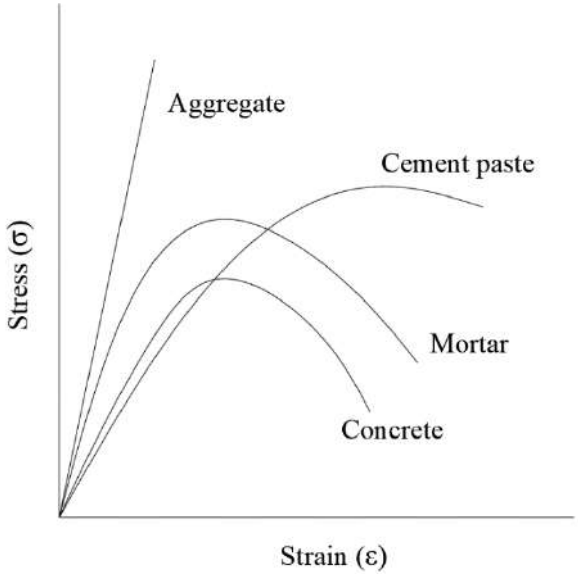

Figure 1. Stress-strain curve for concrete components

One would like to expect that concrete would possess at least the strength of the weaker component which is not the case. This apparent paradox is caused by imperfections that arise when concrete is setting. Micropore and voids, for instance, are responsible for stress concentrations leading to the collapse of the structure with lower stresses than theoretically predicted. A region that play an important role in this behaviour is situated between

the coarse aggregate and bulk cement paste and is usually referred to as *Interfacial Transition Zone* (ITZ) (cf. [1]–[5]). An interesting survey about its properties and influences on the mechanical behaviour of concrete is found in MASO [7]. This zone is generally considered the weakest link in concrete because that is where a great amount of imperfections, such as porosities and voids, is present.

When fractures start to emerge, they will almost always propagate in ITZ. Decrease the water-cement ratio can increase the strength of the cement paste matrix but it will not be the case for ITZ. MINDESS [3] states that silica fume can be employed as a remedy to improve the strength of ITZ because it will partially eliminate the quantity of pores. In any case, the evaluation of its strength depends on various factors that are usually difficult to evaluate by daily tests which makes its assessment challenging.

Outside ITZ, imperfections and flaws are also present, specially in the form of porosities. For heterogeneous solids like concrete, it is one of the main causes for strength-limiting and a parameter commonly used to estimate it is the water-cement ratio. However, other aspects such as aggregate size, curing conditions and rate of loading will influence in a considerable way the mechanical response of the structure (cf. MEHTA and MONTEIRO [4]). In any case, water-cement ratio is a variable which is easy to measure and for practical purposes it still represents a useful criterion to predict some properties of concrete.

3 Thermo-chemical analysis

In order to simulate temperature variations due to hydration of the cement paste, ULM and COUSSY [8], [9] proposed a theoretical framework based on thermodynamics. It considers the cement paste as a chemically reactive porous media, as presented by COUSSY [10]. This methodology was already employed by other researchers such as RITA *et al.* [11], EVSUKOFF *et al*. [12], FERREIRA [13], FERREIRA [14], SILVOSO [15], VALENTIM [16], CERVERA *et al.* [17] and CERVERA *et al.* [18]. In this context, the present chapter will follow the reasoning proposed by ULM and COUSSY [8], ULM and COUSSY [9], COUSSY [10], ULM and COUSSY [19] and ULM and COUSSY [20] to develop a mathematical model that describes the kinetics of hydration reaction.

3.1 Mathematical modelling

Consider the sketch depicted in Figure 2. It represents a picture of the cement paste for a given time instant and at the microscopic level. It consists of free water, hydrated cement, anhydrous cement and micropores. An essential prerequisite of the hydration reaction is that free water must go through the micropores (a process called diffusion) and meet anhydrous cement. When they meet, new layers of hydrate are formed almost instantaneously when compared to diffusion process. Hence, it can be assumed that diffusion is the dominant mechanism behind hydration reaction because it will dictate the formation of hydrated cement.

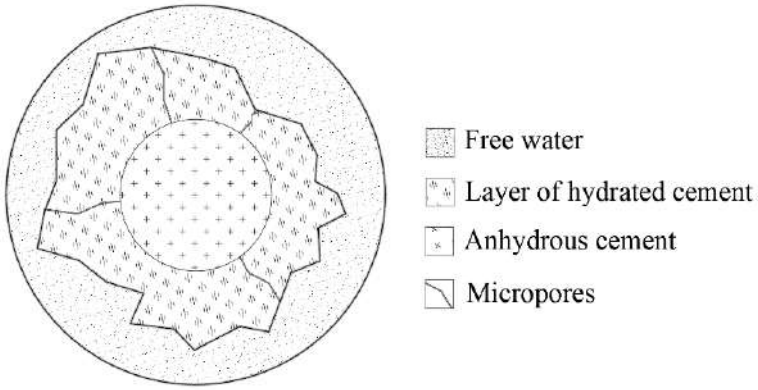

Figure 2. Cement at the microlevel of material description

The scheme represented by Figure 2 can be regarded as a closed system (mass control). It means that matter will not be exchanged with the surrounding medium, only energy. In other words, it implies that, for a given time interval, the change of water mass that combined to form the skeleton (hydrated cement) plus the change of water mass of free water equals zero. Mathematically, it is written as

$$\frac{dm_{sk}}{dt} + \frac{dm_{fw}}{dt} = 0 \tag{3.1}$$

The second law of thermodynamics, which can be given by the Clausius-Duhem inequality, states that the variation of entropy in a closed system is always greater than or equal to the entropy supplied from the surrounding medium. Since closed systems do not exchange matter with the exterior, the source of entropy variation can only be attributed to the heat supplied from the outside

$$\frac{dS}{dt} \geq \frac{Q}{T_{ref}} \rightarrow T_{ref}\,\frac{dS}{dt} \geq Q \tag{3.2}$$

with T_{ref} as a reference temperature. The difference between the left and the right-hand side of Equation 3.2 is equal to the dissipation φ due to hydration reaction

$$\varphi = T_{ref}\,\frac{dS}{dt} - Q \tag{3.3}$$

ULM and COUSSY [9] assume that dissipation is represented by

$$\varphi = \left(g - G\right)\frac{dm_{sk}}{dt} = A_m\,\frac{dm_{sk}}{dt} \geq 0 \tag{3.4}$$

with *g* and *G* as the chemical potential of the free water and of the hydrated cement, respectively. The difference between them can be regarded as the affinity A_m of the reaction. As the thermodynamic imbalance between free water and anhydrous cement increases, affinity grows. ULM and COUSSY [9] assume that dissipation is associated to both irreversible skeleton evolution (chemo-plastic) and hydration reaction (thermo-chemical). In the present study, the former will be neglected.

The dissipation for a closed system, disregarding mechanical effects, is written as

$$\varphi\, dt = \cancel{\sigma : d\varepsilon} - SdT - d\psi \geq 0 \tag{3.5}$$

where ψ denotes the *Helmholtz Free Energy*. It will be assumed that it is a function of two state variables: temperature (*T*) and water mass that reacted with cement to form the skeleton (m_{sk}). Temperature is an external (observable) variable. On the other hand, water mass is considered an internal (hidden) variable which means that it is not controlled from the exterior (cf. ULM [19]). The designation of external and internal variables will depend on whether they are observable from outside the system or not.

$$\psi = \psi\left(T, m_{sk}\right) \tag{3.6}$$

The total differential for a function $f(x_1, x_2, x_3 \ldots x_n)$ is

$$df = \frac{\partial f}{\partial x_1} dx_1 + \frac{\partial f}{\partial x_2} dx_2 + \frac{\partial f}{\partial x_3} dx_3 + \ldots + \frac{\partial f}{\partial x_n} dx_n \tag{3.7}$$

Hence, the total differential of (3.6) will be

$$d\psi = \frac{\partial \psi}{\partial T} dT + \frac{\partial \psi}{\partial m_{sk}} dm_{sk} \tag{3.8}$$

Substituting (3.4) and (3.5) in (3.8) and rearranging it

$$SdT + A_m dm_{sk} = -\frac{\partial \psi}{\partial T} dT - \frac{\partial \psi}{\partial m_{sk}} dm_{sk} \geq 0 \tag{3.9}$$

Comparing the left and right-hand sides of (3.9) leads to

$$S\left(T, m_{sk}\right) = -\frac{\partial \psi}{\partial T} \tag{3.10}$$

and

$$A_m\left(T, m_{sk}\right) = -\frac{\partial \psi}{\partial m_{sk}} \tag{3.11}$$

Because ψ is a function of T and m_{sk}, so will be S and A_m. Taking the total differential of (3.10) and (3.11)

$$dS = -\frac{\partial^2 \psi}{\partial T^2} dT - \frac{\partial^2 \psi}{\partial T \partial m_{sk}} dm_{sk} \tag{3.12}$$

$$dA_m = -\frac{\partial^2 \psi}{\partial T \partial m_{sk}} dT - \frac{\partial^2 \psi}{\partial m_{sk}^{\ 2}} dm_{sk} \tag{3.13}$$

Using (3.12) and (3.3)

$$T_{ref} \frac{\partial^2 \psi}{\partial T^2} \frac{dT}{dt} - T_{ref} \frac{\partial^2 \psi}{\partial T \partial m_{sk}} \frac{dm_{sk}}{dt} - Q - \varphi = C_{th} \dot{T} - L_m \dot{m}_{sk} - Q - \varphi = 0 \tag{3.14}$$

with C_{th} denoting the heat capacity and L_m the latent heat. The dissipation term is small when compared to the latent heat of hydration which makes it negligible. Thus, in the absence of volumetric heat sources, (3.14) can be given by

$$C_{th} \dot{T} - L_m \dot{m}_{sk} - Q = C_{th} \dot{T} - L_m \dot{m}_{sk} - \nabla . \left(k \nabla T \right) = 0 \tag{3.15}$$

with Q as the heat supplied from the exterior and k a scalar denoting the isotropic thermal conductivity. Equation (3.15) is very similar to the standard heat equation.

As mentioned previously, the diffusion of free water through the layers of hydrated cement is considered as the rate-determining (dominant) mechanism behind hydration reaction. Something important to keep in mind is that this process is nonlinear. In other words, as free water combines with anhydrous cement, the layers of hydrate will become thicker, decreasing the velocity of reaction. To illustrate this, consider the following scheme

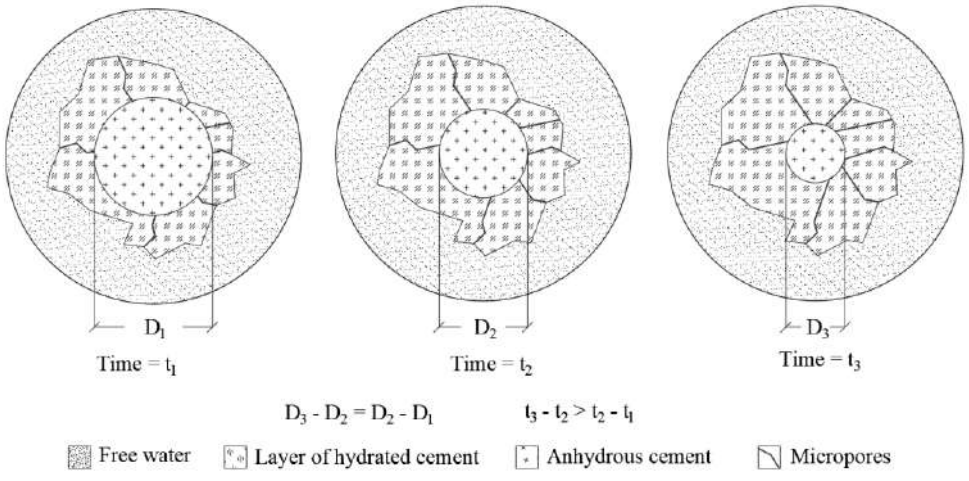

Figure 3. Progressive hydration of the cement paste.

According to Figure 3, as the layers of hydrates become thicker, free water must go through a longer distance to reach anhydrous cement which in turn reduce the affinity. This phenomenon is confirmed by relations $D_3 - D_2 = D_2 - D_1$ and $t_3 - t_2 > t_2 - t_1$. These equations reveal that the time to form a layer of a given thickness increases as time goes by. To translate it mathematically, ULM and COUSSY [9] proposed an Arrhenius-type law to describe it

$$A_m = \eta(\xi)\frac{dm_{sk}}{dt}e^{\left(\frac{E_a}{RT}\right)} \tag{3.16}$$

with $\eta(\xi)$ accounting for the increase of thickness of the layers of hydrate. In addition, the exponential term considers the thermally activated behaviour.

Regarding (3.13), ULM and COUSSY [9] states that the first term of the right-hand side is negligible and, integrating this equation, one has

$$A_m \simeq A_{m0} - a(m_{sk}) = \eta(\xi)\frac{dm_{sk}}{dt}e^{\left(\frac{E_a}{RT}\right)}, \quad \text{with} \quad a(m_{sk}) = \int \frac{\partial^2 \psi}{\partial m_{sk}^{\,2}} dm_{sk} \tag{3.17}$$

with A_{m0} as the initial affinity, i.e., the chemical imbalance between free water and the solid phase and a(m) as the balanced part of this potential difference. Now, defining the hydration degree as

$$\xi(t) = \frac{m_{sk}(t)}{m_{sk}(t \to \infty)} = \frac{m_{sk}(t)}{m_{sk}(\infty)} \tag{3.18}$$

and taking its time derivative

$$\frac{d\xi}{dt} = \frac{1}{m_{sk}(\infty)}\frac{dm_{sk}}{dt} \to m_{sk}(\infty)\frac{d\xi}{dt} = \frac{dm_{sk}}{dt} \tag{3.19}$$

Using (3.16) and (3.19)

$$A_m = \eta(\xi)m_{sk}(\infty)\frac{d\xi}{dt}e^{\left(\frac{E_a}{RT}\right)} \to \frac{d\xi}{dt} = \tilde{A}(\xi)e^{-\left(\frac{E_a}{RT}\right)} \to \tilde{A}(\xi) = \frac{d\xi}{dt}e^{\left(\frac{E_a}{RT}\right)} \tag{3.20}$$

with $\tilde{A}(\xi) = A_m / [\eta(\xi) m_{sk}(\infty)]$ denoting the normalized affinity which accounts for the chemical imbalance and the microdiffusion process given by (3.17).

Considering adiabatic conditions and disregarding spatial gradients, equations (3.15) and (3.19) leads to

$$C_{th}\dot{T}_{ad} - L_m\,\dot{m}_{sk} = C_{th}dT_{ad} - L_m\,dm_{sk} = C_{th}\,dT_{ad} - L\,d\xi = 0 \tag{3.21}$$

where $L = L_m\,m_{sk}(\infty)$ is defined by ULM and COUSSY [9] as the latent heat per unit of hydration degree. Integrating (3.21) with respect to time

$$\int_0^t C_{th}\,dT_{ad}\,dt - \int_0^t L\,d\xi\,dt = C_{th}\left(T_{ad}(t) - T_{ad}(0)\right) - L\left(\xi(t) - \xi(0)\right) = 0 \tag{3.22}$$

with T_{ad} denoting the temperature for adiabatic conditions. For $t = 0$ the hydration degree is zero, that is, concrete is anhydrous $\xi(0) = 0$

$$\xi(t) = \frac{C_{th}}{L}\left(T_{ad}(t) - T_{ad}(0)\right) \tag{3.23}$$

Considering that for $t \to \infty$ concrete is completely hydrated, that is, $\xi(t_\infty) = 1$

$$\frac{L}{C_{th}} = \left(T_{ad}(t_\infty) - T_{ad}(0)\right) \tag{3.24}$$

Using (3.23) and (3.22), the hydration degree can be evaluated as follows

$$\xi(t) = \frac{\left(T_{ad}(t) - T_{ad}(0)\right)}{\left(T_{ad}(t_\infty) - T_{ad}(0)\right)} \tag{3.25}$$

Equations (3.20) and (3.25) are very important in the thermo-chemical analysis. Given an adiabatic temperature curve, the latter allows one to obtain the hydration degree for each time instant while the former is used to evaluate the normalized affinity as a function of the hydration degree which is an input data for the Finite Element modeling.

With the adiabatic temperature curve, one can fit it to obtain $T_{ad}(t)$. Then, one may use (3.25) to evaluate $\xi(t)$ from which it's possible to calculate $\dot{\xi}(t)$. Finally, one can use the derivative of the hydration degree in (3.20) to calculate $\tilde{A}(\xi)$. These calculations are made before the FEM simulation.

3.2 Finite Element formulation

The equations derived in the last section describe the temperature evolution due to hydration reaction. It accounts for the coupling between chemical and thermal processes. Now, they will be used to develop a Finite Element formulation. Considering C_{th} as the product of the density ρ by the specific heat capacity c_p, the governing equations will be

$$\rho c_p \dot{T} = L\dot{\xi} + \nabla\left(k\nabla T\right) \quad \text{for} \quad \Omega_e \quad \text{Temperature field} \tag{3.26}$$

$$q = -k\nabla T \quad \text{for} \quad \Omega_e \quad \text{Constitutive equation (Fourier's law)} \tag{3.27}$$

$$T = \bar{T} \quad \text{for} \quad \Gamma_d \quad \text{(Dirichlet boundary condition)} \tag{3.28}$$

$$-k\nabla T.n = \bar{q} \quad \text{for} \quad \Gamma_n \quad \text{(Neumann boundary condition)} \tag{3.29}$$

$$-k\nabla T.n = h\left(T - T_{ref}\right) \quad \text{for} \quad \Gamma_r \quad \text{(Robin boundary condition)} \tag{3.30}$$

The Finite Element formulation is easily derived after employing Galerkin method and Euler-backward scheme for the time derivatives. In this case, the nonlinear system of equations is given by

$$\left(M + \Delta t\left(K + H\right)\right)T^{t+1} = F_{ct} + F_{hf} + \Delta t\left(F_{chem} + F_{conv}\right) + MT^{t} \tag{3.31}$$

with

$$M = \int_{\Omega_e} N^T \rho c_p N \, d\Omega_e \tag{3.32}$$

$$K = \int_{\Omega_e} B^T k B \, d\Omega_e \tag{3.33}$$

$$H = \int_{\Gamma_r} B^T h B \, d\Gamma_r \tag{3.34}$$

$$F_{ct} = -\left(M + \Delta t\left(K + H\right)\right)\bar{T}^{t+1} \tag{3.35}$$

$$F_{hf} = \oint_{\Gamma_n} B^T \bar{q}\, d\Gamma_n \tag{3.36}$$

$$F_{chem} = \int_{\Omega_e} B^T L\, \dot{\xi}^{t+1}\, d\Omega_e \tag{3.37}$$

$$F_{conv} = \oint_{\Gamma_r} B^T h T_{ref}\, d\Gamma_r \tag{3.38}$$

with (3.35) accounting for the contribution of the prescribed temperature in the right-hand side vector.

Equation (3.31) can be shortly written as

$$AT^{t+1} = b \tag{3.39}$$

with

$$A = \left(M + \Delta t\left(K + H\right)\right) \tag{3.40}$$

$$b = F_{ct} + F_{hf} + \Delta t\left(F_{chem} + F_{conv}\right) + MT^t \tag{3.41}$$

The above system of equations is nonlinear because the temperature depends on the hydration degree and vice versa. This means that the thermo-chemical problem is time-dependent and nonlinear, that is, one must solve it iteratively for each timestep. In this context, the present study employed the Newton-Raphson method to solve it for each timestep due to its good convergence properties, although any other method could be chosen.

Before solving (3.31) one must evaluate the hydration degree for each element. To this end, one must first solve (3.20) iteratively at element level. Applying the Euler-backward scheme for the time derivative (3.20) can be rewritten as

$$\xi_k^{t+1} = \xi^t + \Delta t\, \tilde{A}\left(\xi_k^{t+1}\right) e^{-\left(\frac{E_a T_k^{t+1}}{R}\right)} \tag{3.42}$$

where ξ_k^{t+1} denotes the hydration degree for the current time instant t+1 and an iteration k. Therefore, solving (3.42) means finding the zero of a function and in the present study the *regula-falsi* method was applied. The normalized affinity as a function of the hydration degree is an input data, as remarked in the last section. Besides, (3.42) requires a temperature T_k^{t+1} but an element usually has different temperatures for each node. For linear elements, the average temperature of the nodes is a good approximation. For high-order elements, one can calculate the average temperature of the Gauss points.

3.3 Flowchart for the thermo-chemical model

The logical reasoning for the solution of the thermo-chemical problem is depicted in Figure 4. The condition $\left(\text{if } \xi_{k+1}^{t+1} < \xi^t \Rightarrow \xi_{k+1}^{t+1} = \xi^t, \text{else } \xi_{k+1}^{t+1} = \xi_{k+1}^{t+1}\right)$ states that the hydration degree for the current time instant is always greater than or equal to the hydration degree of the previous time instant. Following the same reasoning, the condition that $\left(\text{if } \xi_{k+1}^{t+1} < \xi_k^{t+1} \Rightarrow \xi_{k+1}^{t+1} = \xi_k^{t+1}, \text{else } \xi_{k+1}^{t+1} = \xi_{k+1}^{t+1}\right)$ means that the hydration degree for the current iteration k + 1 is always greater than or equal to the hydration degree of the previous iteration k. These restrictions imply that the thermo-chemical model is thermodynamically consistent, that is, it obeys the Second Law of Thermodynamics.

The following flowchart presents the general idea of the thermo-chemical analysis so that it is valid for any method for solving nonlinear system of equations. The residual is a function only of the right-hand side vector so it is written as $P(T^{t+1}) = AT^{t+1} - b(T^{t+1})$. In addition, $\|P\|_N$ denotes the normalized norm of the residual vector. In summary, the step-by-step is:

Step 1) Solve (3.42) iteratively for ξ^{t+1} for at element level;

Step 2) Assembly the system of equations (3.31);

Step 3) Solve (3.31) iteratively for T^{t+1} at global level;

Step 4) Go to the next timestep.

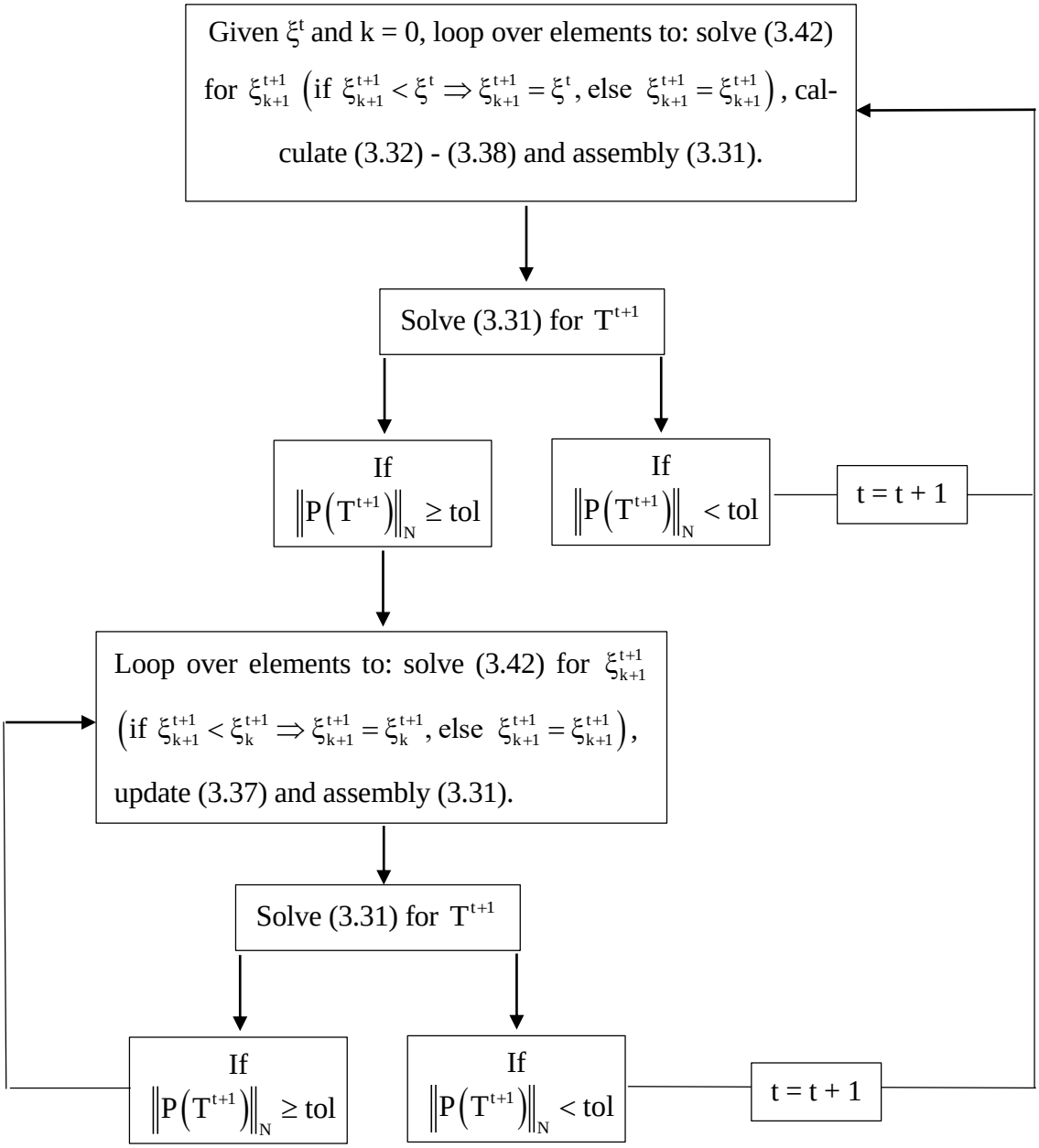

Figure 4. Flowchart for the thermo-chemical model.

3.4 Numerical applications

3.4.1 Adiabatic experiment

Now, two numerical applications of the thermo-chemical model will be presented and compared with experimental data. The analysis is the adiabatic experiment of two concretes whose properties are showed in Table 1. Figure 5 and Figure 6 presented both experimental and numerical results. The agreement between them is qualitatively acceptable.

Properties	Concrete type 1	Concrete type 2
E_a/R (K)	4400.00	4300.00
Adiabatic temperature rise (ºC)	25.60	18.30
Initial temperature (ºC)	20.09	7.21

Table 1. Properties of concretes for adiabatic experiment.

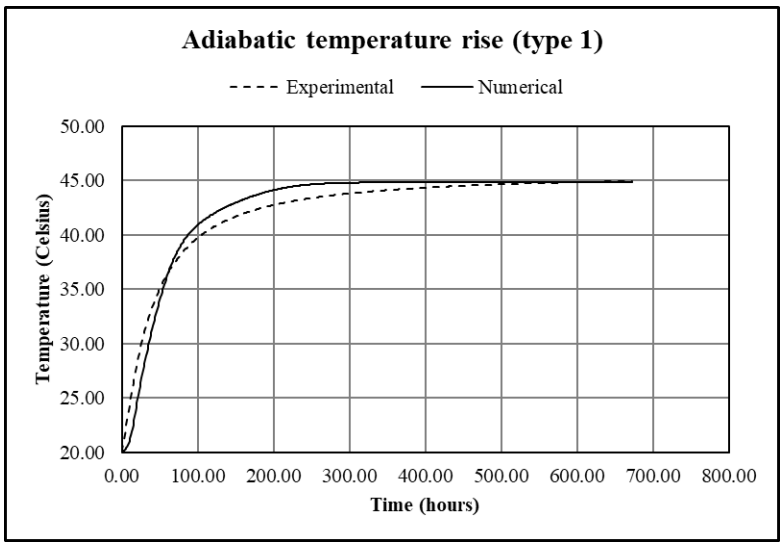

Figure 5. Adiabatic curve for concrete type 1.

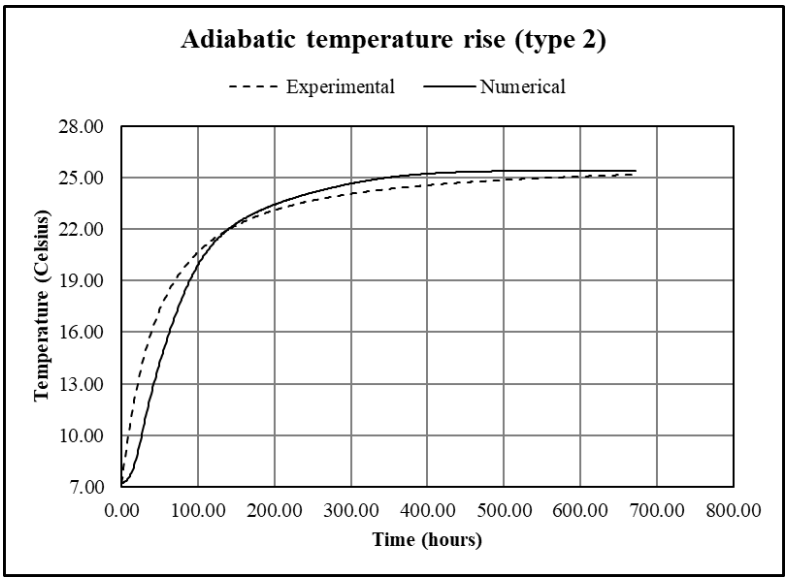

Figure 6. Adiabatic curve for concrete type 2.

3.4.2 Layered simulations

The next example simulates a situation where concrete is placed layer-by-layer. In the pre-processing step, the mesh is generated with a node numbering that, in general, the user cannot control. Thus, to simulate situations like this it is interesting to reorder nodes so that its labels increase with height. This procedure will also be adopted in chapter 5 for a theoretical example of a concrete wall built by layers. The time complexity of this methodology hinges on doing it properly.

Consider the mesh shown in Figure 7 along with its connectivity C and coordinates X arrays. Consider also that this structure will be built layer-by-layer as depicted in Figure 7.

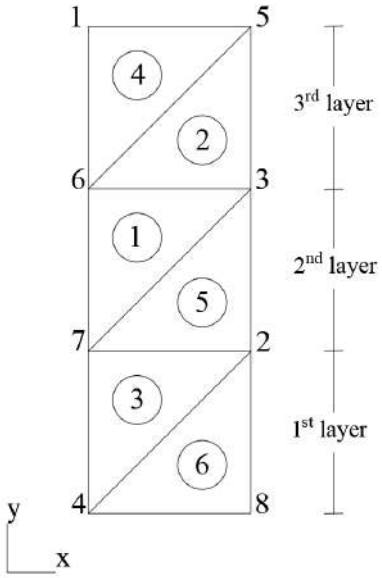

			Coordinates		
			Nodes labels	x	y
Connectivity			1	0.00	3.00
Nodes labels			2	1.00	1.00
3	7	6	3	1.00	2.00
5	6	3	4	0.00	0.00
7	4	2	5	1.00	3.00
1	5	6	6	0.00	2.00
2	7	3	7	0.00	1.00
8	4	2	8	1.00	0.00

Figure 7. Initial mesh along with its initial connectivity and coordinates arrays.

The reordering procedure is the following

Step 1) Reorder the connectivity array in a way that the first *n* rows correspond to the *n* elements of the 1st layer, rows n + 1 until n + k correspond to the *k* elements of the 2nd layer and so on. The coordinates array remains the same for a while. Figure 8 illustrates it.

			Coordinates		
			Nodes labels	x	y
Connectivity			1	0.00	3.00
Nodes labels			2	1.00	1.00
7	4	2	3	1.00	2.00
8	4	2	4	0.00	0.00
2	7	3	5	1.00	3.00
3	7	6	6	0.00	2.00
1	5	6	7	0.00	1.00
5	6	3	8	1.00	0.00

Figure 8. First reordering of the connectivity array.

Step 2) Then, reorder both connectivity and coordinates arrays as follows

Set k = 1

Do i = 1, 2…nº of elements

Do j = 1, 2…nº of nodes per element

If ($k \leq C_{i,j}$) then

In the connectivity array, interchange where C = k and C = $C_{i,j}$.

In the coordinates array, interchange rows $C_{i,j}$ and k.

$k \leftarrow k + 1$

Else

Continue

End if

If (k = total nº of nodes in the mesh) then

Stop

End if

End do

End do

The above reasoning is presented in Figure 9 below

	Old connectivity and coodinates arrays						New connectivity and coodinates arrays					
				Coord.						**Coord.**		
				x	y					x	y	
	Connectivity			0.00	3.00	Since $k \leq C_{i,j}$ obtain new connectivities and coordinates arrays.	**Connectivity**			0.00	1.00	
i = 1	Nodes labels			1.00	1.00		Nodes labels			1.00	1.00	
j = 1	7	4	2	1.00	2.00		1	4	2	1.00	2.00	k = k + 1
k = 1	8	4	2	0.00	0.00		8	4	2	0.00	0.00	
$C_{i,j}$ = 7	2	7	3	1.00	3.00		2	1	3	1.00	3.00	
	3	7	6	0.00	2.00		3	1	6	0.00	2.00	
	1	5	6	0.00	1.00		7	5	6	0.00	3.00	
	5	6	3	1.00	0.00		5	6	3	1.00	0.00	

	Old connectivity and coodinates arrays						New connectivity and coodinates arrays					
				Coord.						**Coord.**		
				x	y					x	y	
	Connectivity			0.00	1.00	Since $k \leq C_{i,j}$ obtain new connectivities and coordinates arrays.	**Connectivity**			0.00	1.00	
i = 1	Nodes labels			1.00	1.00		Nodes labels			0.00	0.00	
j = 2	1	4	2	1.00	2.00		1	2	4	1.00	2.00	k = k + 1
k = 2	8	4	2	0.00	0.00		8	2	4	1.00	1.00	
$C_{i,j}$ = 4	2	1	3	1.00	3.00		4	1	3	1.00	3.00	
	3	1	6	0.00	2.00		3	1	6	0.00	2.00	
	7	5	6	0.00	3.00		7	5	6	0.00	3.00	
	5	6	3	1.00	0.00		5	6	3	1.00	0.00	

	Old connectivity and coodinates arrays						New connectivity and coodinates arrays						
				Coord.						**Coord.**			
				x	y					x	y		
	Connectivity			0.00	1.00	Since $k \leq C_{i,j}$ obtain new connectivities and coordinates arrays.	**Connectivity**			0.00	1.00		
i = 1	Nodes labels			0.00	0.00		Nodes labels			0.00	0.00		
j = 3	1	2	4	1.00	2.00		1	2	3	1.00	1.00	k = k + 1	
k = 3	8	2	4	1.00	1.00		8	2	3	1.00	2.00		
$C_{i,j}$ = 4	4	1	3	1.00	3.00		3	1	4	1.00	3.00		
	3	1	6	0.00	2.00		4	1	6	0.00	2.00		
	7	5	6	0.00	3.00		7	5	6	0.00	3.00		
	5	6	3	1.00	0.00		5	6	4	1.00	0.00		
	Old connectivity and coodinates arrays						New connectivity and coodinates arrays						
				Coord.						**Coord.**			
				x	y					x	y		
	Connectivity			0.00	1.00	Since $k \leq C_{i,j}$ obtain new connectivities and coordinates arrays.	**Connectivity**			0.00	1.00		
i = 2	Nodes labels			0.00	0.00		Nodes labels			0.00	0.00		
j = 1	1	2	3	1.00	1.00		1	2	3	1.00	1.00	k = k + 1	
k = 4	8	2	3	1.00	2.00		4	2	3	1.00	0.00		
$C_{i,j}$ = 8	3	1	4	1.00	3.00		3	1	8	1.00	3.00		
	4	1	6	0.00	2.00		8	1	6	0.00	2.00		
	7	5	6	0.00	3.00		7	5	6	0.00	3.00		
	5	6	4	1.00	0.00		5	6	8	1.00	2.00		

	Old connectivity and coodinates arrays						New connectivity and coodinates arrays						
				Coord.						**Coord.**			
				x	y					x	y		
	Connectivity			0.00	1.00	Since $k > C_{i,j}$ no change is needed.	**Connectivity**			0.00	1.00		
i = 2	Nodes labels			0.00	0.00		Nodes labels			0.00	0.00		
j = 2	1	2	3	1.00	1.00		1	2	3	1.00	1.00	k = k	
k = 5	4	2	3	1.00	0.00		4	2	3	1.00	0.00		
$C_{i,j}$ = 2	3	1	8	1.00	3.00		3	1	8	1.00	3.00		
	8	1	6	0.00	2.00		8	1	6	0.00	2.00		
	7	5	6	0.00	3.00		7	5	6	0.00	3.00		
	5	6	8	1.00	2.00		5	6	8	1.00	2.00		
	Old connectivity and coodinates arrays						New connectivity and coodinates arrays						
				Coord.						**Coord.**			
				x	y					x	y		
	Connectivity			0.00	1.00	Since $k > C_{i,j}$ no change is needed.	**Connectivity**			0.00	1.00		
i = 2	Nodes labels			0.00	0.00		Nodes labels			0.00	0.00		
j = 3	1	2	3	1.00	1.00		1	2	3	1.00	1.00	k = k	
k = 5	4	2	3	1.00	0.00		4	2	3	1.00	0.00		
$C_{i,j}$ = 3	3	1	8	1.00	3.00		3	1	8	1.00	3.00		
	8	1	6	0.00	2.00		8	1	6	0.00	2.00		
	7	5	6	0.00	3.00		7	5	6	0.00	3.00		
	5	6	8	1.00	2.00		5	6	8	1.00	2.00		

	Old connectivity and coodinates arrays						New connectivity and coodinates arrays					
				Coord.						**Coord.**		
				x	y					x	y	
	Connectivity			0.00	1.00		**Connectivity**			0.00	1.00	
i = 3	Nodes labels			0.00	0.00	Since $k > C_{i,j}$	Nodes labels			0.00	0.00	
j = 1	1	2	3	1.00	1.00	no change is	1	2	3	1.00	1.00	k = k
k = 5	4	2	3	1.00	0.00	needed.	4	2	3	1.00	0.00	
$C_{i,j} = 2$	3	1	8	1.00	3.00		3	1	8	1.00	3.00	
	8	1	6	0.00	2.00		8	1	6	0.00	2.00	
	7	5	6	0.00	3.00		7	5	6	0.00	3.00	
	5	6	8	1.00	2.00		5	6	8	1.00	2.00	

	Old connectivity and coodinates arrays						New connectivity and coodinates arrays					
				Coord.						**Coord.**		
				x	y					x	y	
	Connectivity			0.00	1.00		**Connectivity**			0.00	1.00	
i = 3	Nodes labels			0.00	0.00	Since $k > C_{i,j}$	Nodes labels			0.00	0.00	
j = 2	1	2	3	1.00	1.00	no change is	1	2	3	1.00	1.00	k = k
k = 5	4	2	3	1.00	0.00	needed.	4	2	3	1.00	0.00	
$C_{i,j} = 1$	3	1	8	1.00	3.00		3	1	8	1.00	3.00	
	8	1	6	0.00	2.00		8	1	6	0.00	2.00	
	7	5	6	0.00	3.00		7	5	6	0.00	3.00	
	5	6	8	1.00	2.00		5	6	8	1.00	2.00	

	Old connectivity and coodinates arrays						New connectivity and coodinates arrays					
				Coord.						**Coord.**		
				x	y					x	y	
	Connectivity			0.00	1.00		**Connectivity**			0.00	1.00	
i = 3	Nodes labels			0.00	0.00	Since $k \leq C_{i,j}$	Nodes labels			0.00	0.00	
j = 3	1	2	3	1.00	1.00	obtain new	1	2	3	1.00	1.00	k = k + 1
k = 5	4	2	3	1.00	0.00	connectivities	4	2	3	1.00	0.00	
$C_{i,j} = 8$	3	1	8	1.00	3.00	and	3	1	5	1.00	2.00	
	8	1	6	0.00	2.00	coordinates	5	1	6	0.00	2.00	
	7	5	6	0.00	3.00	arrays.	7	8	6	0.00	3.00	
	5	6	8	1.00	2.00		8	6	5	1.00	3.00	

	Old connectivity and coodinates arrays						New connectivity and coodinates arrays					
				Coord.						**Coord.**		
				x	y					x	y	
	Connectivity			0.00	1.00		**Connectivity**			0.00	1.00	
i = 4	Nodes labels			0.00	0.00	Since $k > C_{i,j}$	Nodes labels			0.00	0.00	
j = 1	1	2	3	1.00	1.00	no change is	1	2	3	1.00	1.00	k = k
k = 6	4	2	3	1.00	0.00	needed.	4	2	3	1.00	0.00	
$C_{i,j} = 5$	3	1	5	1.00	2.00		3	1	5	1.00	2.00	
	5	1	6	0.00	2.00		5	1	6	0.00	2.00	
	7	8	6	0.00	3.00		7	8	6	0.00	3.00	
	8	6	5	1.00	3.00		8	6	5	1.00	3.00	

	Old connectivity and coodinates arrays						New connectivity and coodinates arrays						
				Coord.						**Coord.**			
				x	y					x	y		
	Connectivity			0.00	1.00		**Connectivity**			0.00	1.00		
i = 4	Nodes labels			0.00	0.00	Since $k > C_{i,j}$ no change is needed.	Nodes labels			0.00	0.00		k = k
j = 2	1	2	3	1.00	1.00		1	2	3	1.00	1.00		
k = 6	4	2	3	1.00	0.00		4	2	3	1.00	0.00		
$C_{i,j} = 1$	3	1	5	1.00	2.00		3	1	5	1.00	2.00		
	5	1	6	0.00	2.00		5	1	6	0.00	2.00		
	7	8	6	0.00	3.00		7	8	6	0.00	3.00		
	8	6	5	1.00	3.00		8	6	5	1.00	3.00		
	Old connectivity and coodinates arrays						New connectivity and coodinates arrays						
				Coord.						**Coord.**			
				x	y					x	y		
	Connectivity			0.00	1.00	Since $k \leq C_{i,j}$ obtain new connectivities and coordinates arrays.	**Connectivity**			0.00	1.00		
i = 4	Nodes labels			0.00	0.00		Nodes labels			0.00	0.00		
j = 3	1	2	3	1.00	1.00		1	2	3	1.00	1.00		k = k + 1
k = 6	4	2	3	1.00	0.00		4	2	3	1.00	0.00		
$C_{i,j} = 6$	3	1	5	1.00	2.00		3	1	5	1.00	2.00		
	5	1	6	0.00	2.00		5	1	6	0.00	2.00		
	7	8	6	0.00	3.00		7	8	6	0.00	3.00		
	8	6	5	1.00	3.00		8	6	5	1.00	3.00		

	Old connectivity and coodinates arrays						New connectivity and coodinates arrays						
				Coord.						**Coord.**			
				x	y					x	y		
	Connectivity			0.00	1.00	Since $k \leq C_{i,j}$ obtain new connectivities and coordinates arrays.	**Connectivity**			0.00	1.00		
i = 5	Nodes labels			0.00	0.00		Nodes labels			0.00	0.00		
j = 1	1	2	3	1.00	1.00		1	2	3	1.00	1.00		k = k + 1
k = 7	4	2	3	1.00	0.00		4	2	3	1.00	0.00		
$C_{i,j} = 7$	3	1	5	1.00	2.00		3	1	5	1.00	2.00		
	5	1	6	0.00	2.00		5	1	6	0.00	2.00		
	7	8	6	0.00	3.00		7	8	6	0.00	3.00		
	8	6	5	1.00	3.00		8	6	5	1.00	3.00		
	Old connectivity and coodinates arrays						New connectivity and coodinates arrays						
				Coord.						**Coord.**			
				x	y					x	y		
	Connectivity			0.00	1.00	Since $k \leq C_{i,j}$ obtain new connectivities and coordinates arrays.	**Connectivity**			0.00	1.00		k = nº of nodes → stop computations
i = 5	Nodes labels			0.00	0.00		Nodes labels			0.00	0.00		
j = 2	1	2	3	1.00	1.00		1	2	3	1.00	1.00		
k = 8	4	2	3	1.00	0.00		4	2	3	1.00	0.00		
$C_{i,j} = 8$	3	1	5	1.00	2.00		3	1	5	1.00	2.00		
	5	1	6	0.00	2.00		5	1	6	0.00	2.00		
	7	8	6	0.00	3.00		7	8	6	0.00	3.00		
	8	6	5	1.00	3.00		8	6	5	1.00	3.00		

Figure 9. Reordering procedure for the connectivity array.

Finally, the obtained reordered mesh is depicted in Figure 10.

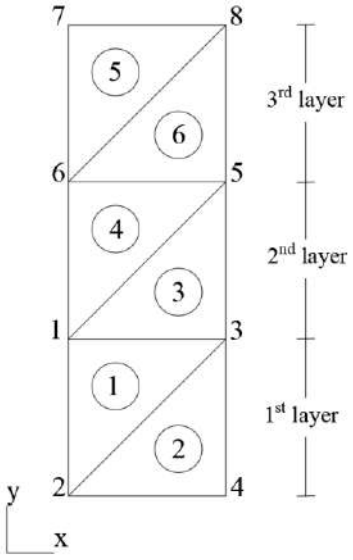

			Coordinates		
			Nodes labels	x	y
Connectivity			1	0.00	1.00
Nodes labels			2	0.00	0.00
1	2	3	3	1.00	1.00
4	2	3	4	1.00	0.00
3	1	5	5	1.00	2.00
5	1	6	6	0.00	2.00
7	8	6	7	0.00	3.00
8	6	5	8	1.00	3.00

Figure 10. Mesh with new nodes' labels and final connectivity and coordinates arrays.

3.4.2.1 Concrete block

This exampled is explored by MEHTA and MONTEIRO [4] and consists in the layered building of a concrete block over a rock foundation which is depicted in Figure 11. The objective of the present analysis is to study the influence of the following parameters on the thermo-chemical behaviour of concrete.

- Pozzolan addition;
- Type of aggregate;
- Placing temperature;
- Number of layers.

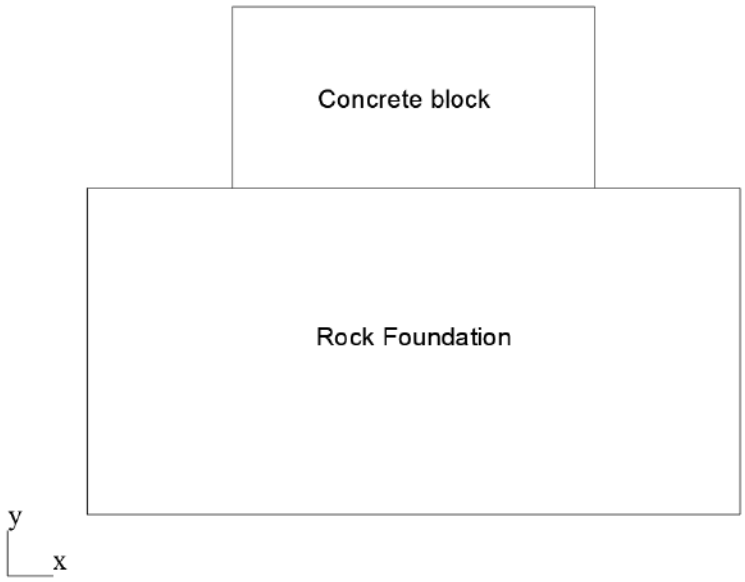

Figure 11. Concrete block built over a rock foundation.

The properties necessary to determine the adiabatic curve are in Table 2. Figure 12, Figure 13 and Figure 14 compare the adiabatic curve for different quantities of Pozzolan. These curves are independent of the type of aggregate used.

Properties	0% Pozzolan	30% Pozzolan	50% Pozzolan
E_a/R (K)	3900.00	3900.00	3900.00
Adiabatic temperature rise (°C)	49.00	44.00	41.00
Initial temperature (°C)	0.00	0.00	0.00

Table 2. Properties of concrete for different portions of Pozzolan.

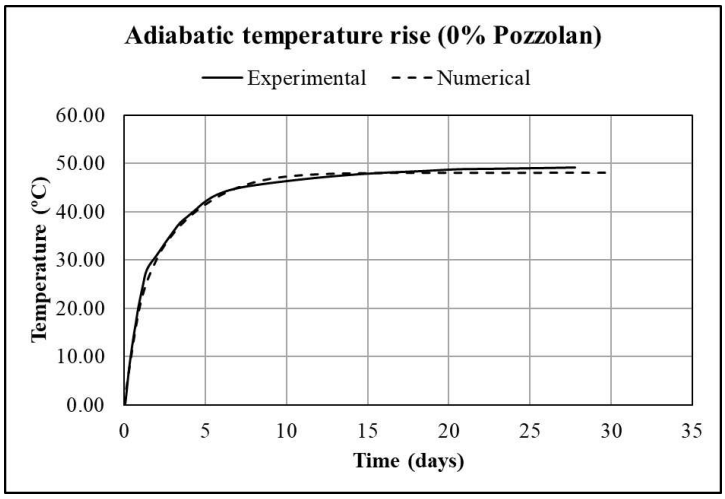

Figure 12. Adiabatic curve for 0% of Pozzolan.

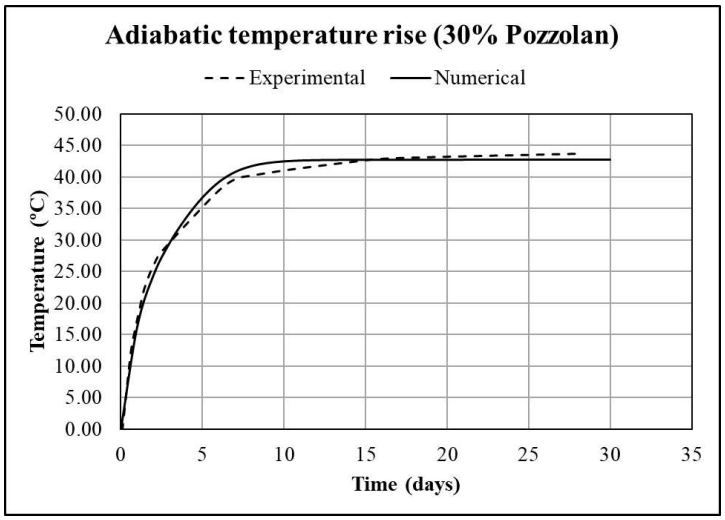

Figure 13. Adiabatic curve for 30% of Pozzolan.

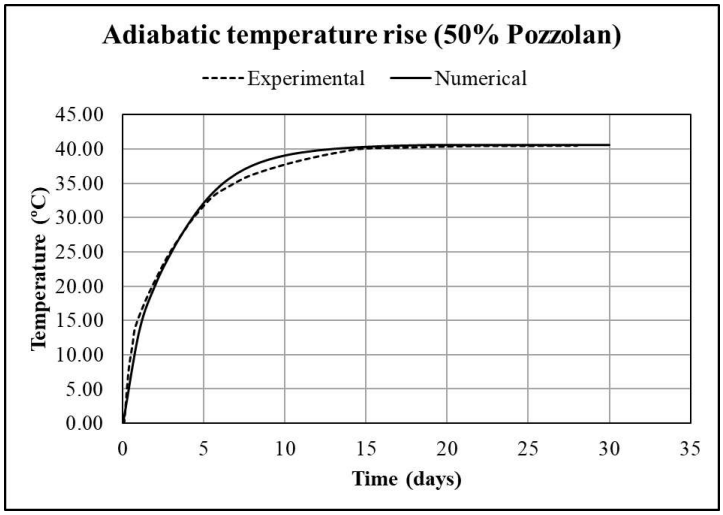

Figure 14. Adiabatic curve for 50% of Pozzolan.

Figure 15 present the nodes that were used to generate the mesh, except point A which is only for temperature evaluation. The coordinates of these nodes are exhibited in Table 3. Similarly, the mesh is in Figure 16 and it has 513 nodes and 955 linear triangular elements.

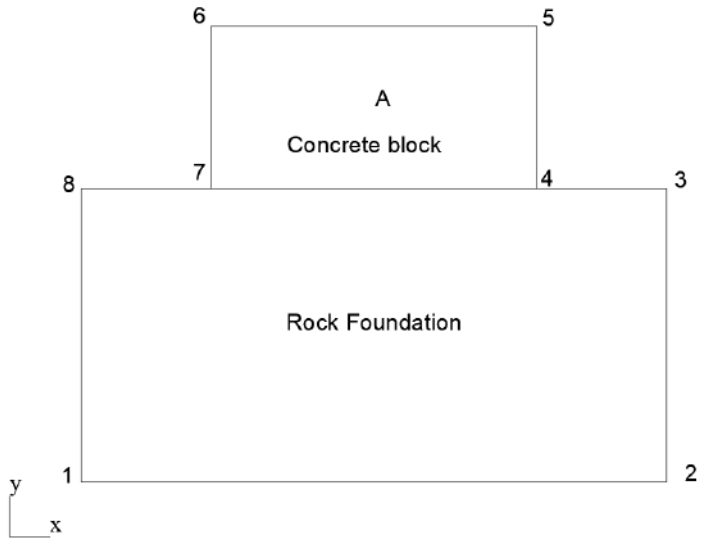

Figure 15. Nodes used to generate the mesh.

Label	1	2	3	4	5	6	7	8	A
x	0.00	10.8	10.8	8.40	8.40	2.40	2.40	0.00	5.40
y	0.00	0.00	5.40	5.40	8.40	8.40	5.40	5.40	6.90

Table 3. Nodes' coordinates of the concrete block.

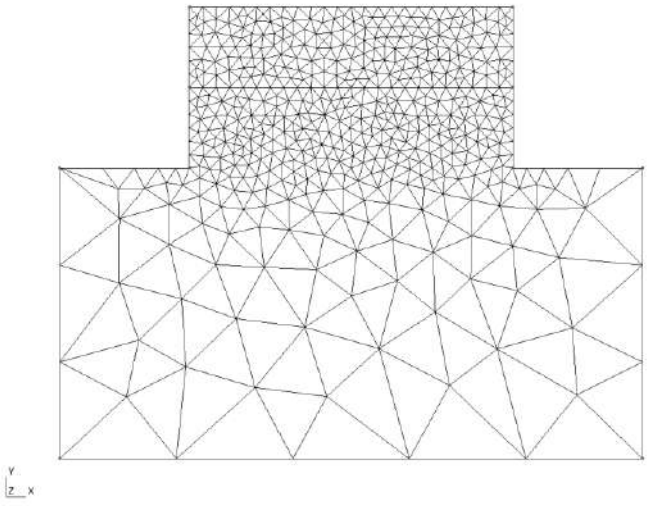

Figure 16. Discretization of the concrete block and rock foundation.

In Table 4 are the properties for the rock foundation and for the aggregates (basalt, granite and gravel). The value of the convective heat transfer coefficient was not provided by MEHTA and MONTEIRO [4]. Thus, it was adopted 20 $J.s^{-1}.m^{-2}.^oC^{-1}$.

Properties	Basalt	Granite	Gravel	Rock
Thermal conductivity ($J.s^{-1}.m^{-1}.^oC^{-1}$)	2.02	2.75	4.29	3.25
Specific heat capacity ($J.kg^{-1}.^oC^{-1}$)	1004.16	962.32	920.48	836.80
Density ($kg.m^{-3}$)	2500.00	2450.00	2400.00	2800.00
E_a/R (K)	3900.00	3900.00	3900.00	--
Convective heat transfer coefficient ($J.s^{-1}.m^{-2}.^oC^{-1}$)	20.00	20.00	20.00	0.00

Table 4. Properties for each aggregate and rock foundation.

In the first and second analyses, it's investigated the influence of the number of layers. For the first analysis, the parameters are in Table 5. The results for 7 days, which presented the maximum temperature distribution, are in Figure 17 and Figure 18.

Aggregate	Granite
Number of layers	2
Placing temperature (^oC)	17.00
Pozzolan addition (%)	0.00
Surrounding temperature (^oC)	17.00
Time interval between each layer (days)	3.00
Layer height (m)	1.50

Table 5. Parameters used in the first analysis.

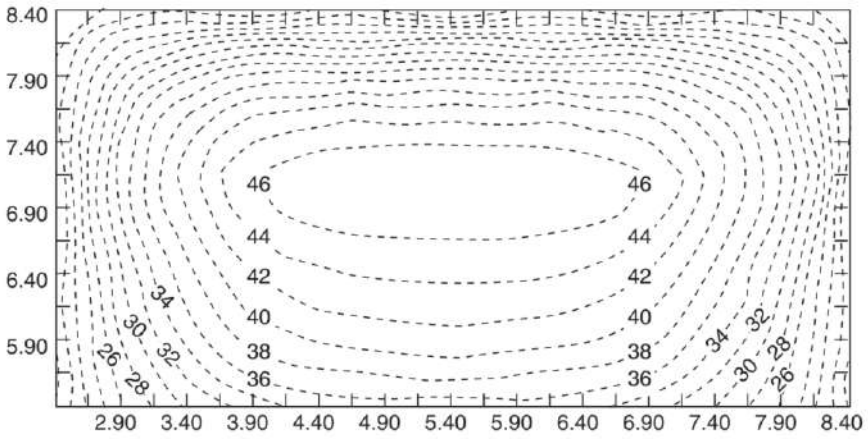

Figure 17. Contour plot for temperature: first analysis (MEHTA and MONTEIRO [4]).

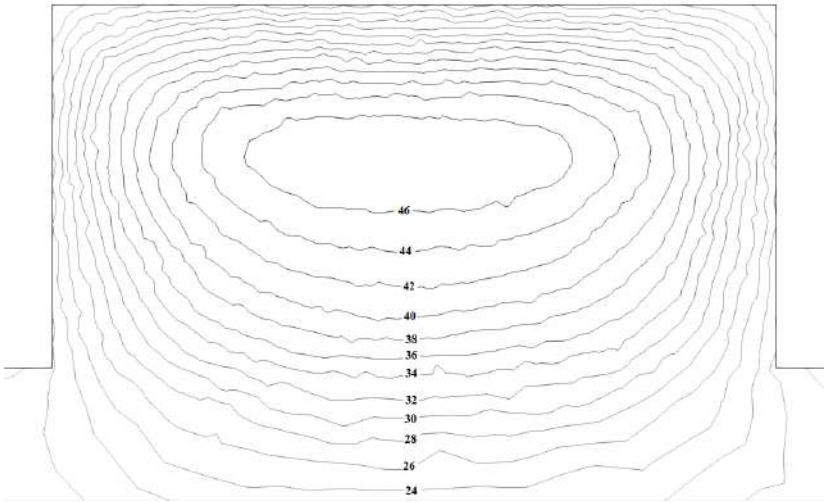

Figure 18. Contour plot for temperature: first analysis (present study).

The parameters for the second analysis are in Table 6. Results for 7 days, which presented the maximum temperature distribution, are in Figure 19 and Figure 20.

Aggregate	Granite
Number of layers	1
Placing temperature (ºC)	17.00
Pozzolan addition (%)	0.00
Surrounding temperature (ºC)	17.00
Layer height (m)	1.50

Table 6. Parameters: second analysis.

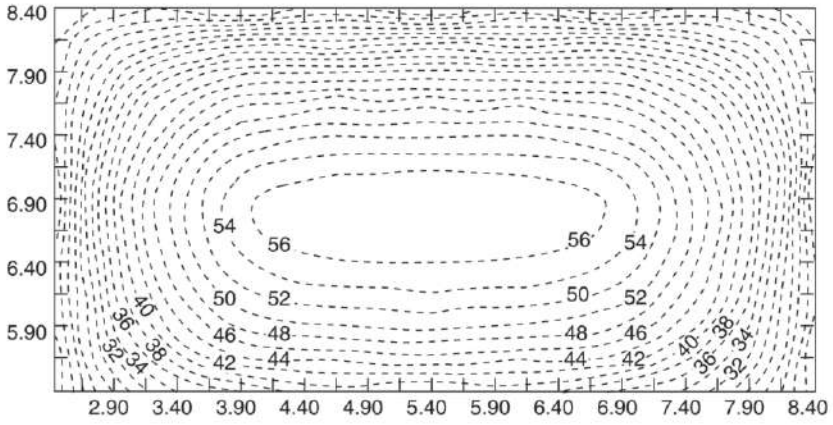

Figure 19. Contour plot for temperature: second analysis (MEHTA and MONTEIRO [4]).

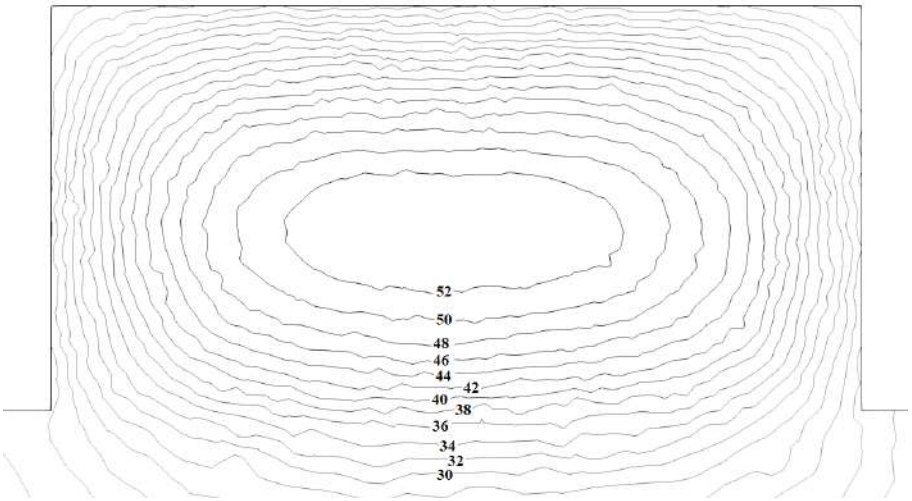

Figure 20. Contour plot for temperature obtained by the present study.

In the third analysis, it was analyzed the effect of the aggregate on the maximum temperature at point A. The parameters are in Table 7 while the results are in Figure 21 and Figure 22.

Number of layers	2
Placing temperature (ºC)	17.00
Pozzolan addition (%)	0.00
Surrounding temperature (ºC)	17.00
Time interval between each layer (days)	3.00
Layer height (m)	1.50

Table 7. Parameters for the third analysis.

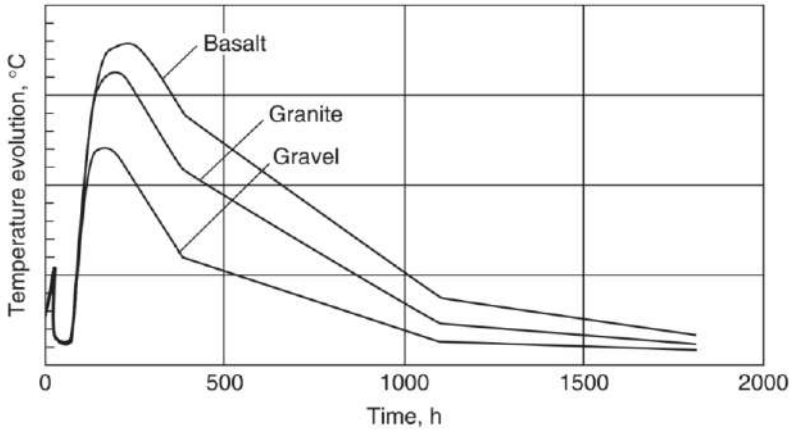

Figure 21. Temperature at point A: third analysis (MEHTA and MONTEIRO [4]).

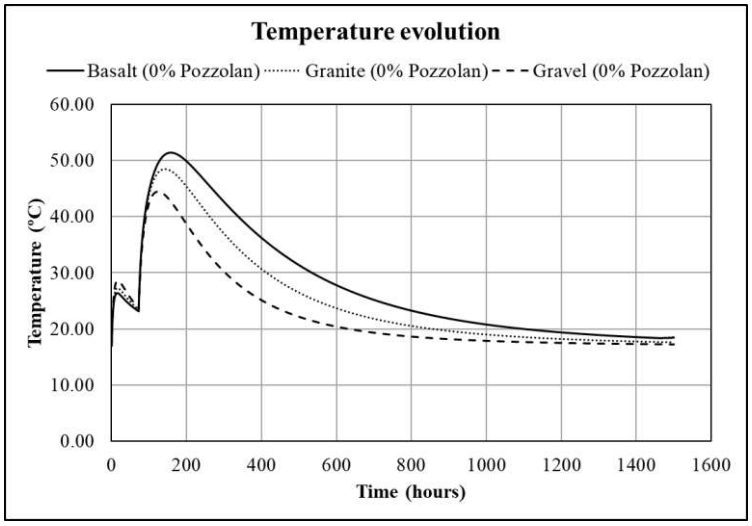

Figure 22. Temperature at point A: third analysis (present study).

In the fourth analysis, it's analyzed the influence of Pozzolan addition on the temperature evolution at point A. In Table 8 are the parameters while results are presented in Figure 23 and Figure 24.

Aggregate	Granite
Number of layers	2
Placing temperature (ºC)	17.00
Surrounding temperature (ºC)	17.00
Time interval between each layer (days)	3.00
Layer height (m)	1.50

Table 8. Parameters for the fourth analysis.

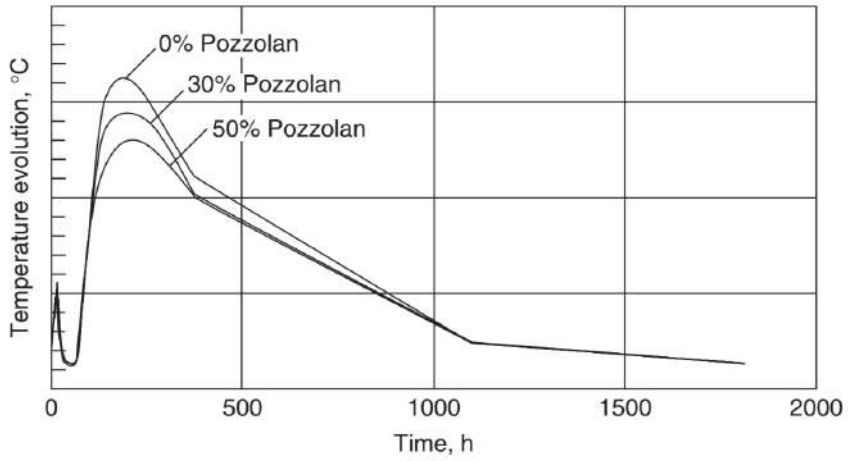

Figure 23. Temperature at point A: fourth analysis (MEHTA and MONTEIRO [4]).

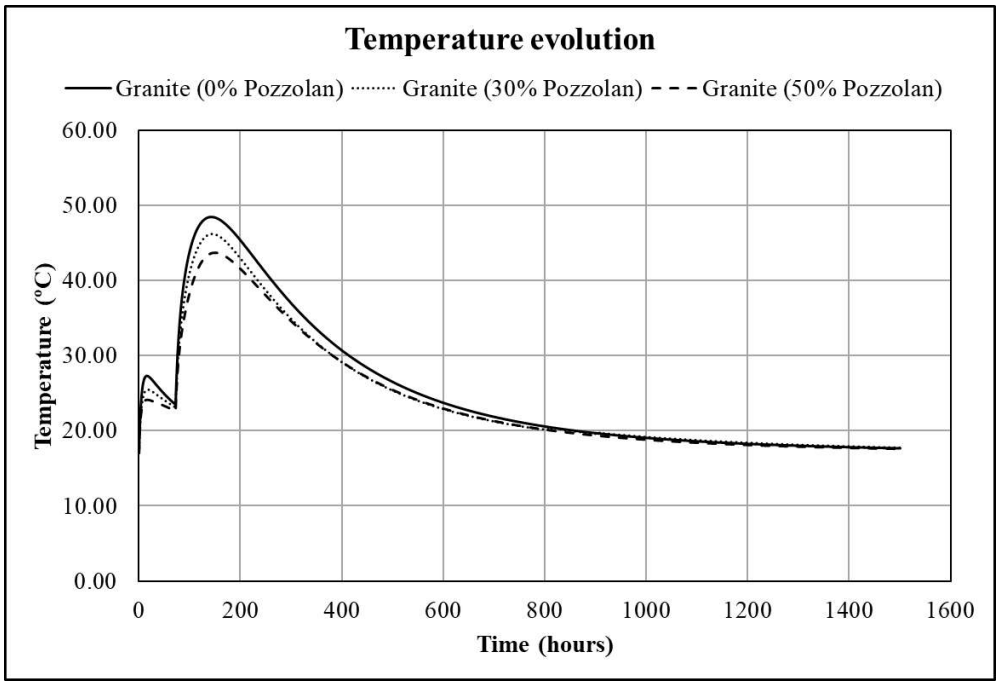

Figure 24. Temperature at point A: fourth analysis (present study).

In fifth and sixth analyses, it was investigated the influence of the placing temperature. For the fifth analysis, the parameters are in Table 9 while results for 7 days, which presented the maximum temperature distribution, are in Figure 25 and Figure 26.

Aggregate	Granite
Number of layers	2
Placing temperature (ºC)	10.00
Surrounding temperature (ºC)	17.00

Time interval between each layer (days)	3.00
Layer height (m)	1.50

Table 9. Parameters for the fifth analysis.

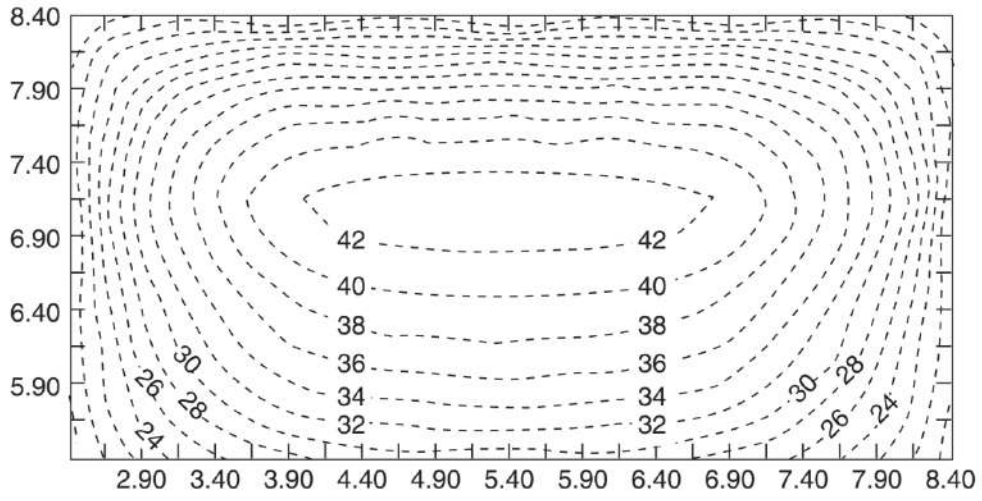

Figure 25. Contour plot for temperature: fifth analysis (MEHTA and MONTEIRO [4]).

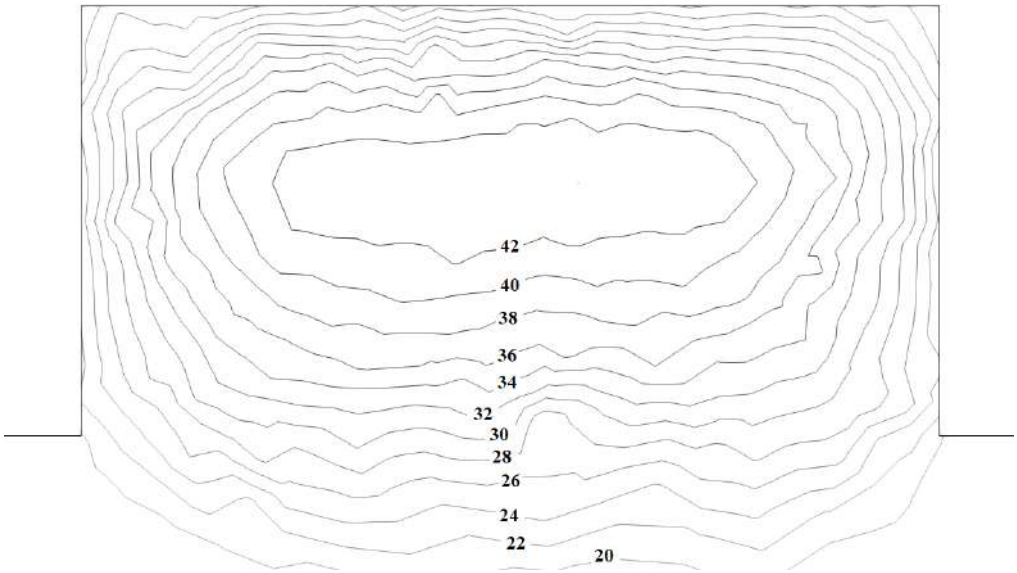

Figure 26. Contour plot for temperature: fifth analysis (present study).

For the sixth analysis, the parameters are in Table 10 while the results for 7 days are in Figure 27 and Figure 28.

Aggregate	Granite
Number of layers	2
Placing temperature (ºC)	25.00
Surrounding temperature (ºC)	17.00
Time interval between each layer (days)	3.00
Layer height (m)	1.50

Table 10. Parameters for the sixth analysis.

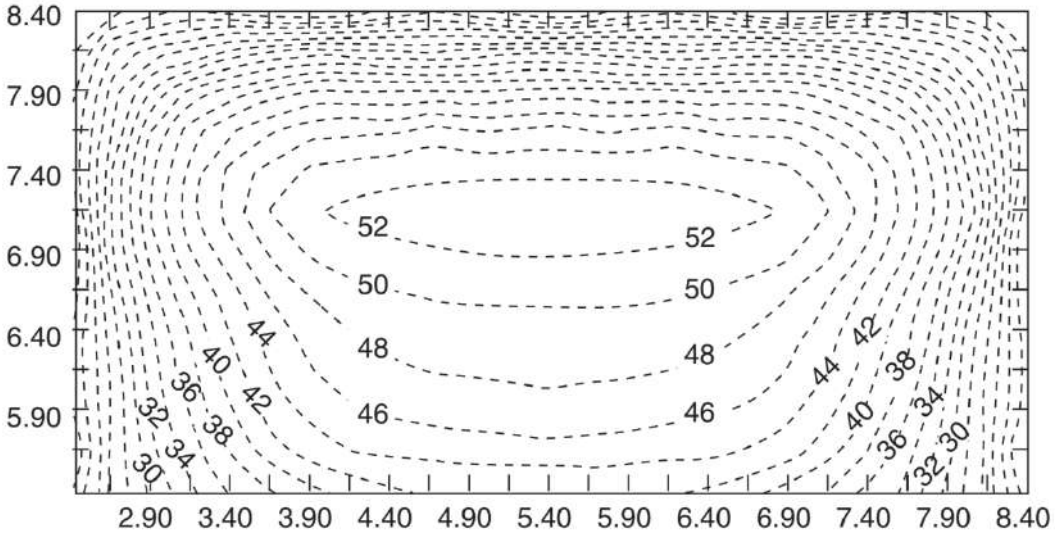

Figure 27. Contour plot for temperature: sixth analysis (MEHTA and MONTEIRO [4]).

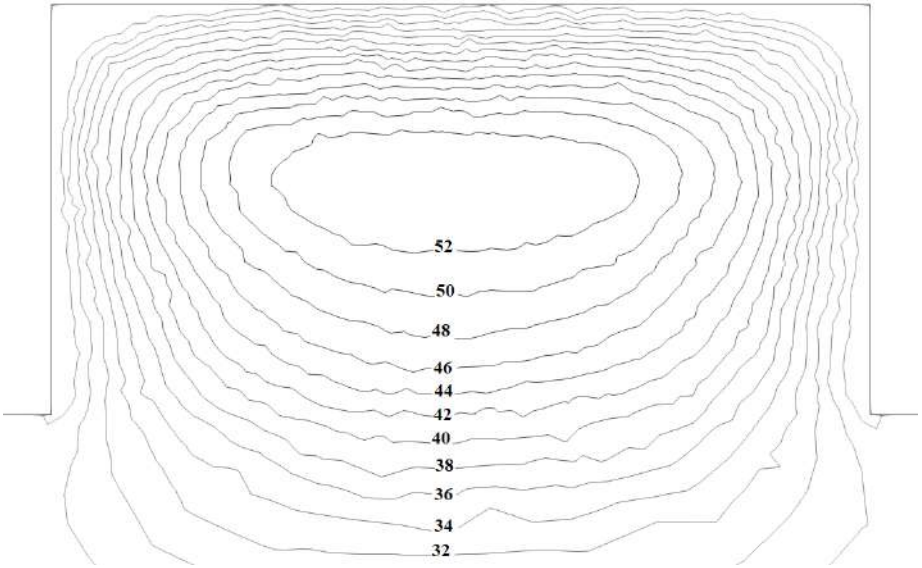

Figure 28. Contour plot for temperature: sixth analysis (present study).

4 Thermo-mechanical model regarding ageing and damage

In the previous chapter, the thermo-chemical model was introduced by using the thermodynamics of chemically reactive porous media. Those equations describe the temperature increase of concrete due to hydration of cement paste. These temperature variations will lead to thermal strains. To this end, this chapter will present a thermo-mechanical model that considers the influence of temperature variations, ageing and damage on the mechanical behaviour of an isotropic and elastic material.

4.1 Constitutive equation for elastic materials with ageing

Before discussing the damage model, it is necessary to make some remarks about elastic materials that present ageing. For these materials, it will not be used the usual constitutive equation $\sigma^{t+1} = \mathbb{C}^{t+1}\,\varepsilon_{elastic}^{t+1}$. Instead, it will be followed the reasoning of MARQUES and CREUS [21], which adopted a different constitutive relationship to model the ageing behaviour. Therefore, the incremental constitutive equation $\dot{\sigma}^{t+1} = \mathbb{C}^{t+1}\,\dot{\varepsilon}_{elastic}^{t+1}$ can be used and this relation preclude that, for a constant stress state, strains decrease with time. This study will not focus on the derivation of the constitutive equation but rather on its usage. A good discussion regarding constitutive equations is presented in OTTOSEN and RISTINMAA [22], ODEN [23], BAŞAR and WEICHERT [24], TRUESDELL and DILL [25], TRUESDELL [26], LIU [27], HAUPT [28], CAPALDI [29], COMAN [30], REDDY [31], BYSKOV [32] and DIMITRIENKO [33].

To illustrate this issue, a Finite Element example will be presented. Consider the governing equations for the mechanical problem using the incremental constitutive equation

$$\nabla.\sigma^{t+1} + b^{t+1} = 0 \quad \text{for} \quad \Omega_e \quad \text{Equilibrium (momentum) equation} \tag{4.1}$$

$$\dot{\sigma} = \mathbb{C}^{t+1}\,\dot{\varepsilon}_{elastic} \approx \Delta\sigma^{t+1} = \mathbb{C}^{t+1}\,\Delta\varepsilon_{elastic}^{t+1} \rightarrow \sigma^{t+1} - \sigma^{t} = \mathbb{C}^{t+1}\left(\varepsilon_{elastic}^{t+1} - \varepsilon_{elastic}^{t}\right) \tag{4.2}$$

$$\varepsilon_{total}^{t+1} = \Im u^{t+1} \quad \text{Strain} - \text{displacement equation} \tag{4.3}$$

$$u = \bar{u} \quad \text{for} \quad \Gamma_d \quad \text{Dirichlet (essential) boundary condition} \tag{4.4}$$

$$\sigma.n = \bar{t} \quad \text{for} \quad \Gamma_n \quad \text{Neumann (natural) boundary condition} \tag{4.5}$$

with $\Im$ denoting the tensor for infinitesimal strains. Employing the Galerkin method, the Finite Element formulation is given by

$$K^{t+1}U^{t+1} = F_{cd}^{t+1} + F_{int}^{t} + F_{tf}^{t+1} + F_{dl}^{t+1} + F_{pd}^{t+1} \tag{4.6}$$

$$K^{t+1} = \int_{\Omega_e} B^T \mathbb{C}^{t+1} B \, d\Omega_e \tag{4.7}$$

$$F_{cd}^{t+1} = -K^{t+1}\bar{U}^{t+1} \tag{4.8}$$

$$F_{int}^{t} = -\int_{\Omega_e} B^T \sigma^t \, d\Omega_e \tag{4.9}$$

$$F_{tf}^{t+1} = \oint_{\Gamma_n} B^T \bar{t}^{t+1} d\Gamma_n \tag{4.10}$$

$$F_{dl}^{t+1} = \int_{\Omega_e} B^T b^{t+1} \, d\Omega_e \tag{4.11}$$

$$F_{pd}^{t+1} = \int_{\Omega_e} B^T \mathbb{C}^{t+1} B \, d\Omega_e U^t = K^{t+1}U^t \tag{4.12}$$

with (4.8) accounting for the contribution of the prescribed displacements on the right-hand side vector. Now, it will be demonstrated the difference between the non-incremental and incremental constitutive equations for modelling ageing. Consider a concrete specimen along with its boundary conditions and mesh discretization depicted in Figure 29. It has 0.3m length, 0.1m height and 0.1m width. It will be loaded in tension by a constant displacement of 1mm on the right-hand edge when t = 1 hour. The Young's modulus is assumed to evolve with time through the following function

$$E(t) = E_0 \frac{t}{t_f} \quad \forall \quad t > 0 \tag{4.13}$$

with t_f as the final instant time analyzed (10 hours for this analysis), E_0 the initial Young's modulus which was chosen as 3 GPa and $\nu = 0.30$ for the Poisson coefficient. The analysis was made using the Plane Stress theory and time interval $\Delta t = 1$ hour. The evolution of Young's modulus is in Figure 30 and the results of the simulation are in Figure 31. When using the non-incremental constitutive equation, stresses increase with time for a constant strain state which is not correct. For the incremental constitutive equation, stress remain constant for a constant strain state which is physically coherent.

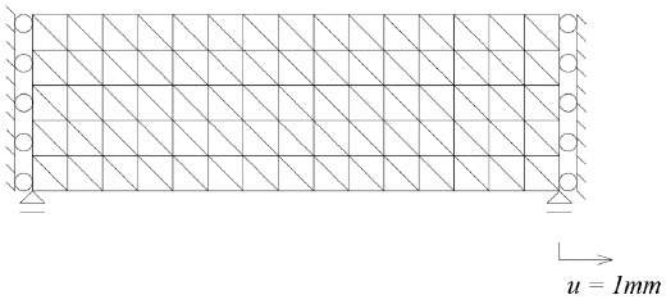

Figure 29. Concrete specimen and its boundary conditions.

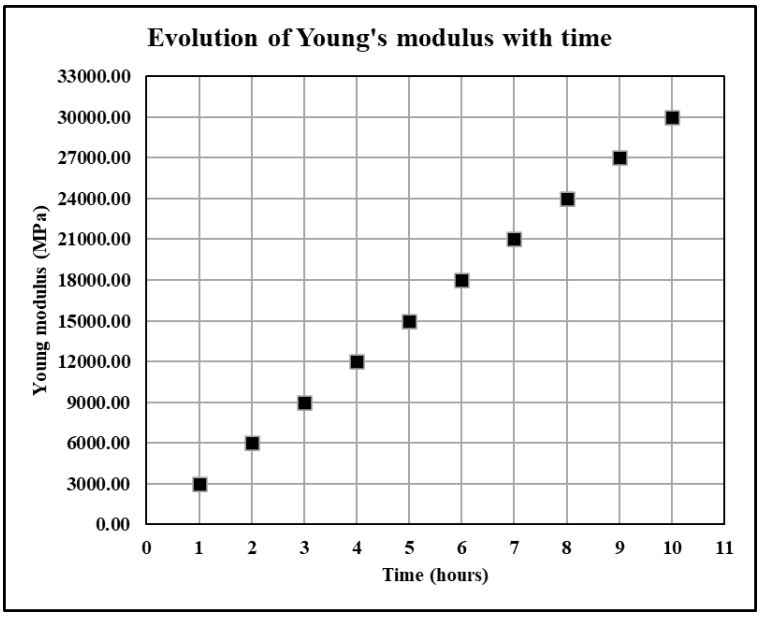

Figure 30. Evolution of Young's modulus.

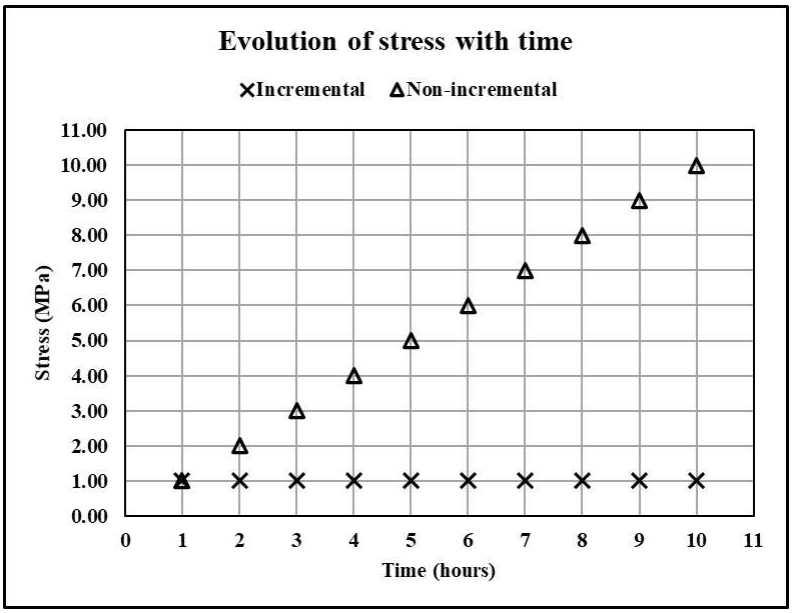

Figure 31. Evolution of stress measured on the support for both incremental and non-incremental constitutive equation.

4.2 Mathematical modelling regarding ageing and damage

The word "damage" in the context of *Continuum Damage Mechanics* is generally used to describe the deterioration of a material due to loss of stiffness. The concept of damage was first proposed by KACHANOV [34] when studying creep and the author used a scalar variable to evaluate the damage state of the material. The idea was further developed by RABOTNOV [35], HAYHURST [36], KRAJCINOVIC and FONSEKA [37], KRAJCINOVIC and FONSEKA [38], LECKIE and HAYHURST [39], LEMAITRE and CHABOCHE [40], LEMAITRE [41], LEMAITRE and DESMORAT [42], MURAKAMI [43], among others.

Now, a mathematical model that takes into account both ageing and damage will be derived. The consideration of ageing is linked to the incremental constitutive equation discussed in the previous section. Hence, damage must be incorporated to it and that's the main concern of this section. To discuss damage, two fundamental concepts must be presented, namely: *Effective Stress* and *Principle of Strain-Equivalence*.

4.2.1 Effective Stress

Consider a small region of a mesoscale taken from a body under external loads (Figure 32). The dimensions of this region are such that its defects and mechanical properties are statistically homogeneous. The smallest volume that satisfies these conditions is referred to as Representative Volume Element (RVE).

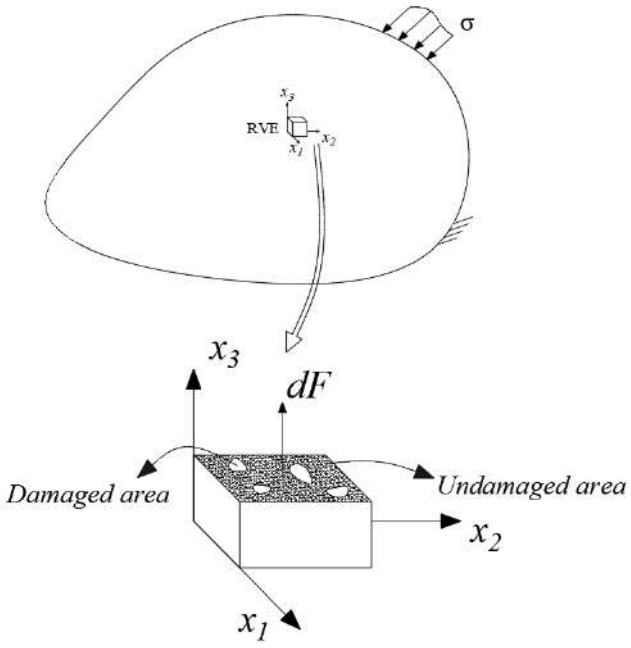

Figure 32. Body under external loads and its Representative Volume Element.

Consider a plane cutting the RVE, as depicted in Figure 32. For a given time instant, a force dF acts on it. Besides, its total area is written as

$$dA_{total} = dA^{t+1}_{damaged} + dA^{t+1}_{undamaged} \tag{4.14}$$

Considering damage as a scalar variable, it can be given by

$$D^{t+1} = \frac{dA^{t+1}_{damaged}}{dA_{total}} \rightarrow dA^{t+1}_{damaged} = D^{t+1} dA_{total} \tag{4.15}$$

Thus, the material is undamaged for *D = 0*, that is, in the absence of defects and completely damaged for *D = 1*, i.e., when the damaged area corresponds to the total area and the material loses its load-carrying capacity.

The nominal stress is given by

$$\sigma^{t+1} = \frac{dF^{t+1}}{dA_{total}} \tag{4.16}$$

while the effective stress is written as

$$\tilde{\sigma}^{t+1} = \frac{dF^{t+1}}{dA^{t+1}_{undamaged}} \tag{4.17}$$

Using (4.14), (4.15), (4.16) and (4.17) the relation between nominal and effective stresses is given by

$$\begin{aligned} &\frac{\sigma^{t+1}}{\tilde{\sigma}^{t+1}} = \frac{dA^{t+1}_{undamaged}}{dA_{total}} = \frac{dA_{total} - dA^{t+1}_{damaged}}{dA_{total}} = \frac{dA_{total} - D^{t+1}dA_{total}}{dA_{total}} = \left(1 - D^{t+1}\right) \\ &\rightarrow \tilde{\sigma}^{t+1} = \frac{\sigma^{t+1}}{\left(1 - D^{t+1}\right)} \end{aligned} \tag{4.18}$$

4.2.2 Principle of Strain-Equivalence

The Principle of Strain-Equivalence (cf. LEMAITRE [40] and MURAKAMI [43]), illustrated in Figure 33, affirms that the strain state for an undamaged material subjected to effective stress is equal to the strain state for a damaged material under nominal stress.

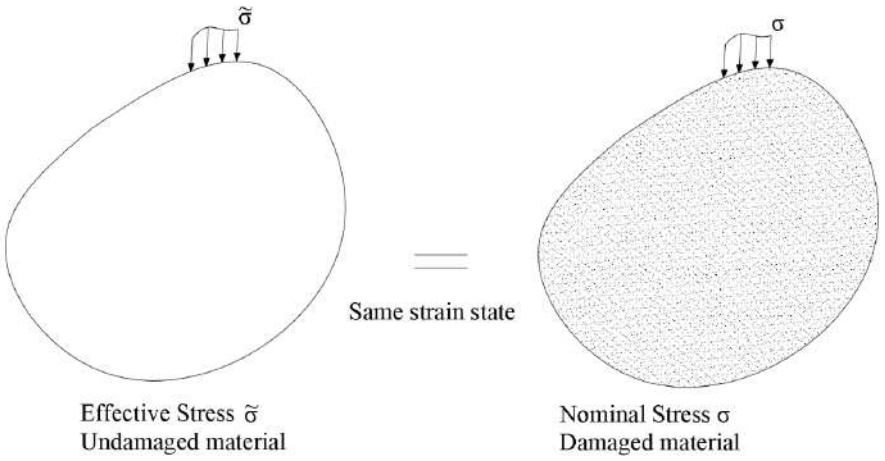

Figure 33. Principle of Strain-Equivalence showing the equivalence of the strain state between a damaged and an undamaged body.

The undamaged material has Young's modulus E so that its constitutive matrix is $\mathbb{C}$. The damaged material has modulus $\tilde{E}$ which makes its constitutive matrix be $\tilde{\mathbb{C}}$. Using the incremental constitutive equation, the strain for a given time instant $t+1$ is

$$\varepsilon_{\text{elastic}}^{t+1} = \mathbb{C}^{-1}\left(\sigma^{t+1} - \sigma^{t}\right) + \varepsilon_{\text{elastic}}^{t} \tag{4.19}$$

Mathematically, the hypothesis of strain-equivalence is written as

$$\begin{aligned} &\mathbb{C}^{-1}\left(\tilde{\sigma}^{t+1} - \tilde{\sigma}^{t}\right) + \varepsilon_{\text{elastic}}^{t} = \tilde{\mathbb{C}}^{-1}\left(\sigma^{t+1} - \sigma^{t}\right) + \varepsilon_{\text{elastic}}^{t} \rightarrow \\ &\mathbb{C}^{-1}\left(\tilde{\sigma}^{t+1} - \tilde{\sigma}^{t}\right) = \tilde{\mathbb{C}}^{-1}\left(\sigma^{t+1} - \sigma^{t}\right) \end{aligned} \tag{4.20}$$

Using the concept of effective stress, equation (4.20) is rewritten as

$$\mathbb{C}^{-1}\left(\frac{\sigma^{t+1}}{\left(1-D^{t+1}\right)} - \frac{\sigma^{t}}{\left(1-D^{t}\right)}\right) = \tilde{\mathbb{C}}^{-1}\left(\sigma^{t+1} - \sigma^{t}\right) \tag{4.21}$$

Rearranging (4.21)

$$\Delta\sigma = \tilde{\mathbb{C}}\,\mathbb{C}^{-1}\frac{\left(\Delta\sigma - \sigma^{t+1}D^{t} + \sigma^{t}D^{t+1}\right)}{\left(1-D^{t+1}\right)\left(1-D^{t}\right)} \tag{4.22}$$

In addition, the constitutive equation for a damaged material is

$$\Delta\sigma = \tilde{\mathbb{C}}\,\Delta\varepsilon_{\text{elastic}} \tag{4.23}$$

Hence, combining (4.22) and (4.23), the constitutive equation that considers ageing and damage is written as

$$\sigma^{t+1} = \left(1-D^{t+1}\right)\mathbb{C}\,\Delta\varepsilon_{\text{elastic}} + \frac{\left(1-D^{t+1}\right)}{\left(1-D^{t}\right)}\sigma^{t} \tag{4.24}$$

noting that in the absence of damage, equation (4.24) becomes the incremental constitutive relation (4.2).

4.2.3 Finite Element formulation

Now, the mathematical model developed previously will be used to derive its numerical formulation using the FEM. To this end, consider the governing equations

$$\nabla.\sigma^{t+1} + b^{t+1} = 0 \quad \text{for} \quad \Omega_e \quad \text{Equilibrium (momentum) equation} \tag{4.25}$$

$$\sigma^{t+1} = \left(1 - D^{t+1}\right)\mathbb{C}\,\Delta\varepsilon_{elastic} + \frac{\left(1 - D^{t+1}\right)}{\left(1 - D^{t}\right)}\sigma^{t} \quad \text{Constitutive equation} \tag{4.26}$$

$$\varepsilon_{total}^{t+1} = \Im u^{t+1} \quad \text{Strain} - \text{displacement equation} \tag{4.27}$$

$$u = \bar{u} \quad \text{Dirichlet boundary condition} \tag{4.28}$$

$$\sigma.n = \bar{t} \quad \text{Neumann boundary condition} \tag{4.29}$$

For the thermo-mechanical problem, the total (observable) strain is the sum of elastic and thermal strains

$$\varepsilon_{total}^{t+1} = \varepsilon_{elastic}^{t+1} + \varepsilon_{thermal}^{t+1} \tag{4.30}$$

Using the Galerkin method, the Finite Element formulation of the thermo-mechanical model considering ageing and damage is given by

$$K^{t+1}U^{t+1} = F_{cd}^{t+1} + F_{int}^{t} + F_{term}^{t+1} + F_{tf}^{t+1} + F_{dl}^{t+1} + F_{pd}^{t+1} \tag{4.31}$$

$$K^{t+1} = \left(1 - D^{t+1}\right)\int_{\Omega_e} B^{T}\mathbb{C}^{t+1}B\,d\Omega_e \tag{4.32}$$

$$F_{cd}^{t+1} = -\left(1 - D^{t+1}\right)K^{t+1}\bar{U}^{t+1} \tag{4.33}$$

$$F_{int}^{t} = -\frac{\left(1 - D^{t+1}\right)}{\left(1 - D^{t}\right)}\int_{\Omega_e} B^{T}\sigma^{t}\,d\Omega_e \tag{4.34}$$

$$F_{term}^{t+1} = \left(1 - D^{t+1}\right) \int_{\Omega_e} \alpha B^T \mathbb{C}^{t+1} \left(T^{t+1} - T^t\right) d\Omega_e \tag{4.35}$$

$$F_{tf}^{t+1} = \oint_{\Gamma_n} B^T \bar{t}^{t+1} d\Gamma_n \tag{4.36}$$

$$F_{dl}^{t+1} = \int_{\Omega_e} B^T b^{t+1} d\Omega_e \tag{4.37}$$

$$F_{pd}^{t+1} = \left(1 - D^{t+1}\right) \int_{\Omega_e} B^T \mathbb{C}^{t+1} B \, d\Omega_e U^t = \left(1 - D^{t+1}\right) K^{t+1} U^t \tag{4.38}$$

with (4.33) taking into account the contribution of prescribed displacements on the right-hand side vector. Equation (4.31) can be shortly written ass

$$A\left(U^{t+1}\right) U^{t+1} = b\left(U^{t+1}\right) \tag{4.39}$$

where

$$A\left(U^{t+1}\right) = K^{t+1} \tag{4.40}$$

$$b\left(U^{t+1}\right) = F_{cd}^{t+1} + F_{int}^{t} + F_{term}^{t+1} + F_{tf}^{t+1} + F_{dl}^{t+1} + F_{pd}^{t+1} \tag{4.41}$$

The two major parts of a FEM simulation are the loop on the elements to assembly the system of equations and the solution of the system of equations, where the latter is usually the most time-consuming part. Usually, non-stationary iterative methods are used for solving the system of equations and their efficiency hinge on the condition number of the matrix. The problem is that, as damage develops, the stiffness matrix K^{t+1} of the element approaches zero which in turn increase the ill-conditioning of the system of equations. Hence, iterative methods will take more iterations to converge as damage advances. From a numerical point of view, this aspect is one of the greatest drawbacks of damage models.

4.2.4 Flowchart of the thermo-mechanical model

The flowchart for the thermo-mechanical model with ageing and damage is depicted in Figure 34. Its reasoning is similar to thermo-chemical, presented in section 3.3. Note that both matrix A and right-hand side vector b are nonlinear. Hence, both must be updated during the computations. The residual vector is $P(U^{t+1}) = A(U^{t+1})\, U^{t+1} - b(U^{t+1})$. $\|P\|_N$ denotes the normalized norm of the residual vector. Similar to the hydration degree in the thermo-chemical model, damage always increases in order to be thermodynamically consistent.

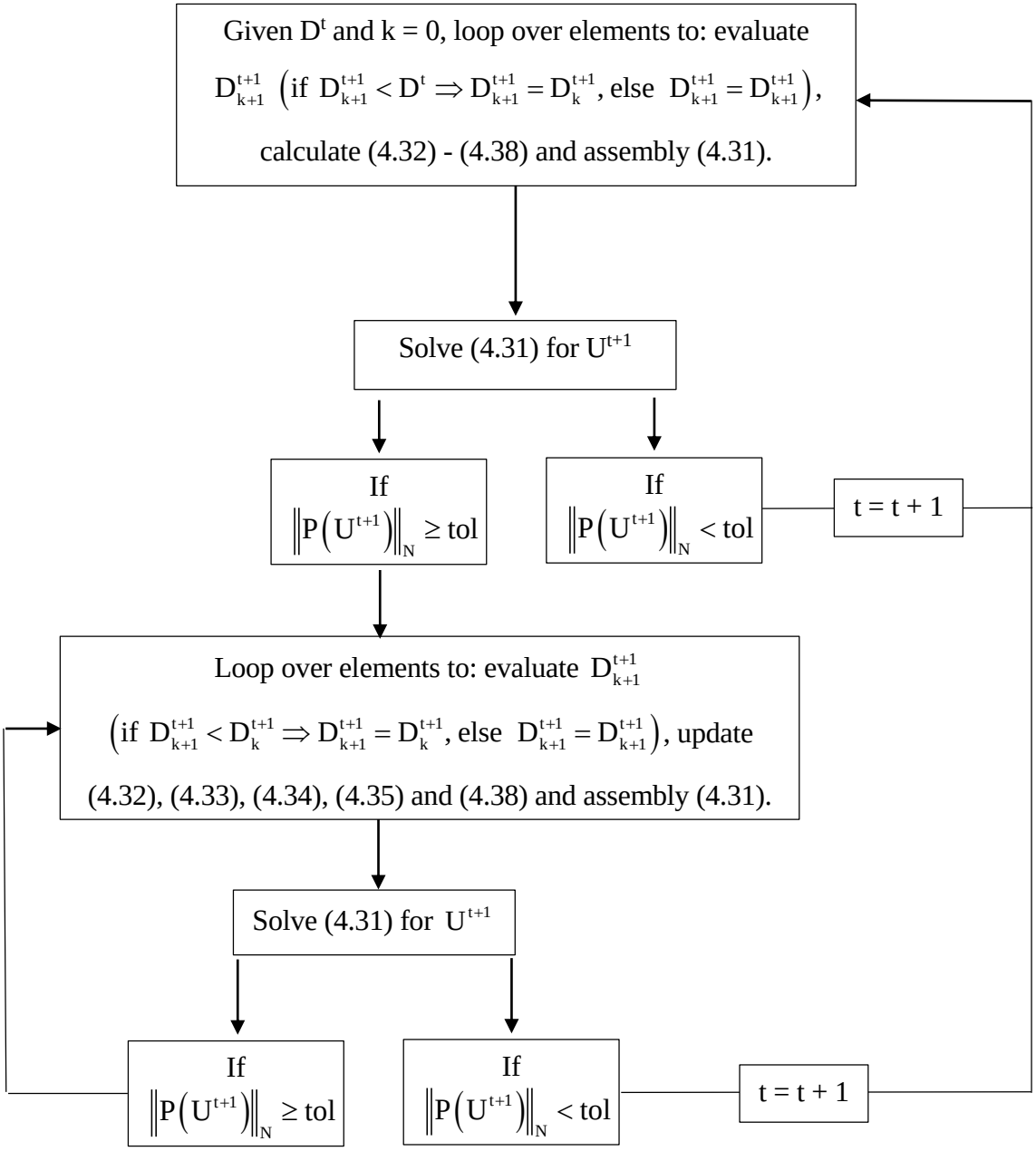

Figure 34. Flowchart for the thermo-mechanical model.

4.3 Lack of objectivity due to strain localization

As mentioned by JIRÁSEK [44], strain-softening models were not immediately accepted by the scientific community because they did not converge to results physically coherent. Upon mesh refinement, these models used to converge to crack propagation with less energy dissipation. This behaviour is related to the transformation of a continuum problem into a discrete one. Hence, this issue is not related to the damage model. In addition, it is not associated with the Finite Element Method but actually with the discretization. From a physical point of view, it can be regarded as a instability problem and BAŽANT and CEDOLIN [45] present a good discussion about it.

To illustrate the problem of lack of objectivity due to strain localization caused by softening, consider the rod of length *L* in Figure 35 and its discretization by *n* elements with length *l* each. It will be assumed that the material has the stress-strain curve also depicted in Figure 35. It is linear-elastic until its tensile strength $f_t = E\varepsilon_{d0}$. Beyond this point, that is, between ε_{d0} and ε_{ult}, the material starts to damage (microcrack), following a linear softening until it reaches its ultimate strain ε_{ult} where the material is completely damaged (an observable macrocrack appears), that is, the material loses its load-carrying capacity.

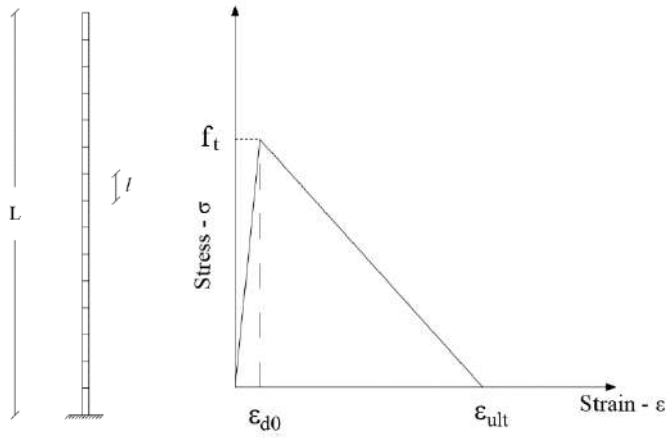

Figure 35. FEM discretization of a rod (left) and stress-strain curve for its material (right).

Consider that the rod is loaded in tension by a prescribed displacement in the upper edge. From the initial state until it attains the tensile strength, all the elements have the same stress-strain behaviour. Strains, stresses and displacements evolutions throughout the rod are in Figure 36, Figure 37 and Figure 38, respectively. Until now, no problem at all.

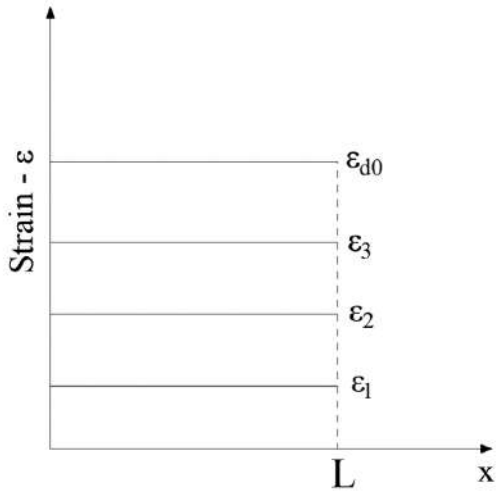

Figure 36. Evolution of strains until the tensile strength.

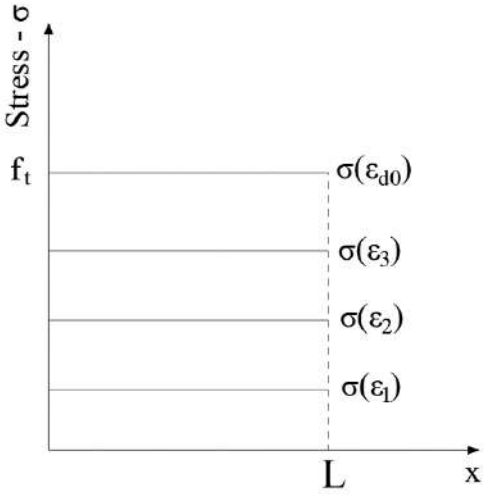

Figure 37. Evolution of stresses until tensile strength.

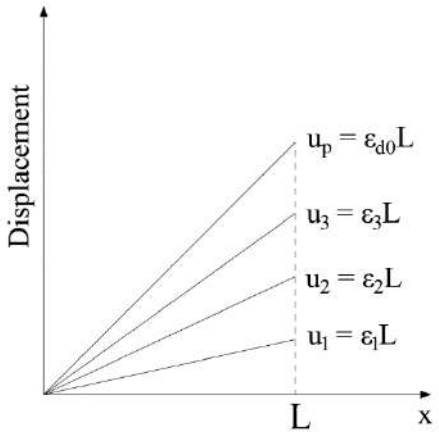

Figure 38. Evolution of displacements until tensile strength.

Real materials contain already in the initial state a multitude of defects (cf. GROSS and SEELIG [46]). In order to consider these defects, assume that the tensile strength of a given element is slightly lower than the rest of the mesh. When the weaker element reaches its tensile strength, it will start to soften, that is, decrease its stress and increase its strain. On the other hand, the other elements will unload elastically which means that their stresses will also decrease but their strains will decrease since their tensile strength were not exceeded. This means that, beyond ε_{d0}, strains will localize in the weaker element and any additional deformation of the rod is related to the deformation of the weaker element. This phenomenon is called *strain localization* and is demonstrated graphically in Figure 39.

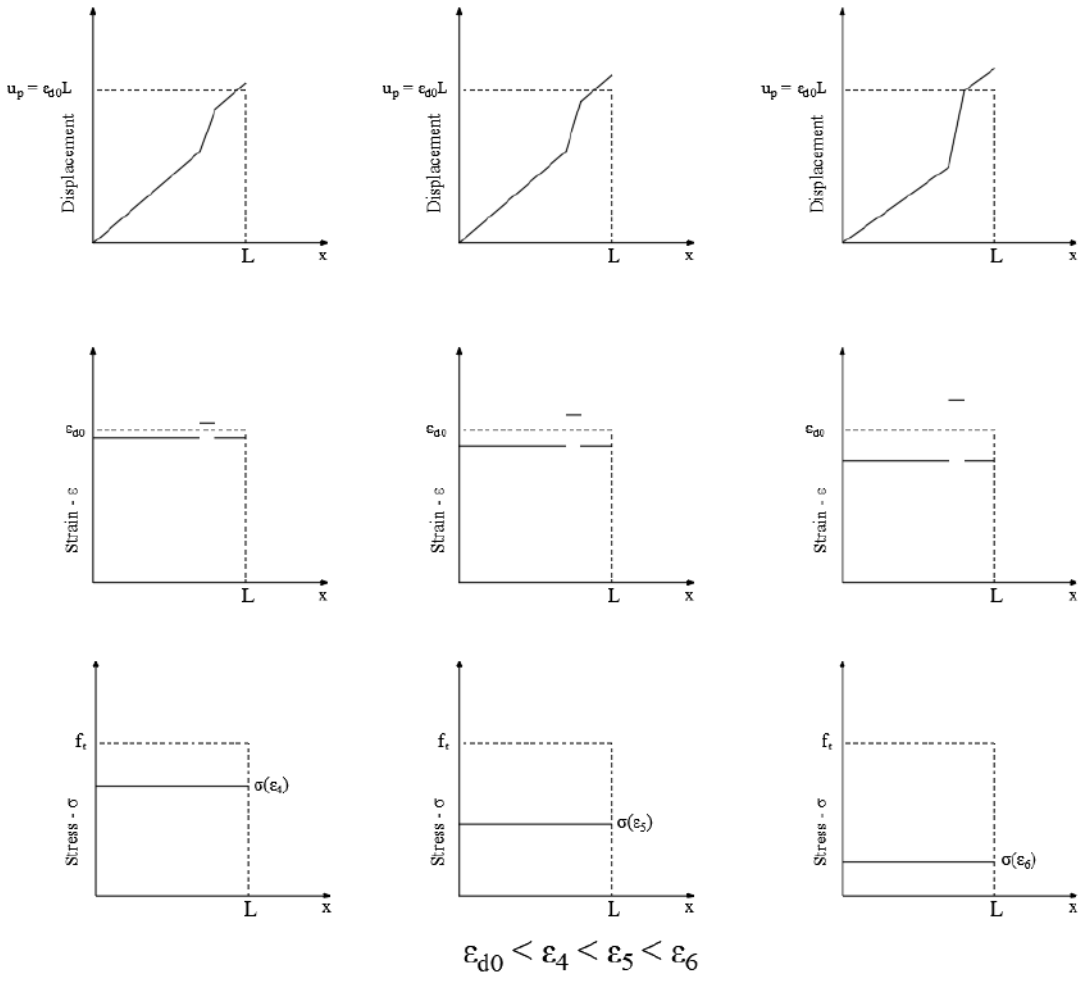

Figure 39. Evolution of displacements, strains and stresses throughout the rod during softening.

Remember that the stress-strain response is given by the stress σ measured in the support versus the strain ΔL of the rod. Once localization occurs, strains will be limited to the weaker element which from the onset of damage (microcrack) until the completely failure of the element (macrocrack) will stretch by $\varepsilon_{d0} - \varepsilon_{ult} = \Delta l/l$. Therefore, the weaker element will dictate the post-peak behaviour of the structure because a decrease in l will reduce the weaker element strain Δl which in turn will diminish ΔL.

To illustrate it, consider again that the rod from Figure 35 but now its discretization by an increasing number n of elements with the hatched element weaker than the others (Figure 40). As $n \rightarrow \infty$, then $\Delta l \rightarrow 0$. Therefore, $\Delta L \rightarrow 0$ which in turn leads to $\Delta L/L \rightarrow 0$. That's why, as n approaches infinity, the post-peak strain of the bar is almost zero, i.e., it converges to a perfectly brittle rupture which is completely incorrect. This behaviour is usually referred to as *Lack of objectivity* or *Non-objectivity* and is in Figure 41.

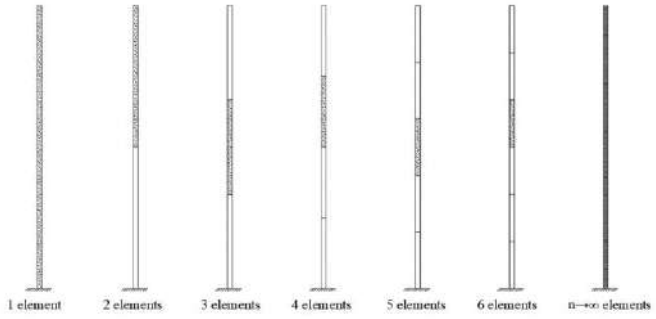

Figure 40. Increasing discretization of the rod with one of the elements weaker than the others.

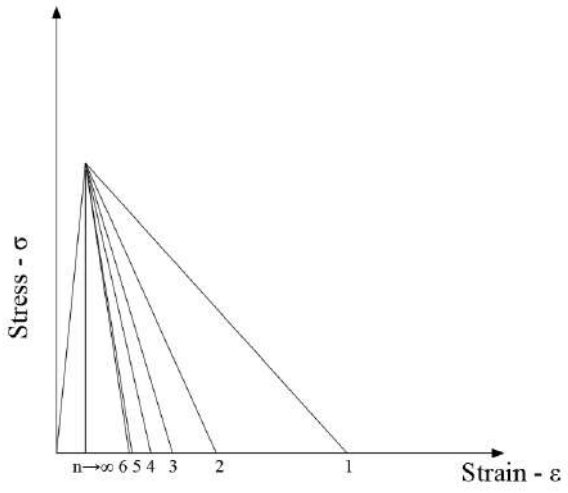

Figure 41. Non-objective stress-strain curve for increasing number of elements.

The discussion presented in this section leads one to conclude that the Lack of objectivity is not related to the Finite Element Method. In addition, it is not associated with damage since others nonlinear models such as plasticity also manifest it. In fact, this pathological behaviour has to do with the discretization of softening problems. Thus, nonlinear models with *hardening* will not undergo Lack of objectivity because they will not develop strain localization. Actually, even the linear-elastic branch of the stress-strain curve can be regarded as a hardening, that is, increasing strains accompanied by growing stresses.

Now, the Finite Element formulation developed in section 4.2 will be used to demonstrate the Lack of objectivity by simulating a tensile test through a Plane Stress analysis. To this end, the concrete specimen of Figure 29 will be considered again with three different meshes, as presented in Figure 42. Neither ageing nor temperature variations will be considered in this example.

Height	Width	Thickness	Young modulus	Tensile strength	
0.3 m	0.1 m	0.1 m	30 GPa	1.5 MPa (non-hatched elements)	1.47 MPa (hatched elements)

Table 11. Properties of the concrete specimen.

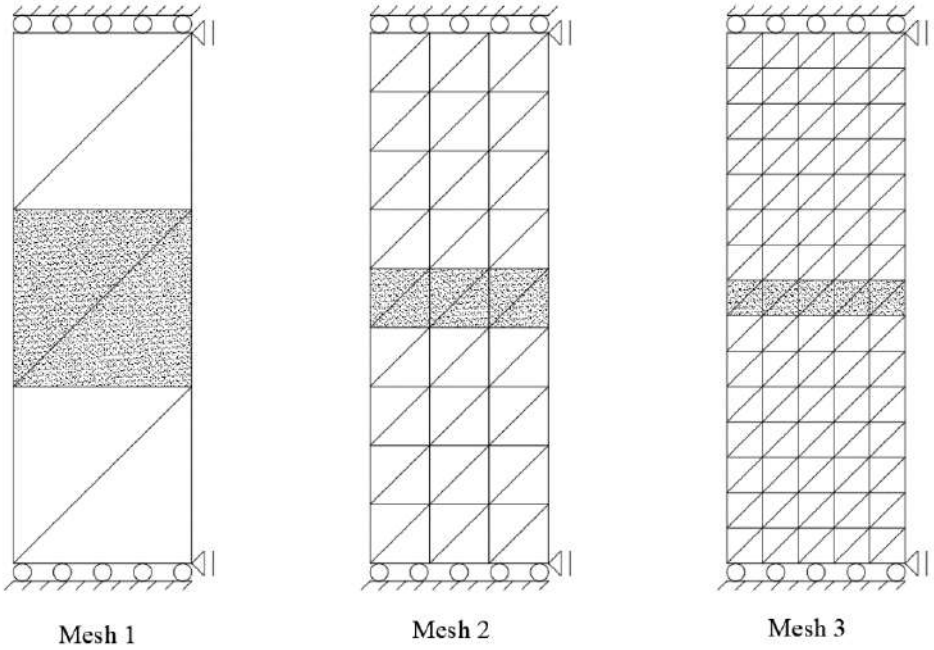

Figure 42. Discretization of the concrete specimen: Mesh 1 (left), Mesh 2 (center) and Mesh 3 (right).

For the sake of simplicity, the following linear damage law will be employed with $\varepsilon_{d0} = 5_x10^{-5}$ as the strain related to the tensile strength and $\varepsilon_{fi} = 5_x10^{-4}$ the strain for which the material is completely damaged.

$$D(\varepsilon_{eq}) = \begin{cases} 0 \quad \forall \quad \varepsilon_{eq} \le \varepsilon_{d0} \\ 1 - \dfrac{\varepsilon_{d0}}{\varepsilon_{eq}} \left[1 - \dfrac{\left(\varepsilon_{eq} - \varepsilon_{d0}\right)}{\left(\varepsilon_{fi} - \varepsilon_{d0}\right)} \right] \quad \forall \quad \varepsilon_{d0} < \varepsilon_{eq} < \varepsilon_{fi} \\ 1 \quad \forall \quad \varepsilon_{eq} \ge \varepsilon_{fi} \end{cases} \tag{4.42}$$

The damage law (4.42) is a function of a variable called *equivalent strain*, ε_{eq}, which is commonly used to describe damage. Several definitions for it have been presented in the literature but throughout this study the Mazars' definition (4.43) will be employed. Henceforth, the summation convention will be adopted.

$$\varepsilon_{eq} = \sqrt{\left\langle {}^{p}\varepsilon_{ii} \right\rangle \left\langle {}^{p}\varepsilon_{ii} \right\rangle} \tag{4.43}$$

with $\langle \ \rangle$ denoting the Macaulay brackets and the upper-left superscript p denoting the principal tensor. Equation (4.43) is useful for materials like concrete since it considers that damage occur majorly due to tensile strains, that is, when the material is stretched.

Although a bidimensional mesh was chosen, the analysis boils down to a case of a one-dimensional rod. In this case, $\varepsilon_{eq} = \varepsilon$ and the stress-strain equation can be written as

$$\sigma(\varepsilon) = \begin{cases} E\varepsilon \quad \forall \quad \varepsilon \le \varepsilon_{d0} \\ \left(1 - D(\varepsilon_{eq})\right) E\varepsilon \quad \forall \quad \varepsilon > \varepsilon_{d0} \end{cases} \tag{4.44}$$

The damage evolution using (4.42) as function of the equivalent strain is presented in Figure 43. The results of the FEM simulation for the stress (measured on the support) versus the strain of the bar is depicted in Figure 44. These results suffer from the lack of objectivity since it converges to a brittle rupture as the mesh is refined.

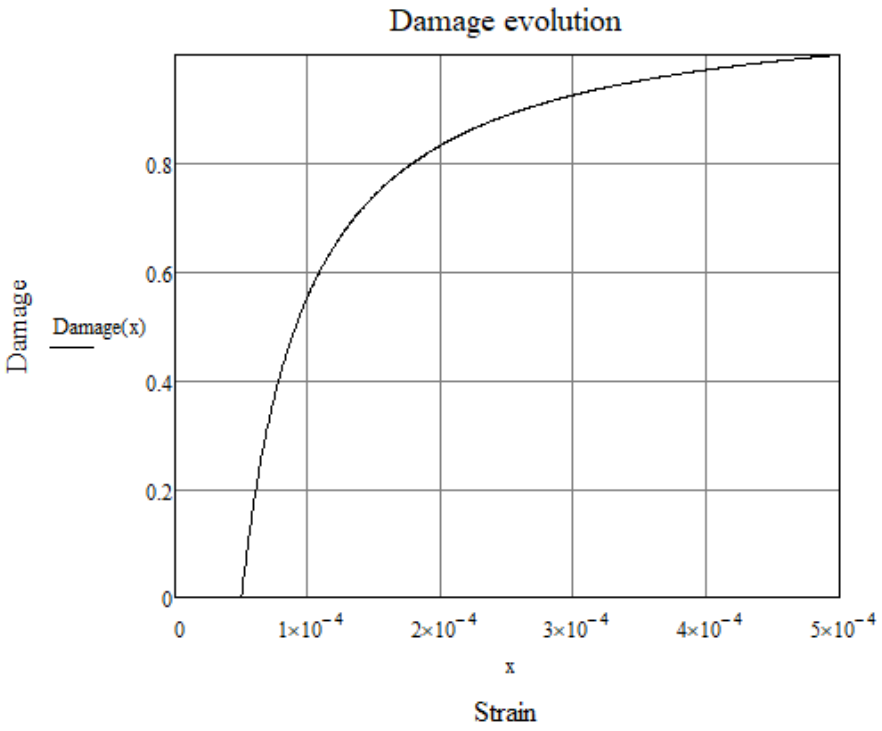

Figure 43. Damage evolution using equation (4.44).

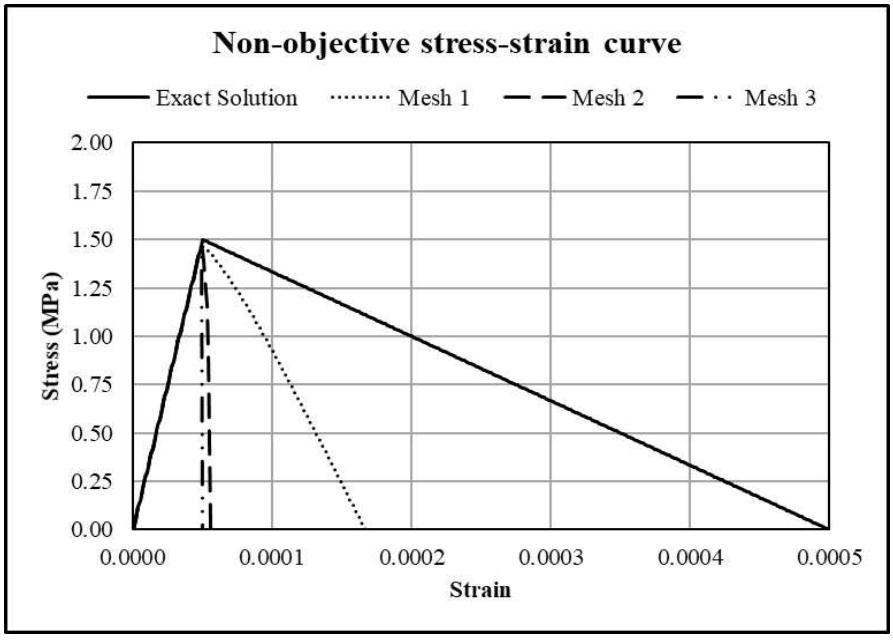

Figure 44. Non-objective stress-strain curve for the three meshes considered.

Figure 45 - Figure 53 present the development of displacements, strains and stresses throughout the bar for Mesh 1. These figures demonstrate the phenomenon of strain localization.

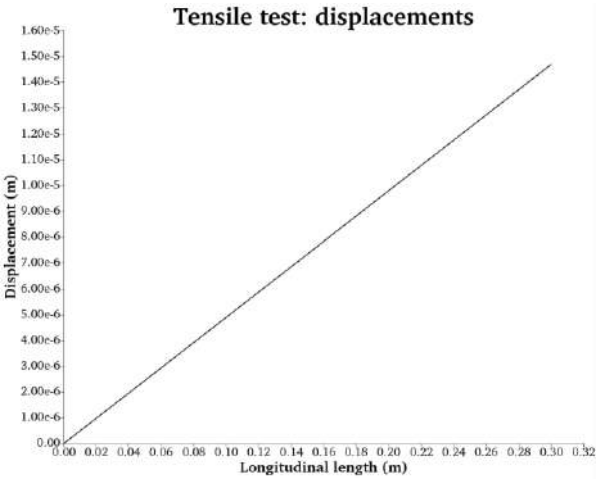

Figure 45. Displacement-length curve for Mesh 1 immediately before the weaker (hatched) elements reach their tensile strength.

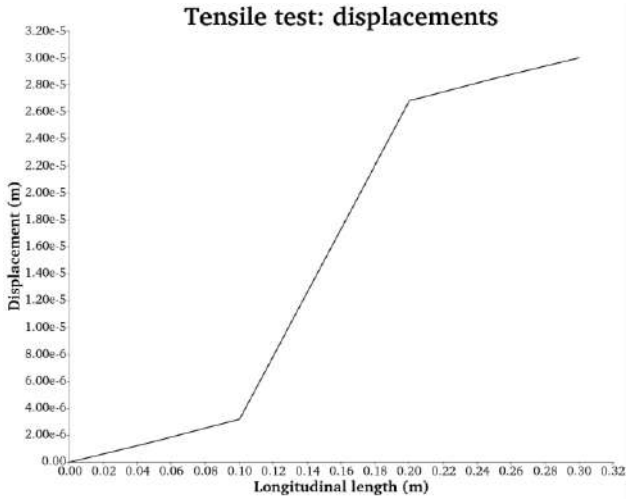

Figure 46. Displacement-length curve for Mesh 1 during the damage process.

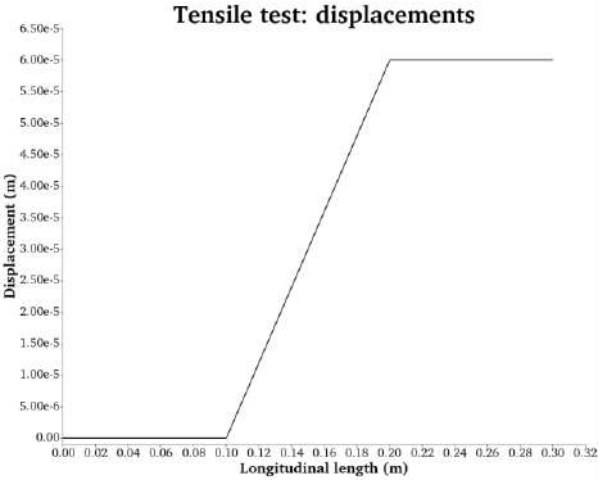

Figure 47. Displacement-length curve for Mesh 1 when damage is complete.

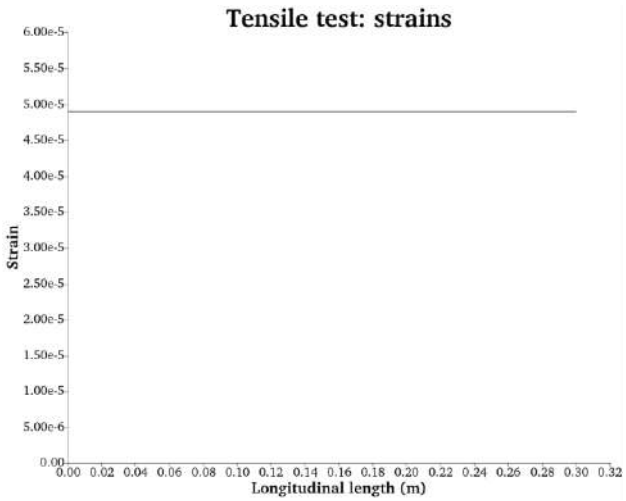

Figure 48. Strain-length curve for Mesh 1 immediately before the weaker (hatched) elements reach their tensile strength.

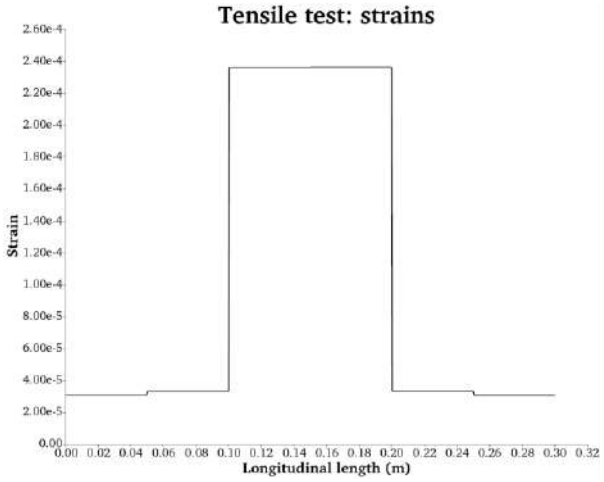

Figure 49. Strain-length curve for Mesh 1 during the damage process.

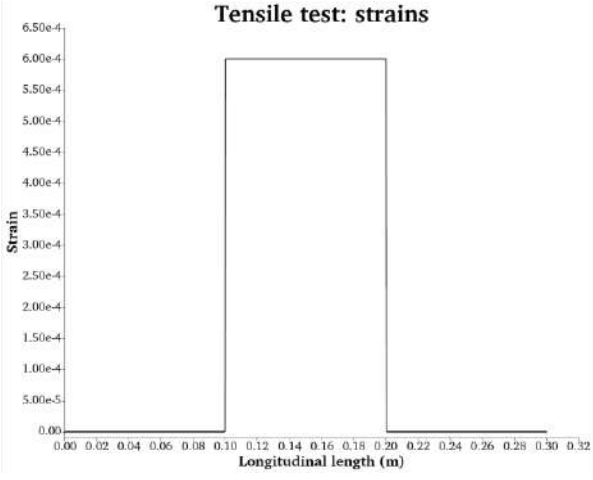

Figure 50. Strain-length curve for Mesh 1 when damage is complete.

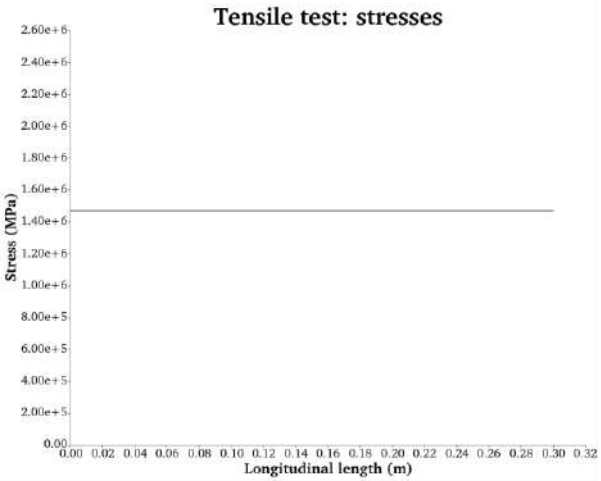

Figure 51. Stress-length curve for Mesh 1 immediately before the weaker (hatched) elements reach their tensile strength.

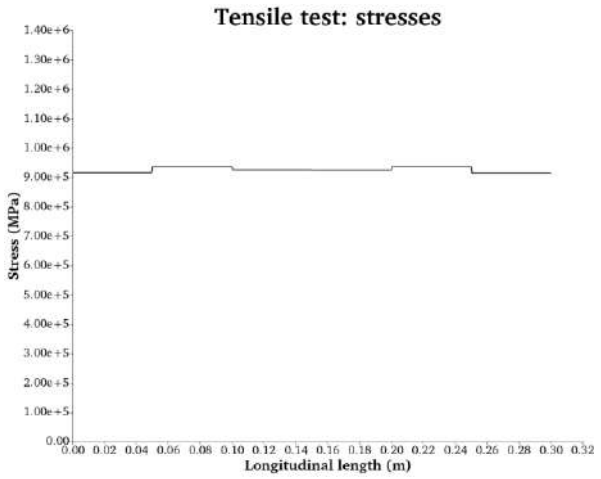

Figure 52. Stress-length curve for Mesh 1 during the damage process.

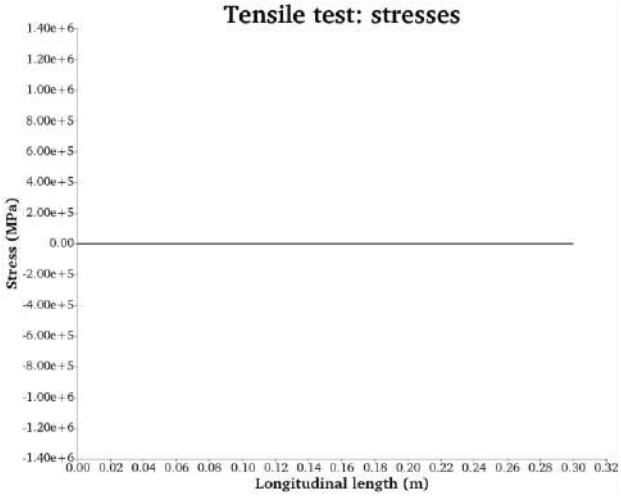

Figure 53. Stress-length curve for Mesh 1 when damage is complete.

Considering Mesh 1 yet, Figure 54 presents the stress-strain curve for the hatched elements, i.e., those that undergo damage. Figure 55 shows the damage evolution for these elements and the graph is similar to Figure 43. In addition, Figure 56 present the stress-strain curve for the elements that don't undergo damage. Some interesting remarks must be made regarding these figures. First, Figure 54 shows that, at element level, the stress-strain response of the structure is still objective. Remember that the lack of objectivity discussed previously occur only when evaluating the global response of the structure but at the element level it remains objective. Second, Figure 56 demonstrates that elements that do not undergo damage return to their initial configuration. This last remark is also depicted in Figure 57.

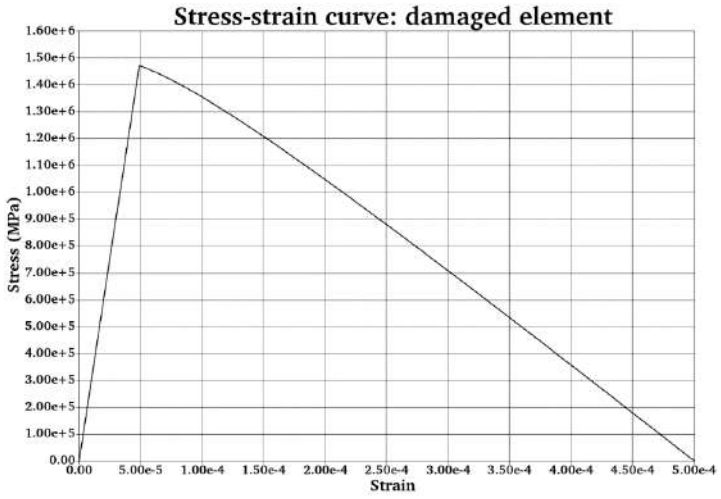

Figure 54. Stress-strain curve for hatched elements (Mesh 1).

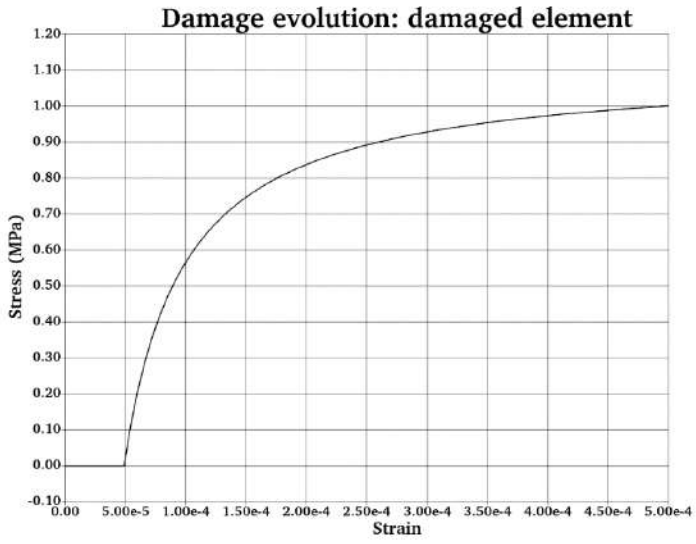

Figure 55. Damage evolution for hatched elements (Mesh 1).

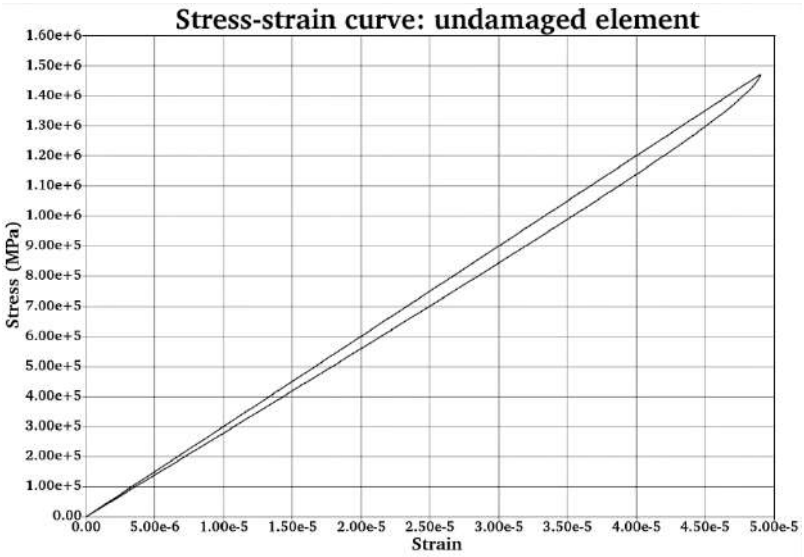

Figure 56. Stress-strain curve for an element without damage.

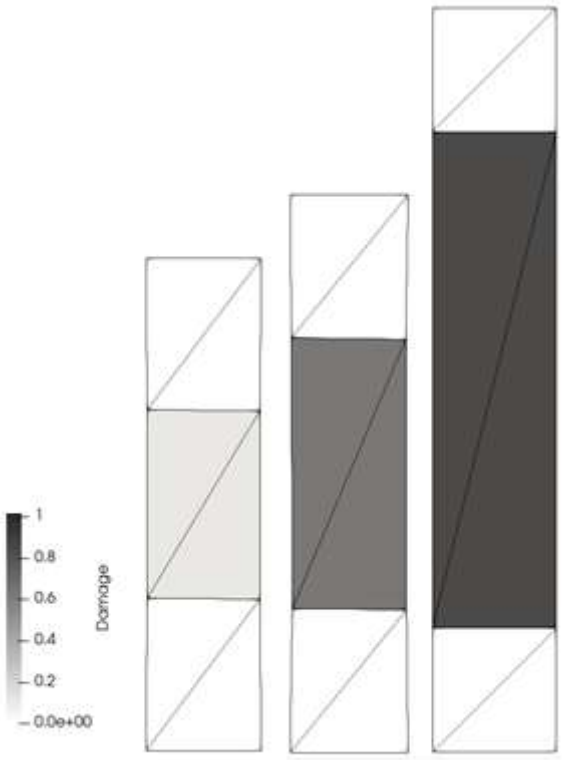

Figure 57. Deformed shape of the rod for three different strain states: on the onset of damage (left), during damage (center) and when damage is complete (right).

4.3.1 Nonlocal regularization technique

In the last decades, some remedies have been proposed to circumvent the lack of objectivity, namely: integral-type Nonlocal, gradient-enhanced, Cosserat-type continua, Fracture Energy, etc. Nonlocal models were originally proposed by PIJAUDIER-CABOT and BAŽANT [47] and are quite appealing since they are easy to implement on an existing Finite Element code without much effort. Hence, that's why the present study chose this technique. A didactic presentation of Nonlocal technique is presented by JIRÁSEK [48].

The main idea of Nonlocal models is to replace the local equivalent strain by its nonlocal counterpart. This aspect is what makes it attractive since the logical scheme to calculate damage remains the almost the same. Therefore, the only difference is that equivalent strain will be evaluated considering the influence of near elements. With this in mind, the nonlocal equivalent strain is determined by equations (4.45), (4.46) and (4.47) if one adopts the Gauss distribution function (Figure 58) or (4.45), (4.46) and (4.48) if one employs the Truncated quartic polynomial (Figure 59), respectively.

$$\bar{\varepsilon}_{eq} = NL\varepsilon_{eq} \tag{4.45}$$

$$NL_{ij} = \frac{w_j \left|J_j\right| \alpha_0(x_i, x_j)}{\sum_{k=1}^{k=NGP} \left[w_k \left|J_k\right| \alpha_0(x_i, x_k) \right]} \tag{4.46}$$

$$\alpha_0(x_i, x_j) = e^{-\left(\frac{\left(\left\| x_i - x_j \right\| \right)^2}{2d^2} \right)} \tag{4.47}$$

$$\alpha_0(x_i, x_j) = \left(1 - \frac{\left(\left\| x_i - x_j \right\| \right)^2}{d^2} \right)^2 \tag{4.48}$$

with ε_{eq} and $\bar{\varepsilon}_{eq}$ denoting, respectively, the vectors of local equivalent strain and its nonlocal counterpart for each Gauss Point in the mesh. *NPG* denotes the number of Gauss points that interact with Gauss Point i, w_j the integration weight for point j, $|J_j|$ the determinant of the Jacobian matrix at this point, d is an input parameter and stands for the maximum

distance for which two Gauss points interact with each other and $||x_i - x_j||$ the distance between Gauss points *i* and *j* measured in some norm (usually Euclidian).

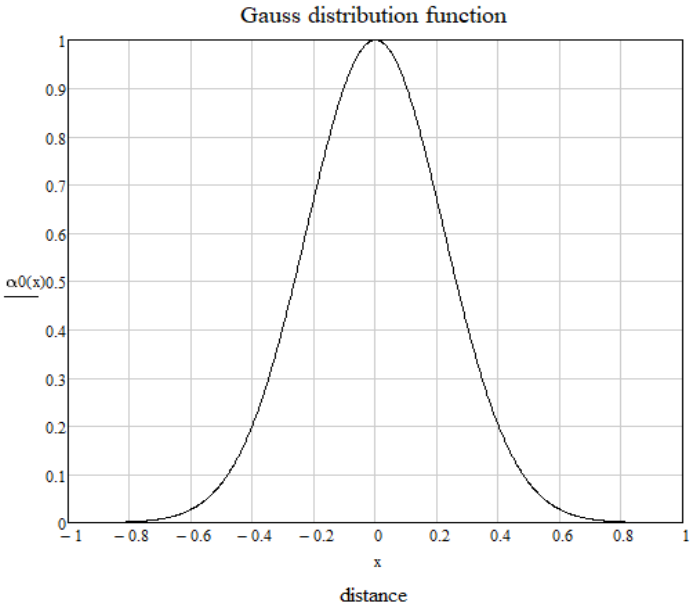

Figure 58. Gauss distribution function.

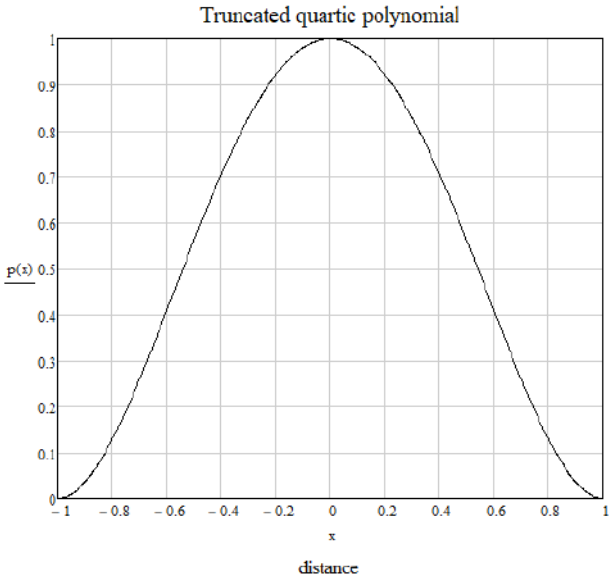

Figure 59. Truncated quartic polynomial.

Higher interaction radius will lead to more accurate results. On the other hand, computations will increase its complexity in terms of memory. However, these calculations are

done a single time only and can be made as soon as connectivity and coordinates are obtained. These computations will generate the array NL in equation (4.45) that can be stored and reused during the evaluation of damage.

Something important to keep in mind is that the calculation of strains, stresses, displacements, etc. will remain the same. The only difference is that after evaluating the equivalent strain (given by equation 4.43, for example) its nonlocal counterpart will be determined using the previous equations.

Now, the same example presented in Figure 42 will be explored again but this time using the Nonlocal technique with Gauss distribution function and interaction radius of 0.50m. The results for meshes 1, 2 and 3 are exhibited in Figure 60, Figure 61 and Figure 62, respectively. The agreement between exact (analytical) and numerical solutions is qualitatively acceptable. Therefore, results became mesh-independent only by changing the way equivalent strains are evaluated.

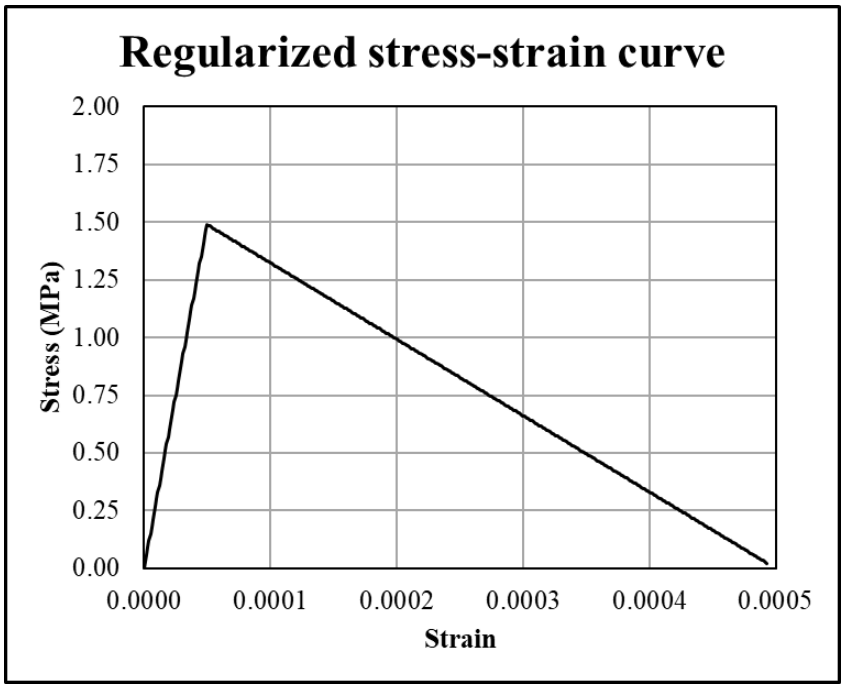

Figure 60. Regularized stress-strain curve for Mesh 1.

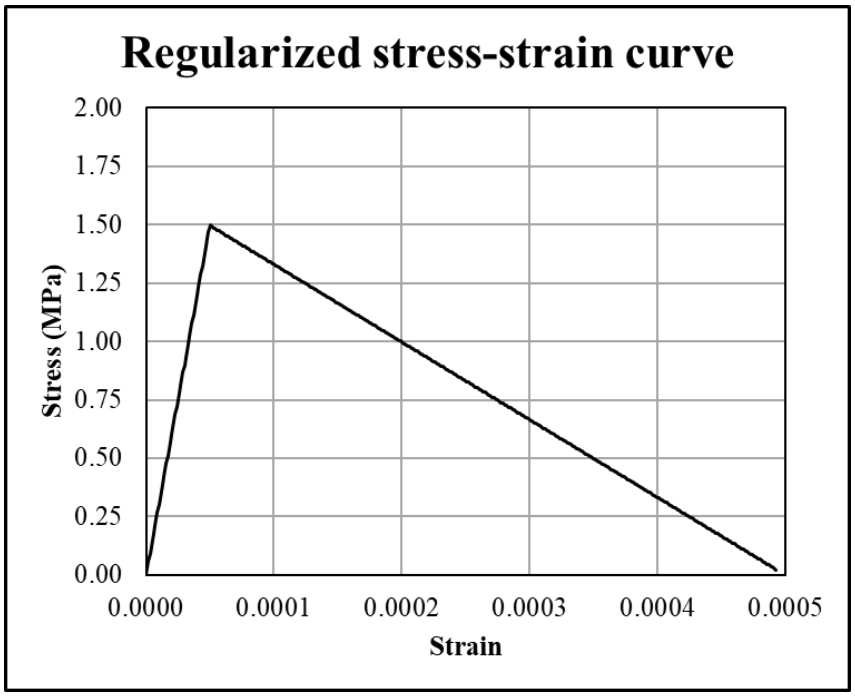

Figure 61. Regularized stress-strain curve for Mesh 2.

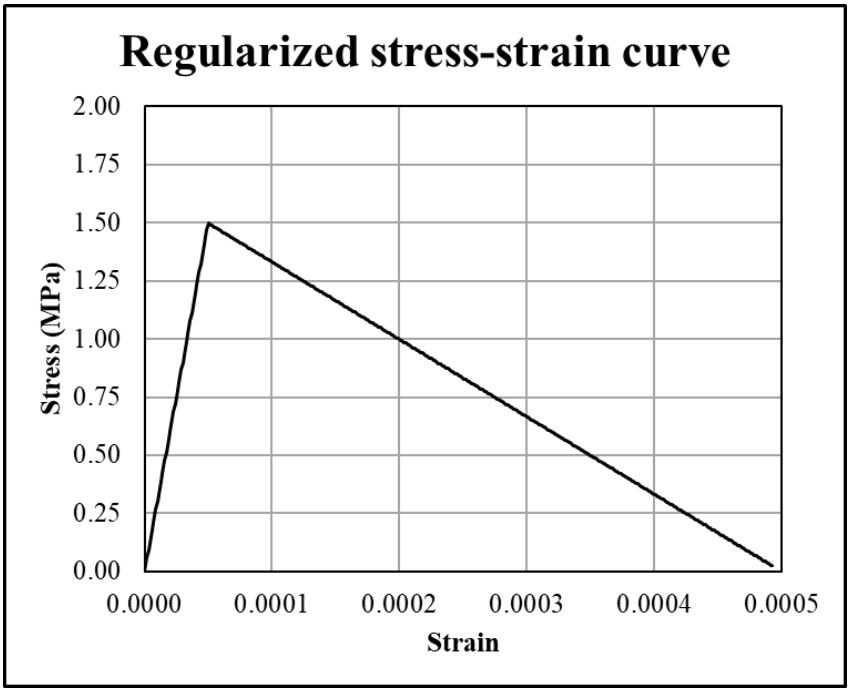

Figure 62. Regularized stress-strain curve for Mesh 3.

4.4 Mazars damage model

In the last section, a simple damage law was presented. Its usage was only for didactic purposes. When material is subjected to any external influence it is interesting to consider a model that encompasses it. The Mazars damage model is a good starting point for concrete and it was originally proposed by MAZARS [49]. The main features of this model are:

- It is elastic. Hence, permanent deformations are completely disregarded;
- Damage is isotropic which is good for quasi-static or cyclic loadings but might be an oversimplification for other types of loadings;
- Damage only take place when material is stretched as remarked by (4.43).

Recall the relation between the effective (damaged) stress tensor $\tilde{\sigma}$ and the nominal (undamaged) stress tensor σ

$$\tilde{\sigma} = \left(1 - D\left(\varepsilon_{eq}\right)\right)\sigma \tag{4.49}$$

The Mazars model determines damage through the following procedure (remembering that the superscript p on the left-hand side denotes the tensor of principal stresses or strains)

$${}^{p}\tilde{\sigma} = {}^{p}_{+}\tilde{\sigma} + {}^{p}_{-}\tilde{\sigma} \tag{4.50}$$

$${}^{p}_{+}\tilde{\sigma}_{ij} = \frac{1}{2}\left({}^{p}_{+}\tilde{\sigma}_{ij} + \left|{}^{p}_{+}\tilde{\sigma}_{ij}\right|\right) \tag{4.51}$$

$${}^{p}_{-}\tilde{\sigma}_{ij} = \frac{1}{2}\left({}^{p}_{-}\tilde{\sigma}_{ij} - \left|{}^{p}_{-}\tilde{\sigma}_{ij}\right|\right) \tag{4.52}$$

$${}^{p}\varepsilon = {}^{p}_{T}\varepsilon + {}^{p}_{C}\varepsilon \tag{4.53}$$

$${}^{p}_{T}\varepsilon_{ij} = \frac{1+\nu}{E}\,{}^{p}_{+}\tilde{\sigma}_{ij} - \frac{\nu}{E}\,{}^{p}_{+}\tilde{\sigma}_{kk} \tag{4.54}$$

$${}^{p}_{C}\varepsilon_{ij} = \frac{1+\nu}{E}\,{}^{p}_{-}\tilde{\sigma}_{ij} - \frac{\nu}{E}\,{}^{p}_{-}\tilde{\sigma}_{kk} \tag{4.55}$$

$$ {}^{p}_{T}\varepsilon = {}_{T+}{}^{p}\varepsilon + {}_{T-}{}^{p}\varepsilon \tag{4.56} $$

$$ {}_{T+}{}^{p}\varepsilon_{ij} = \frac{1}{2}\left({}_{T+}{}^{p}\varepsilon_{ij} + \left| {}_{T+}{}^{p}\varepsilon_{ij} \right| \right) \tag{4.57} $$

$$ {}_{T-}{}^{p}\varepsilon_{ij} = \frac{1}{2}\left({}_{T-}{}^{p}\varepsilon_{ij} - \left| {}_{T-}{}^{p}\varepsilon_{ij} \right| \right) \tag{4.58} $$

$$ {}^{p}_{C}\varepsilon = {}_{C+}{}^{p}\varepsilon + {}_{C-}{}^{p}\varepsilon \tag{4.59} $$

$$ {}_{C+}{}^{p}\varepsilon_{ij} = \frac{1}{2}\left({}_{C+}{}^{p}\varepsilon_{ij} + \left| {}_{C+}{}^{p}\varepsilon_{ij} \right| \right) \tag{4.60} $$

$$ {}_{C-}{}^{p}\varepsilon_{ij} = \frac{1}{2}\left({}_{C-}{}^{p}\varepsilon_{ij} - \left| {}_{C-}{}^{p}\varepsilon_{ij} \right| \right) \tag{4.61} $$

$$ \varepsilon_{V}^{+} = {}_{T+}{}^{p}\varepsilon_{ii}\ {}_{C+}{}^{p}\varepsilon_{ii} \tag{4.62} $$

$$ \alpha_{T} = \frac{{}_{T+}{}^{p}\varepsilon_{ii}}{\varepsilon_{V}^{+}} \tag{4.63} $$

$$ \alpha_{C} = \frac{{}_{C+}{}^{p}\varepsilon_{ii}}{\varepsilon_{V}^{+}} \tag{4.64} $$

$$ D_{T} = 1 - \frac{\varepsilon_{d0}\left(1 - A_{T}\right)}{\varepsilon_{eq}} - \frac{A_{T}}{e^{\left[B_{T}\left(\varepsilon_{eq} - \varepsilon_{d0}\right)\right]}} \tag{4.65} $$

$$ D_{C} = 1 - \frac{\varepsilon_{d0}\left(1 - A_{C}\right)}{\varepsilon_{eq}} - \frac{A_{C}}{e^{\left[B_{C}\left(\varepsilon_{eq} - \varepsilon_{d0}\right)\right]}} \tag{4.66} $$

Finally, damage is calculated as

$$ D(\varepsilon_{eq}) = \alpha_{T} D_{T} + \alpha_{C} D_{C} \tag{4.67} $$

The parameters A_T, B_T, A_C and B_C are determined from experiments. SANTOS [50] states that the values suggested by MAZARS [49] are

$$ 0.7 \le A_{T} \le 1.0 \quad 10^{4} \le B_{T} \le 10^{5} \quad 1.0 \le A_{C} \le 1.5 \quad 10^{3} \le B_{C} \le 2 \times 10^{3} \tag{4.68} $$

Each one of them has a specific influence on the nonlinear branch of the stress-strain curve. For an uniaxial tensile test, $\varepsilon_{eq} = \varepsilon$ and the stress-strain equation will be

$$\sigma(\varepsilon) = \begin{cases} E\varepsilon \quad \forall \quad \varepsilon \le \varepsilon_{d0} \\ \left(1 - D(\varepsilon)\right) E\varepsilon = \left(\dfrac{\varepsilon_{d0}\left(1 - A_T\right)}{\varepsilon} + \dfrac{A_T}{e^{\left[B_T\left(\varepsilon - \varepsilon_{d0}\right)\right]}} \right) E\varepsilon \quad \forall \quad \varepsilon > \varepsilon_{d0} \end{cases} \tag{4.69}$$

Considering f_t = 3 MPa and E = 30 GPa, then $\varepsilon_{d0} = 10^{-4}$. The effects of A_T and B_T on the stress-strain equation (4.69) are, respectively, in Figure 63 and Figure 64.

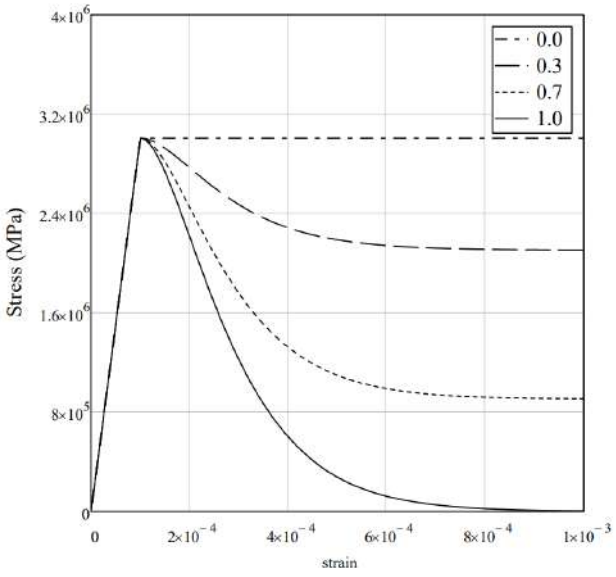

Figure 63. Influence of the parameter A_T of the Mazars model on the stress-strain curve.

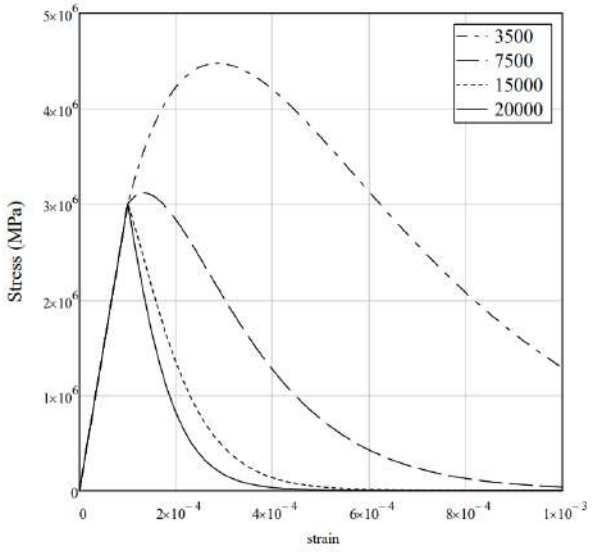

Figure 64. Influence of the parameter B_T of the Mazars model on the stress-strain curve.

For an uniaxial compression test, $\varepsilon_{eq} = \nu\varepsilon$ and the stress-strain equation will be

$$\sigma(\varepsilon) = \begin{cases} E\varepsilon \quad \forall \quad \varepsilon \le \varepsilon_{d0} \\ \left(1 - D(\varepsilon_{eq})\right) E\varepsilon = \left(\dfrac{\varepsilon_{d0}\left(1 - A_C\right)}{\nu\varepsilon} + \dfrac{A_C}{e^{\left[B_C(\nu\varepsilon - \varepsilon_{d0})\right]}} \right) E\varepsilon \quad \forall \quad \varepsilon > \varepsilon_{d0} \end{cases} \tag{4.70}$$

Considering f_t = 3 MPa and E = 30 GPa, then $\varepsilon_{d0} = 10^{-4}$. The effects of A_C and B_C on the stress-strain equation (4.70) are, respectively, in Figure 65 and Figure 66.

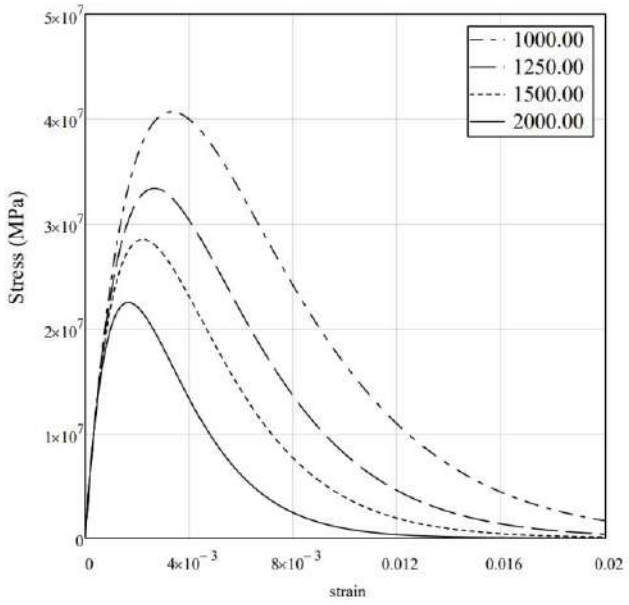

Figure 65. Influence of the parameter A_C of the Mazars model on the stress-strain curve.

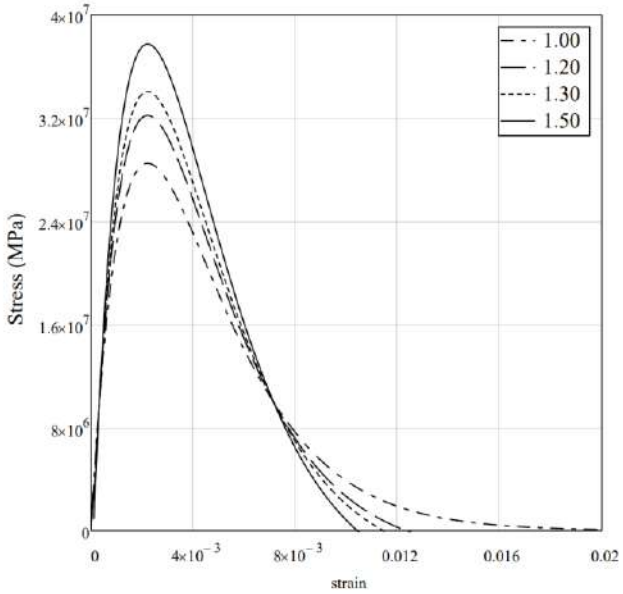

Figure 66. Influence of the parameter B_C of the Mazars model on the stress-strain curve.

4.4.1 Numerical application: Mazars beam

Now, the Mazars damage model will be used for a numerical application. It's consists in a three-point bending test (Figure 67). It has a reinforcement composed by two rebars. Its properties are presented in Table 12. The beam is loaded by an applied force in the middle of the upper surface. The Nonlocal technique presented in section 4.3.1 was adopted in order to avoid lack of objectivity due to strain localization.

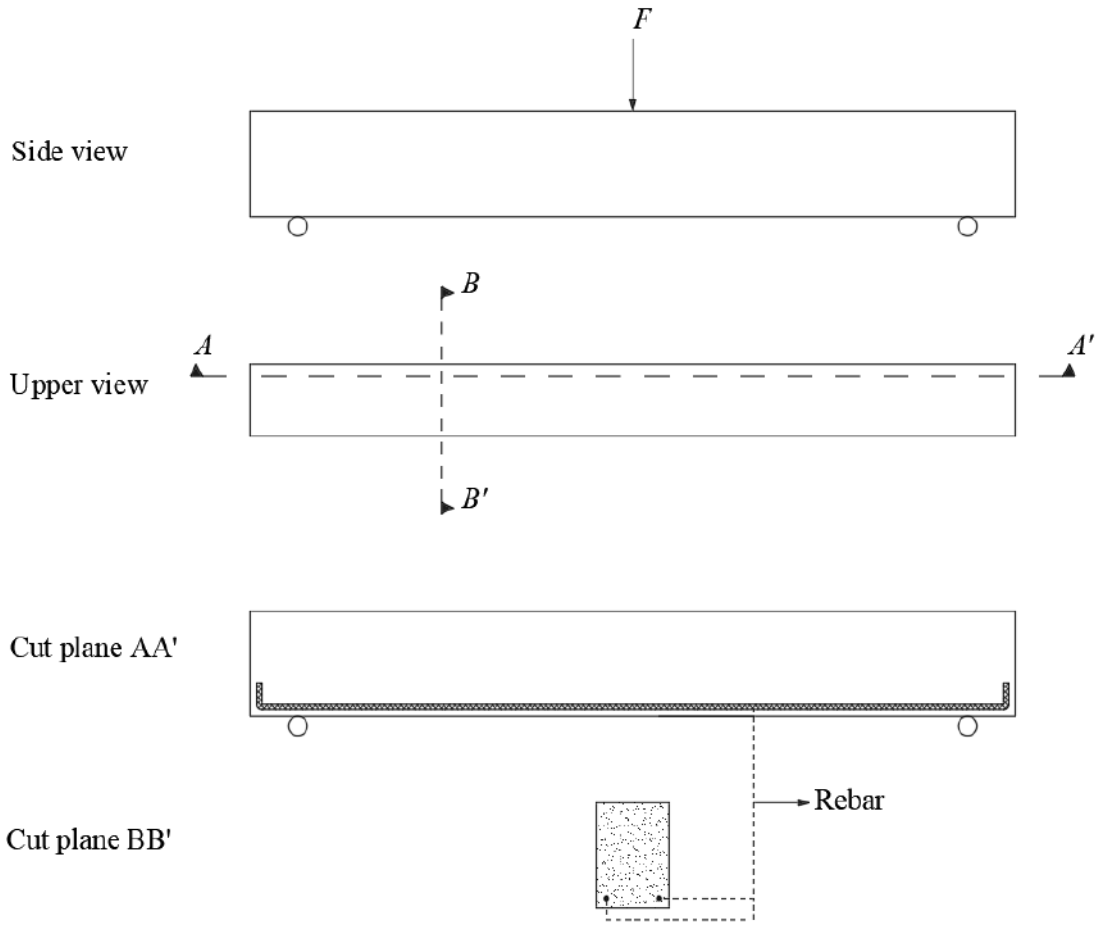

Figure 67. Sketch of the Mazars beam.

Length	Span	Height	Width	Rebar area	Cover	$E_{concrete}$
1.6 m	1.4 m	0.22 m	0.15 m	226.19 mm²	1.5 cm	30 GPa
E_{steel}	A_T	B_T	A_C	B_C	f_t	ν
196 GPa	0.8	20000	1.4	1850	3.45 MPa	0.20

Table 12. Properties of the Mazars beam.

The deformed beam as well as its crack pattern are exposed in Figure 68, Figure 69, Figure 70 and Figure 71. As expected, cracks start in the middle of the bottom edge because this part reaches the tensile strength first since it presents the maximum bending moment. Besides, one can observe that, as cracks distance from the middle, they start skewing. This behaviour is also expected and it is attributed to the influence of shear stresses.

In the middle of the upper edge and in the left and the right of the bottom edge are little intermediate supports. They were used only for numerical purposes so that they do not damage due to the presence of stress concentration. However, its Young's modulus is 10% of concrete's modulus, that is, 3GPa so that it does not affect significantly the results.

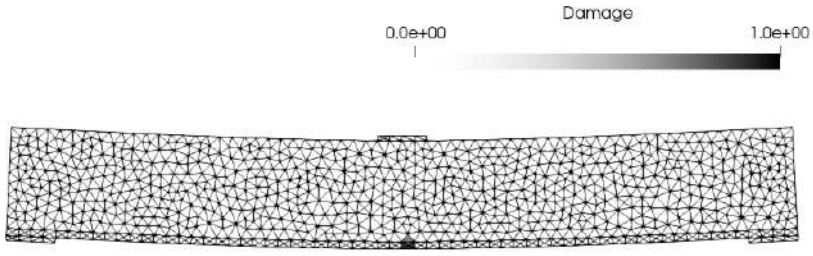

Figure 68. Deformed shape of Mazars beam for F = 15kN.

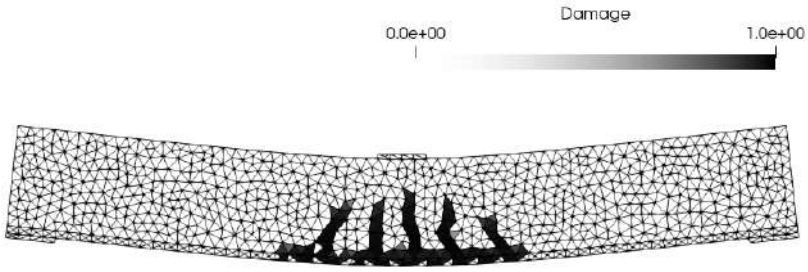

Figure 69. Deformed shape of Mazars beam for F = 20kN.

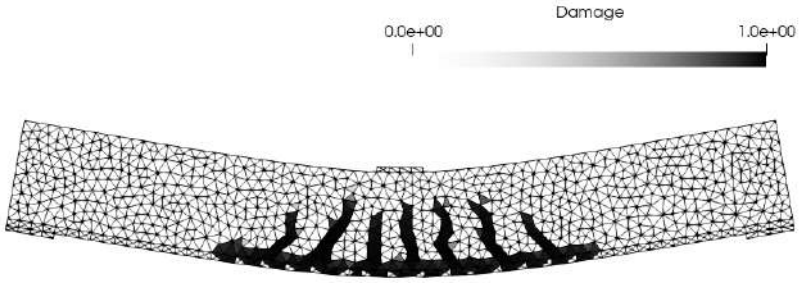

Figure 70. Deformed shape of Mazars beam for F = 25kN.

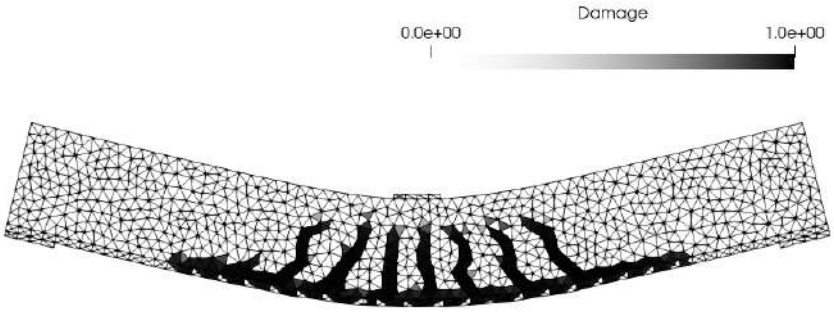

Figure 71. Deformed shape of Mazars beam for F = 30kN.

This problem was analyzed originally by MAZARS [49] and later by SANTOS [50]. The results showed by these authors are compared with those obtained in the present study (Figure 72). The comparison between them demonstrate a good agreement.

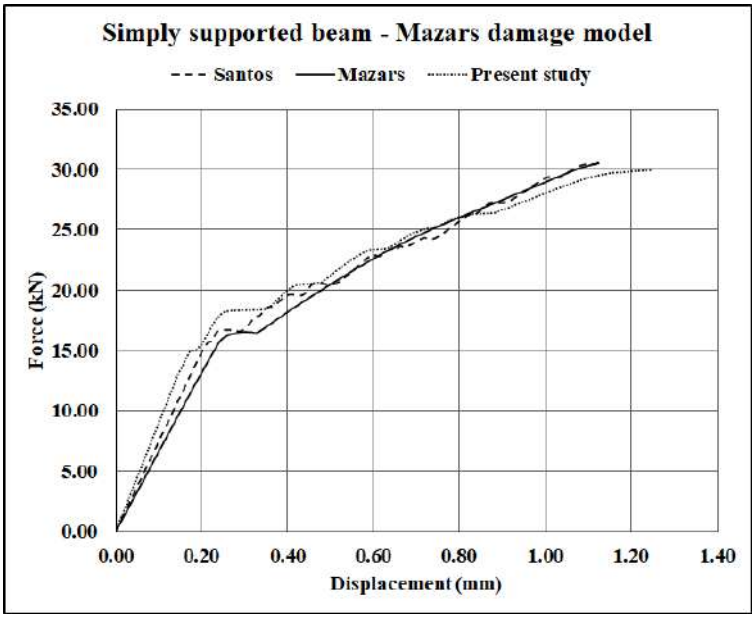

Figure 72. Force-displacement curve for the point where force is applied.

5 Thermo-chemo-mechanical model with ageing and damage

So far, the thermo-chemical and thermo-mechanical models were discussed separately. However, the main objective of this research is to model the thermo-chemo-mechanical behaviour of concrete structures regarding ageing and damage and that is the main concern of the present chapter. The principal theoretical aspects of the thermo-chemo-mechanical analysis were already developed in chapters 3 and 4 when deriving the thermo-chemical and thermo-mechanical models. Now, they will be combined in order to form the thermo-chemo-mechanical model which is nothing but solving, for each time instant, the thermo-chemical model first and thermo-mechanical model subsequently.

This analysis is quite important for concrete structures specially for massive ones because concrete usually does not dissipate heat fast enough. Generally, this is not a problem for daily structures. However, as its dimensions increase, thermal effects might lead to propagation of cracks. In addition, when both ageing and thermal deformations are occurring together residual stresses without observable strains can take place which might result in the rupture of the structure with lower strains than predicted. In this context, the present chapter will demonstrate the thermo-chemo-mechanical behaviour of concrete considering ageing and damage. To this end, two theoretical examples will be discussed: a concrete specimen and a generic concrete wall. Although theoretical, these examples indicate what happens to concrete structures when the hydration of the cement paste is no longer negligible.

The thermo-chemo-mechanical FE analysis is composed by the thermo-chemical and thermo-mechanical problems which are solved one at time. First, the thermo-chemical model is solved obtaining the temperature for each node of the mesh. Then, the thermo-mechanical problem is solved wherein displacements are calculated for each node. Something important to mention is that these two models are weakly coupled, that is, temperature variations cause deformations (thermo→mechanical) but not the other way around. In some situations, this assumption is not correct and the mechanical→thermal coupling must be considered as well. This is the case for some types of polymeric materials so that the full thermo-mechanical coupling should be taken into account because the deformation of the structure will increase its own temperature.

5.1 Flowchart for the thermo-chemo-mechanical analysis

The flowchart for the thermo-chemo-mechanical model is the following

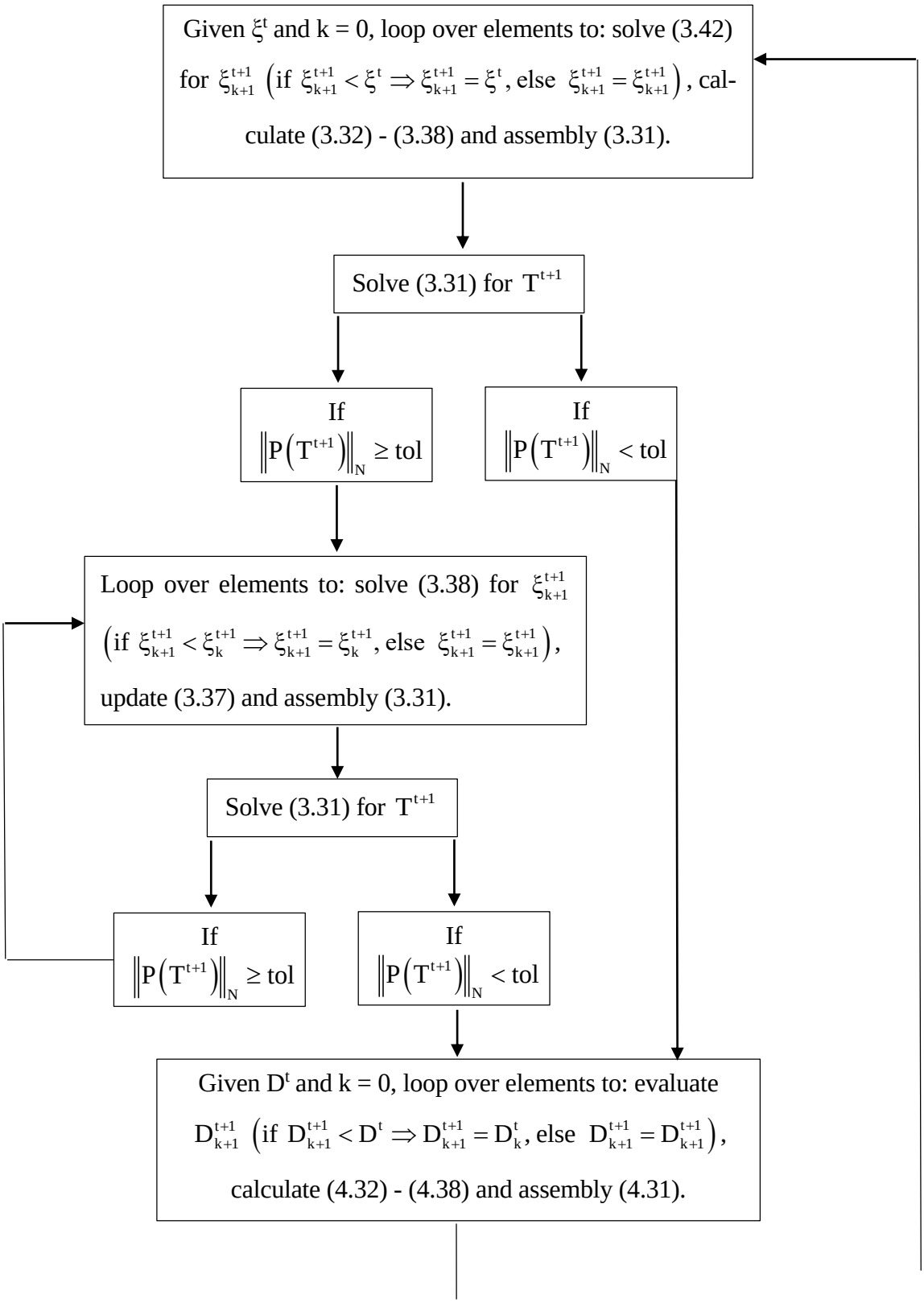

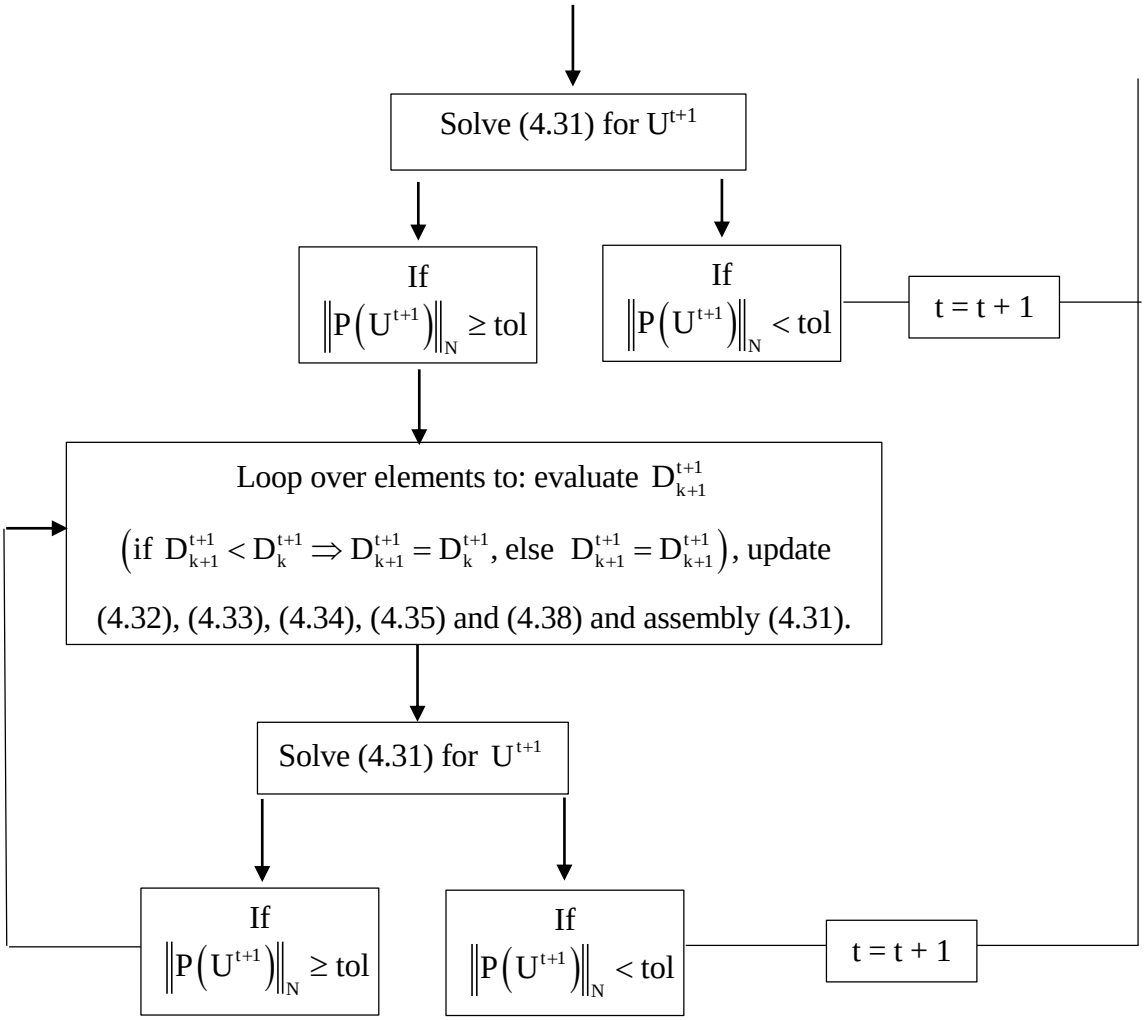

Figure 73. Flowchart for the thermo-chemo-mechanical analysis.

5.2 Numerical applications

5.2.1 Concrete specimen

The first example is a concrete specimen similar those already considered previous sections. Its geometry, boundary conditions and mesh are depicted in Figure 74. Its physical properties are presented in Table 13 where Young's modulus is considered as functions of the hydration degree in order to take concrete ageing into account. Similar to previous analysis, the hatched elements in the middle have lower tensile strength than the rest of the mesh. The Mazars damage model was adopted to simulate the nonlinear behaviour and its parameters are also in Table 13.

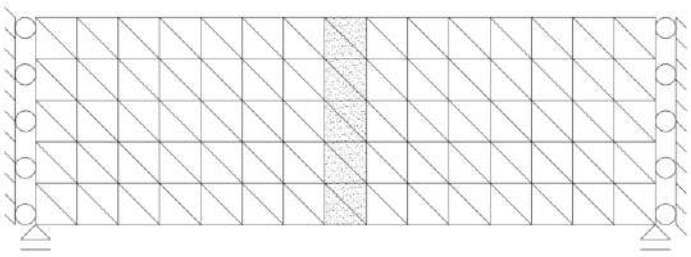

Figure 74. Discretization of the concrete specimen with weaker elements in the middle.

Length (m)	0.30
Height (m)	0.10
Width (m)	0.10
Thermal conductivity ($W.m^{-1}.K^{-1}$)	2.00
Adiabatic temperature rise (°C)	25.6
Convective heat transfer coefficient ($W.m^{-2}.K^{-1}$)	0.85
Density ($kg.m^{-3}$)	2500.00
Specific heat capacity ($J.kg^{-1}.K^{-1}$)	800.00
Environment temperature (°C)	22.00
Specimen's initial temperature (°C)	22.00
Poisson's coefficient	0.30
Dilatation coefficient ($°C^{-1}$)	10^{-5}
Young's modulus (GPa)	30.00ξ
A_T	0.98
B_T	20000.00
Tensile strength for hatched elements (MPa)	1.47
Tensile strength for non-hatched elements (MPa)	1.50

Table 13. Properties of the concrete specimen for the thermo-chemo-mechanical analysis.

The mechanical model was formulated using Plane Stress theory. Although its simplicity, this example simulates what happens to concrete structures that are already restrained at the time of its placing (cf. HILAIRE *et al.* [51]). The main objective of this problem is to analyze the effect of residual stresses due to hydration reaction.

Figure 75 shows the average temperature evolution of the bar. Figure 76 and Figure 77 show the average strain evolution of the bar using non-incremental and incremental constitutive equations, respectively.

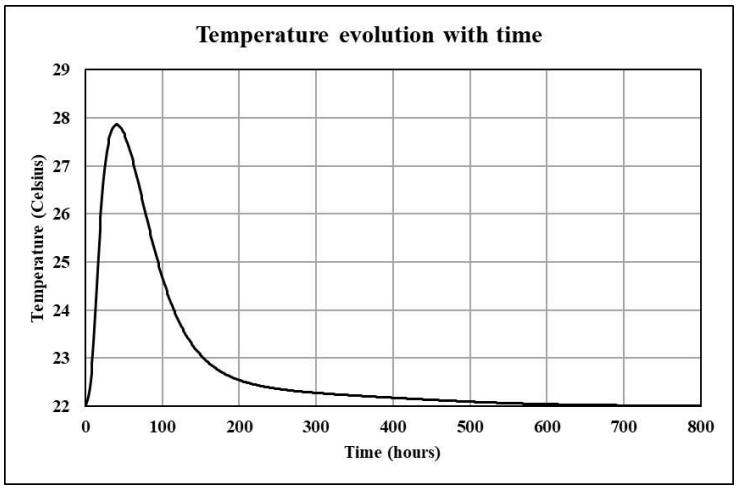

Figure 75. Temperature evolution: average of all nodes.

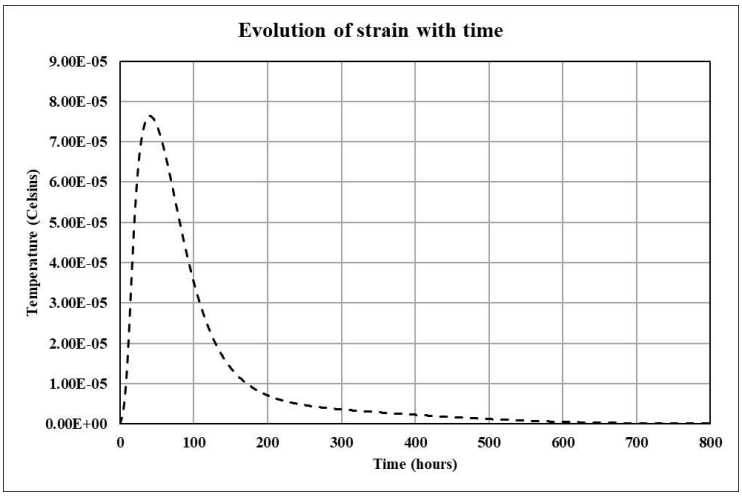

Figure 76. Strain evolution for non-incremental constitutive equation: average of all elements.

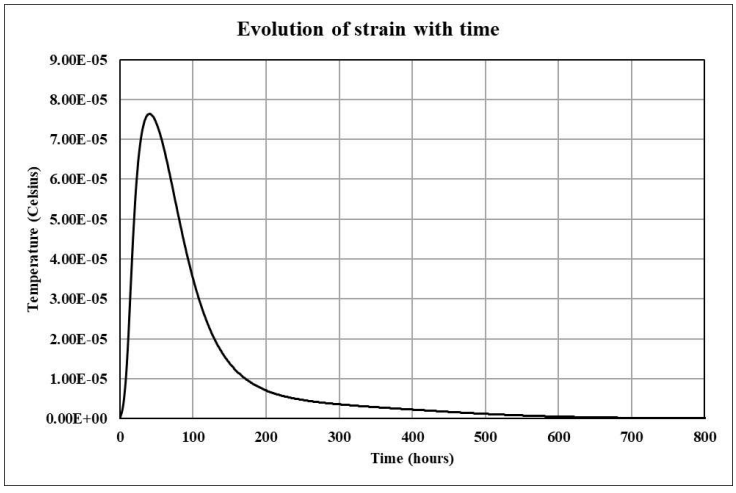

Figure 77. Strain evolution for incremental constitutive equation: average of all elements.

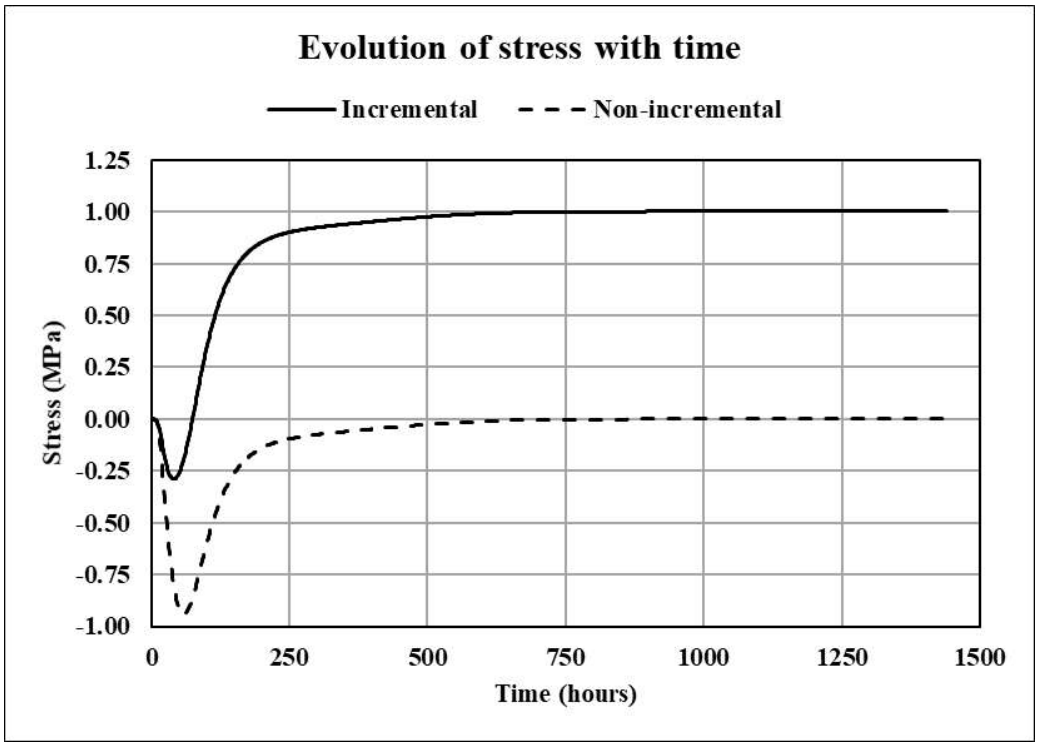

Figure 78. Stress measured on the support for non-incremental and incremental constitutive equations.

Figure 78 show again the necessity of an incremental constitutive relation for ageing materials like concrete. Regarding Figure 76 and Figure 77, one can conclude that the strains development in the specimen are the same. However, when using the incremental constitutive equation, remaining stresses take place (correct) while for non-incremental relation it does not happens (incorrect). The presence of residual stresses must be avoided because this will lead to the collapse of the structure with lower strains than predicted.

To simulate it, a tensile test was conducted in the specimen 1500h after pouring so that the hydration process was already done. The sample was loaded in tension on the right-hand edge by a prescribed displacement, similar to what was done in previous sections. To avoid lack of objectivity, the nonlocal technique was employed using the Gauss distribution and an interaction radius of 50 cm. In order to simulate the nonlinear behaviour, the Mazars damage model was adopted with parameters already mentioned in Table 13. Parameters A_C and B_C are not important for this analysis since it is a pure tensile test. The resulting stress-strain curve is depicted in Figure 79 along with the curve for a specimen without initial stresses.

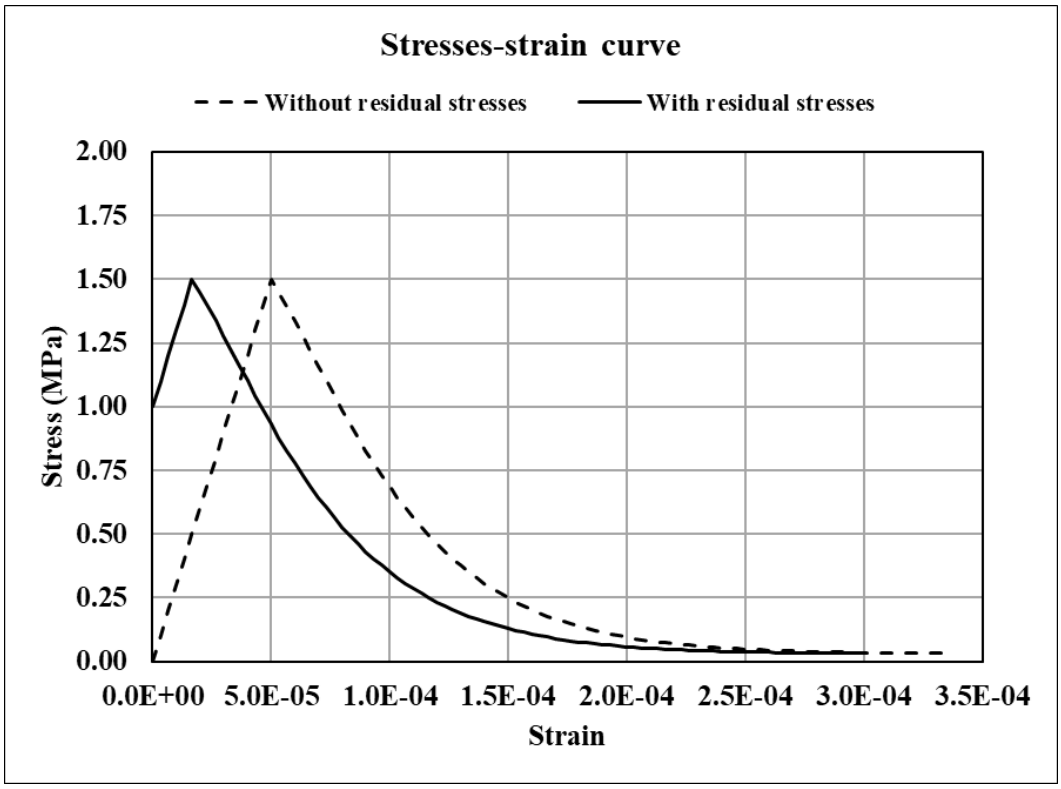

Figure 79. Effect of residual stresses on the stress-strain curve for the tensile test.

Figure 79 exhibits what was expected: the specimen collapses before the one without residual stresses. This situation is dramatic because such premature collapse is caused by lower strains than theoretically predicted. Therefore, this pathological behaviour should be avoided or at least took into account already in design stage given that it's difficult to measure stresses accurately in daily concrete structures.

5.2.2 Generic concrete wall

The following example is a case study of a generic concrete wall, similar to a dam. Its sketch is in Figure 80. It's was built layer-by-layer with a total number of 50 layers with the same height (1.07 m). They were built 7 days apart. The concretes used are the same as those presented in section 3.4.1. The main objective of this analysis is the investigation of damage propagation on a massive concrete structure due to thermal strains caused by hydration of concrete. This example resembles a concrete dam which is a structure that commonly suffers the undesirable effects of concrete hydration.

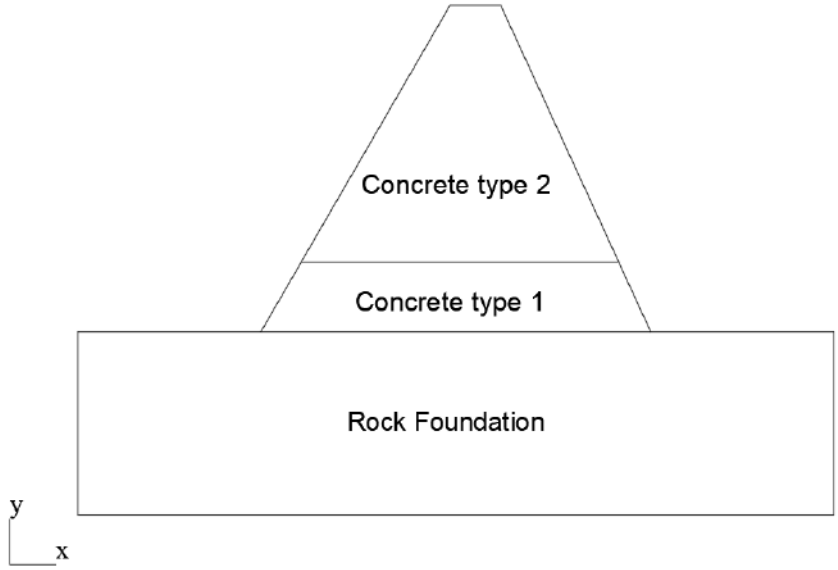

Figure 80. Sketch of the concrete wall.

In Figure 81 are the nodes used to generate the mesh and its coordinates are in Table 14.

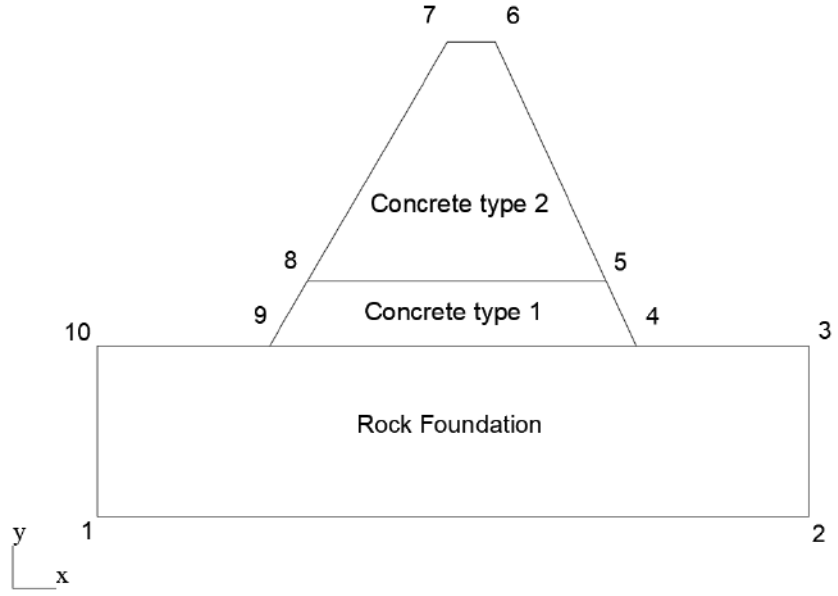

Figure 81. Points used to generate the mesh of the concrete wall.

Label	1	2	3	4	5	6	7	8	9	10
x	0.00	123.96	123.96	93.96	88.69	69.35	61.03	36.64	30.00	0.00
y	0.00	0.00	30.00	30.00	41.45	83.50	83.50	41.45	30.00	30.00

Table 14. Coordinates for the nodes used to generate the mesh.

The discretization is in Figure 82. It consists of 11181 nodes and 22060 linear triangular elements. The Plane Stress theory was adopted for the thermo-mechanical analysis. Robin (convection) boundary conditions were assumed throughout the whole boundary for the thermo-chemical model. For the thermo-mechanical problem, it was considered that boundary nodes with $y \geq 30m$ are constrained only in x direction, boundary nodes with $y < 30m$ are completely constrained and all the interior nodes are unconstrained.

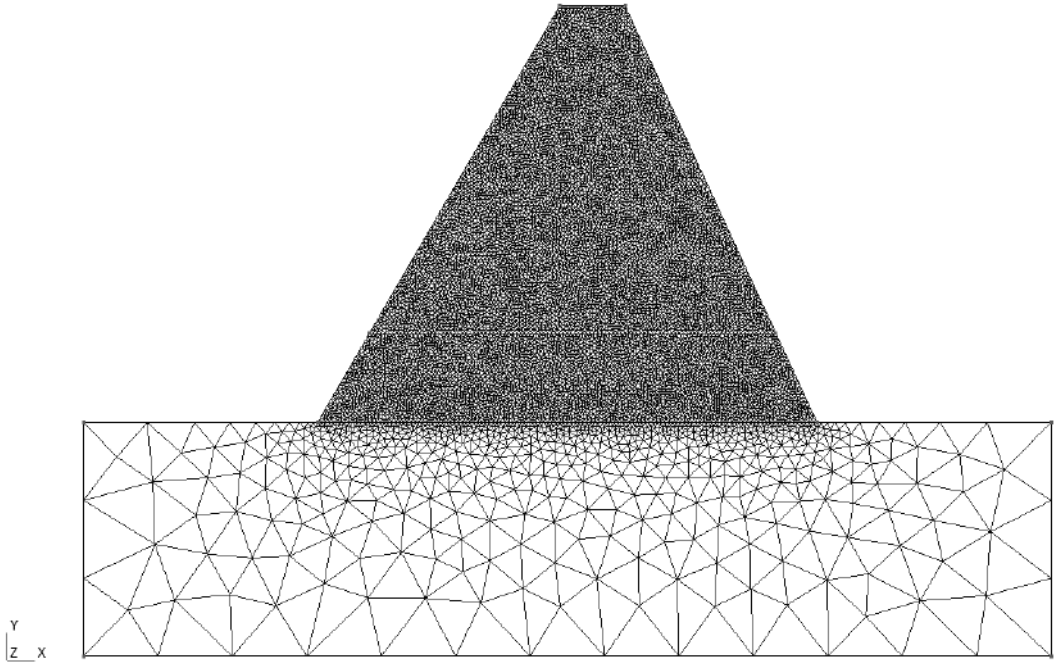

Figure 82. Discretization of the concrete wall.

In Table 15 are the thermal and mechanical properties of the concrete wall

Properties	Concrete type 1	Concrete type 2	Rock foundation
Thermal conductivity ($W.m^{-1}.K^{-1}$)	2.00	2.00	2.00
Specific heat capacity ($J.kg^{-1}.K^{-1}$)	890.00	890.00	900.00
Density ($kg.m^{-3}$)	2600.00	2650.00	2950.00
E_a/R (K)	4400.00	4300.00	--
Placement temperature of the layers (°C)	22.00	22.00	22.00
Convective heat transfer coefficient ($W.m^{-2}.K^{-1}$)	10.00	10.00	0.00
Young's modulus (GPa)	42.00ξ	44.00ξ	50.00
Poisson coefficient	0.20	0.20	0.30
Coefficient of thermal expansion ($°C^{-1}$)	8×10^{-6}	8×10^{-6}	2.5×10^{-6}

Tensile strength (MPa)	2.80ξ	2.20ξ	--
A_T (Mazars model)	0.80	0.80	--
B_T (Mazars model)	20000.00	20000.00	--
A_C (Mazars model)	1.20	1.20	--
B_C (Mazars model)	1850.00	1850.00	--
Gravity acceleration ($m.s^{-2}$)	9.81	9.81	9.81
Thickness in *z* direction (m)	10.00	10.00	10.00

Table 15. Physical properties of the concrete wall.

Both Young's modulus and tensile strength were considered as a function of the hydration degree in order to consider ageing. In Figure 83 - Figure 98 are presented the obtained results for temperature, horizontal displacements, vertical displacements and damage pattern.

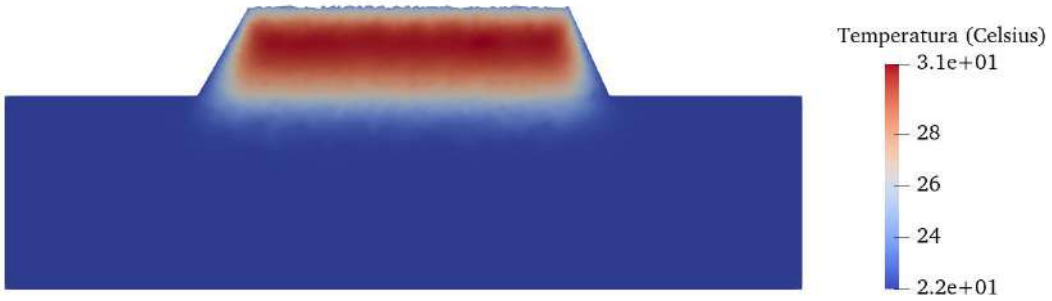

Figure 83. Temperature distribution for the concrete wall after 90 days.

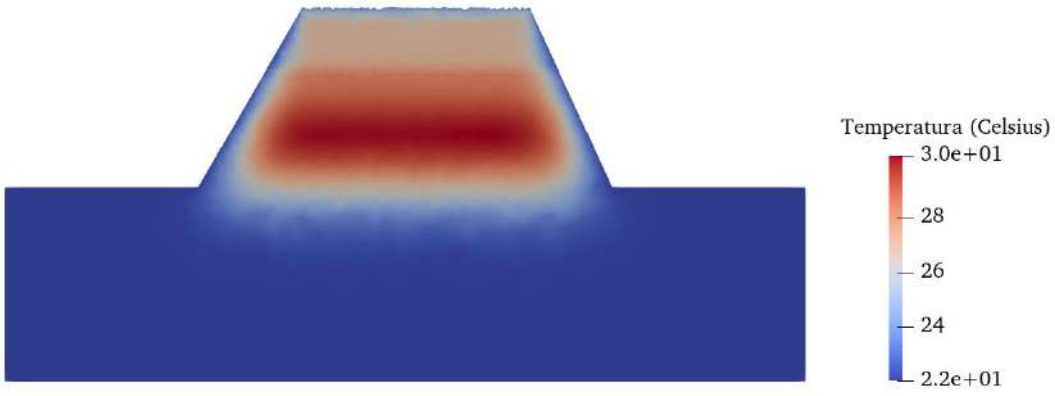

Figure 84. Temperature distribution for the concrete wall after 180 days.

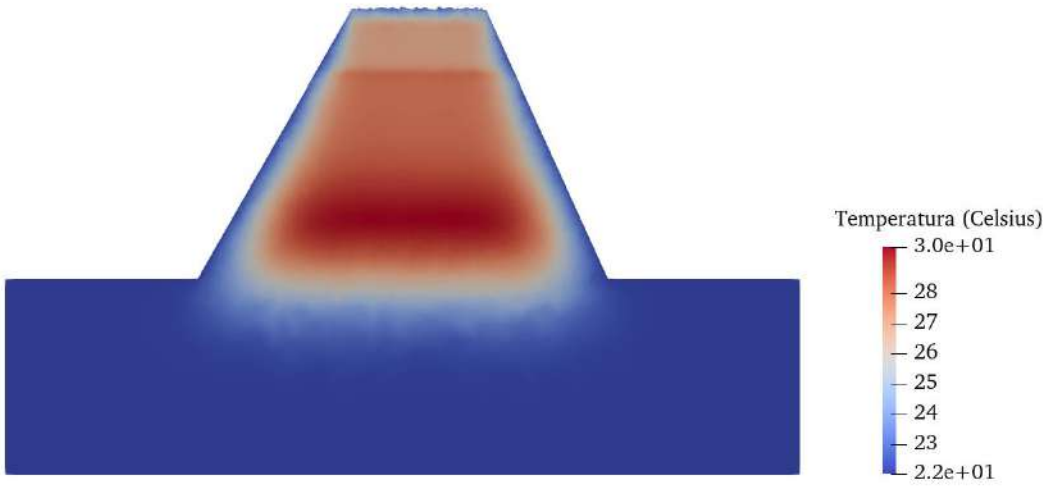

Figure 85. Temperature distribution for the concrete wall after 270 days.

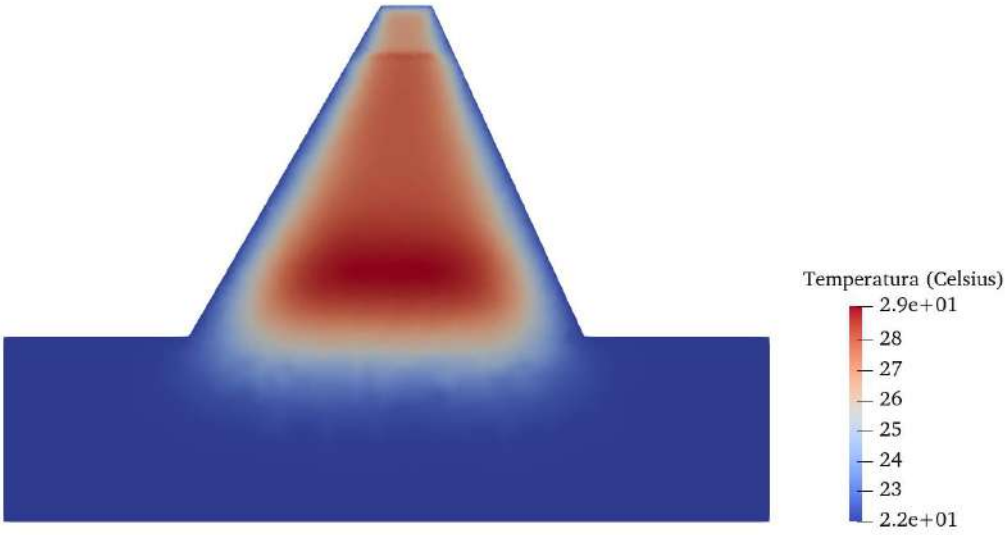

Figure 86. Temperature distribution for the concrete wall after 360 days.

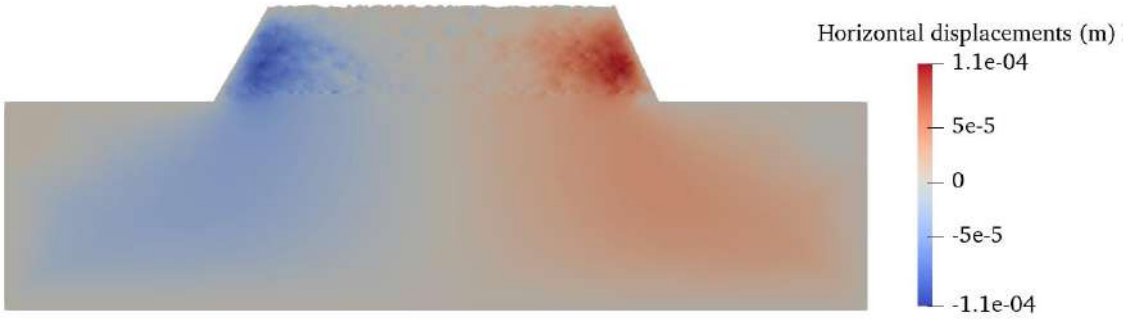

Figure 87. Displacement in *x* direction for the concrete wall after 90 days.

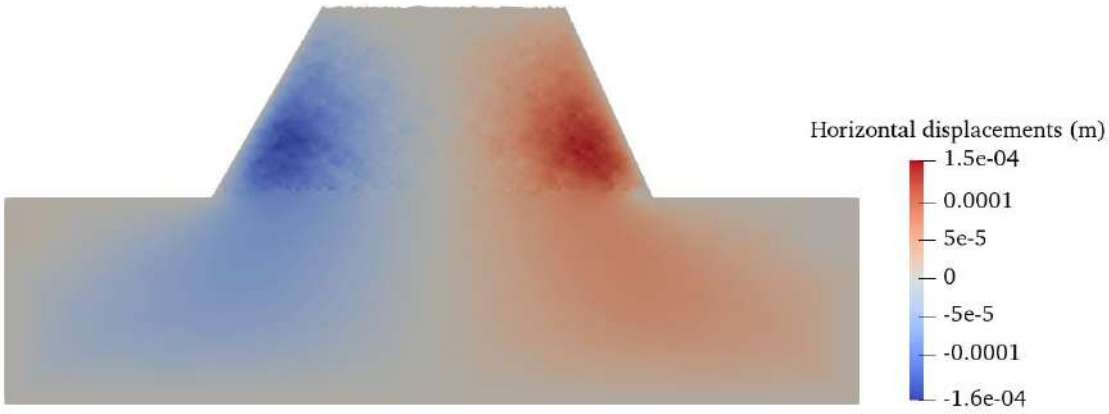

Figure 88. Displacement in x direction for the concrete wall after 180 days.

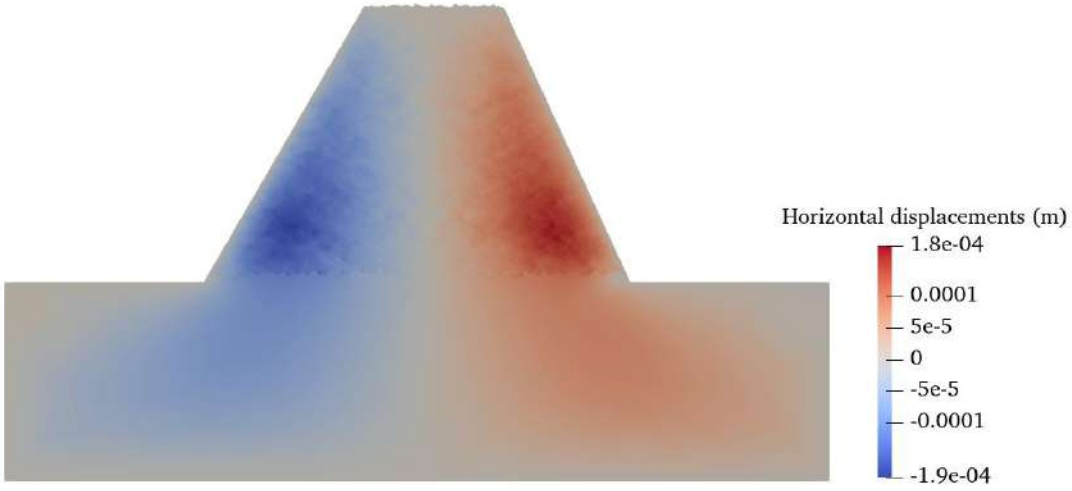

Figure 89. Displacement in x direction for the concrete wall after 270 days.

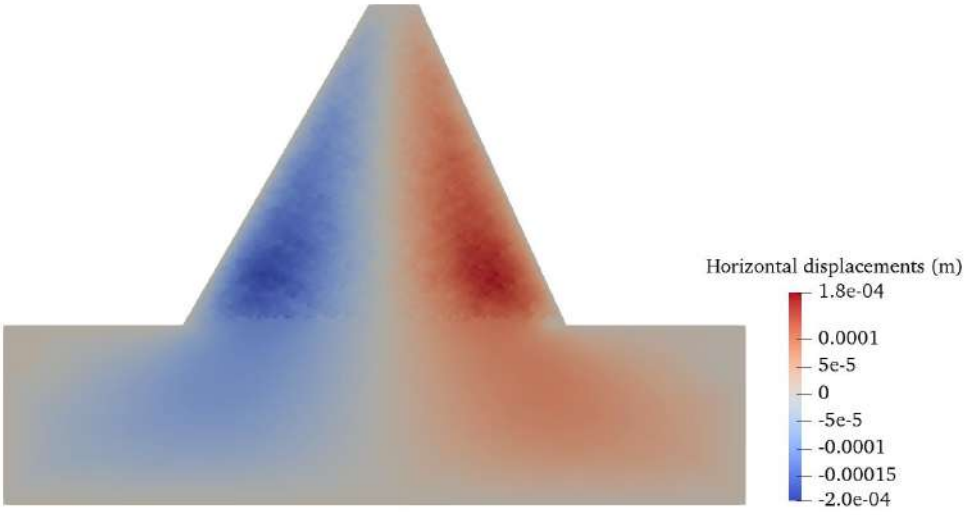

Figure 90. Displacement in x direction for the concrete wall after 360 days.

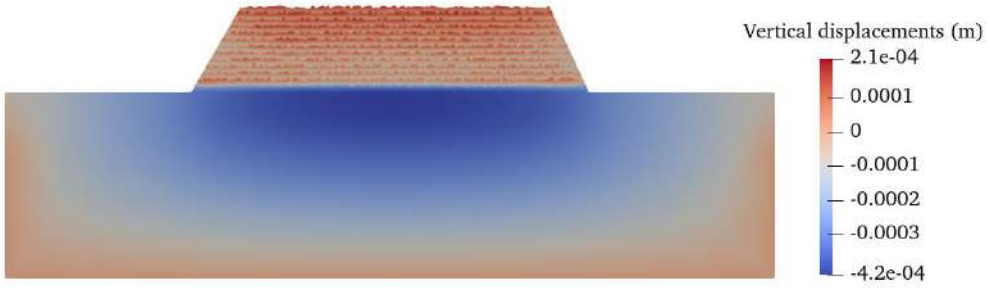

Figure 91. Displacement in y direction for the concrete wall after 90 days.

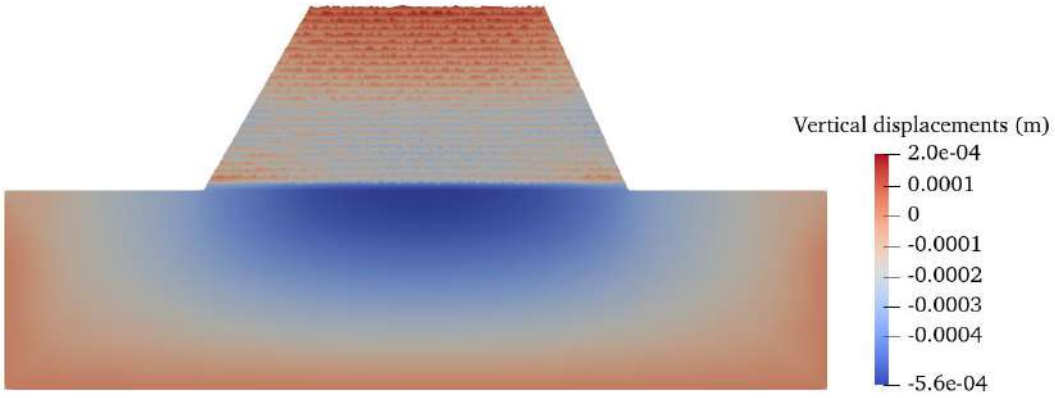

Figure 92. Displacement in y direction for the concrete wall after 180 days.

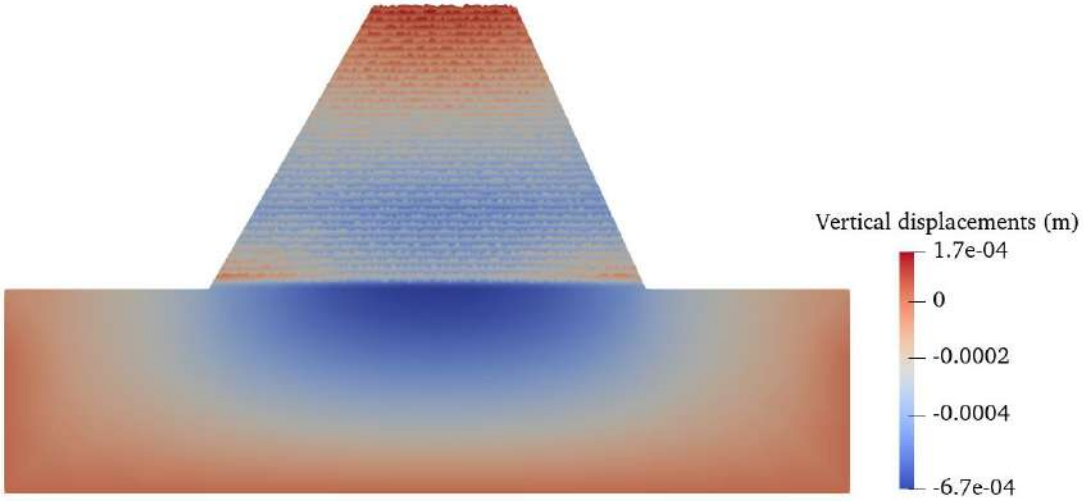

Figure 93. Displacement in y direction for the concrete wall after 270 days.

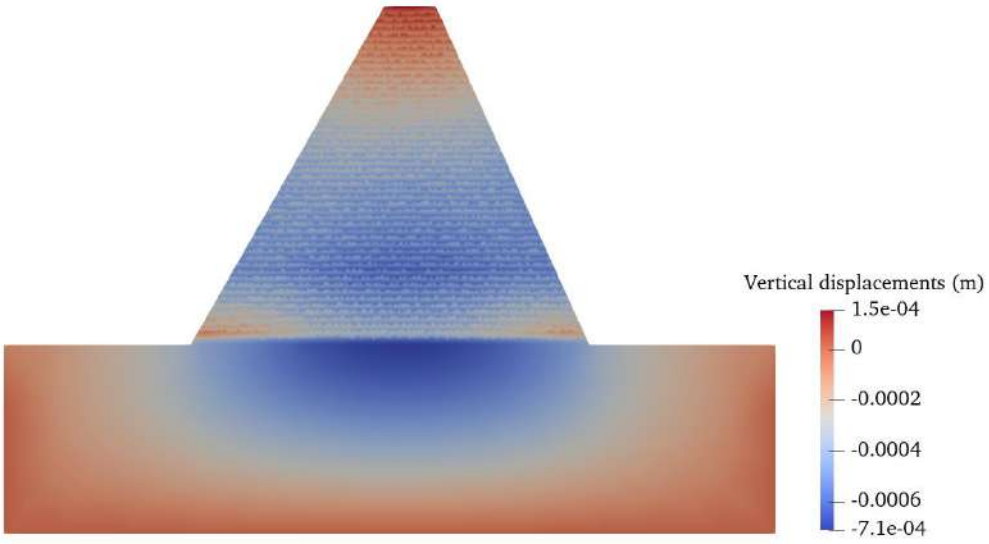

Figure 94. Displacement in y direction for the concrete wall after 360 days.

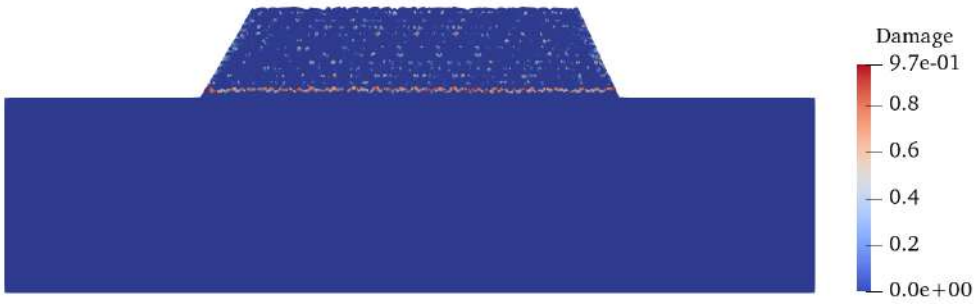

Figure 95. Damage pattern for the concrete wall after 90 days.

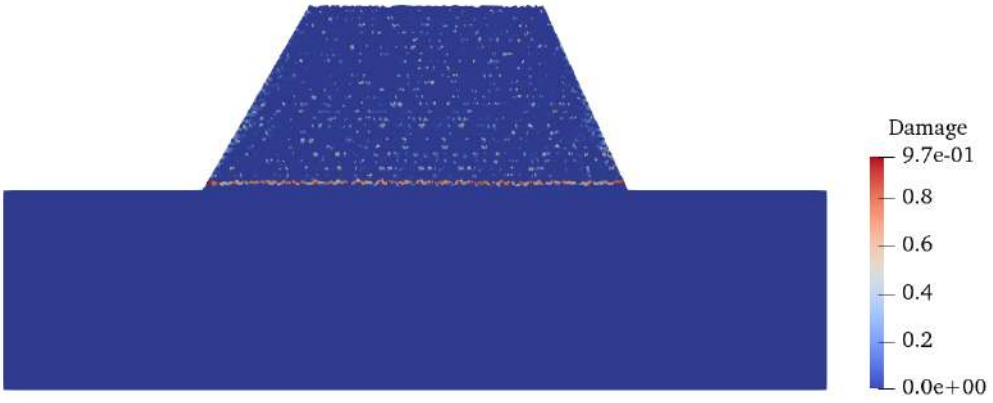

Figure 96. Damage pattern for the concrete wall after 180 days.

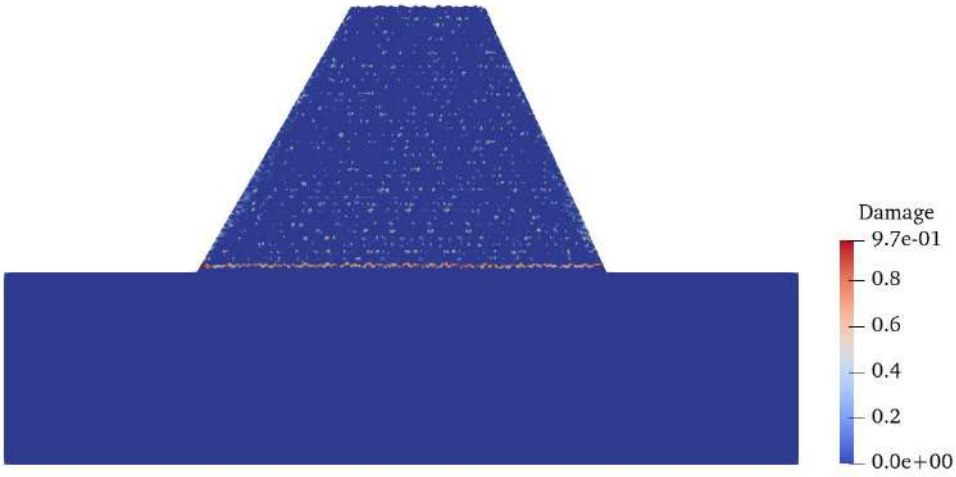

Figure 97. Damage pattern for the concrete wall after 270 days.

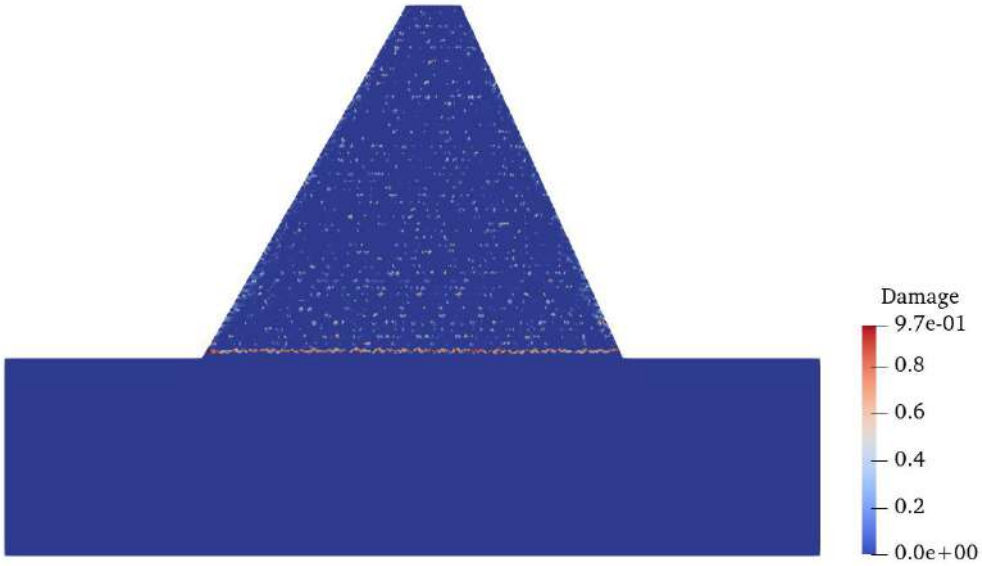

Figure 98. Damage pattern for the concrete wall after 360 days.

From the results in Figure 83 - Figure 86 it's possible to observe the core of the structure is always hotter than the boundary, as expected. It's the same pattern that was obtained in section 3.4.2.1.

Figure 87 - Figure 90 depict the displacement in *x* direction. These results are physically coherent because, as nodes approach the boundaries, their horizontal displacements increase. Similarly, the nodes close to the middle are zero. Since the geometry is not perfectly symmetric, the line with zero displacements isn't exactly in the middle but near to it.

Besides, as nodes increase in *y* direction, their horizontal displacements decrease which is also coherent.

Figure 91 - Figure 94 demonstrate the vertical displacements. The displacements near to the link between the concrete wall and the rock is negative, forming a region of negative displacements below the wall which is due to the dead load. In addition, it's possible to observe that the vertical displacements near to the top of the layers are initially positive but, as next layers are placed, they become negative. This means that the thermal expansion is initially greater than the deformation due to dead load. However, as time goes by, the dead load becomes the predominant influence and these points present negative vertical displacements.

Figure 95 - Figure 98 show the damage pattern of the concrete wall. It's possible to observe that damage is present already in the early ages. Besides, there's a high concentration of damaged elements near to the link between the rock foundation and the wall. This behaviour is commonly present in concrete dams. In addition, the wall hasn't observable cracks because the maximum value reached for damage was approximately 0.97. Hence, the wall is only microcracked. In any case, the integrity of the structure is already prejudicated already in the early age. This will lead to the premature rupture of the wall if not considered in the in advance.

6 Concluding remarks

In the present study, the thermo-chemo-mechanical behaviour of concrete structures regarding ageing and damage was studied. To this end, it was developed mathematical models based on consistent frameworks. First, it was derived the thermo-chemical formulation using the thermodynamics of chemically reactive porous media. The Second Law of thermodynamics allowed one to derive a robust model that considers irreversibility of hydration process. Then, it was proposed a FEM formulation for the thermo-chemical model based on the Galerkin method. After, numerical applications were presented in order to demonstrate the feasibility of the proposed methodology. One of these examples consisted of a layered construction for which a node renumbering strategy was proposed.

Subsequently, the thermo-mechanical model was exposed. It was discussed the importance of an incremental constitutive equation for modelling ageing concrete. Then, using the concept of Effective Stress and the Principle of Strain-Equivalence, it was possible to derive a constitutive equation that considers both ageing and damage. In the following, it was introduced the problem of lack of objectivity due to strain localization. The Nonlocal technique was employed as a remedy to circumvent it. Then, the Mazars damage model was derived and a numerical application for a three-point bending test was presented. It was also briefly discussed the influence of damage models on iterative solvers.

Finally, the thermo-chemo-mechanical analysis considering ageing and damage was proposed. The hypothesis of weak coupling allowed to separate it in two models, namely: thermo-chemical and thermo-mechanical. The thermo-chemo-mechanical model is nothing but solving the thermo-chemical model first and thermo-mechanical subsequently. Two theoretical examples were discussed in order to demonstrate the mechanical effects in concrete structures due to hydration of concrete. In the first example, it was exposed the phenomenon of residual stress without observable strains for a concrete specimen. In the second example, it was investigated the temperature and displacements evolution and damage pattern for a concrete wall which was built layer-by-layer. The results showed that microcracks took place already in the early age which might reduce to a great extent the load-carrying capacity of the concrete wall. This, in turn, might lead to the premature collapse of the structure.

7 References

[1] A. M. Neville and J. J. Brooks, *Concrete technology*, 2nd ed. Prentice Hall, 2010.

[2] Z. Li, *Advanced Concrete Technology*. John Wiley & Sons, Inc, 2011.

[3] S. Mindess, J. F. Young, and D. Darwin, *Concrete*, 2nd ed. Prentice Hall, 2003.

[4] P. K. Mehta and P. J. M. Monteiro, *Concrete: microstructure, properties and materials*. McGraw-Hill, 2006.

[5] S. Popovics, *Concrete materials: Properties, specifications and testing*, 2nd ed. Noyes Publications, 1992.

[6] R. Springenschmid, *Prevention of Thermal Cracking in Concrete at Early Ages*. E.& F.N. Spon, 1998.

[7] J. C. Maso, *Interfacial Transition Zone in Concrete: state-of-the-art report*, 1st ed. E.& F.N. Spon, 1996.

[8] F. J. Ulm and O. Coussy, "Modeling of thermochemomechanical couplings of concrete at early ages," *J. Eng. Mech.*, 1995, doi: 10.1061/(ASCE)0733-9399(1995)121:7(785).

[9] F. J. Ulm and O. Coussy, "Strength growth as chemo-plastic hardening in early age concrete," *J. Eng. Mech.*, 1996, doi: 10.1061/(ASCE)0733-9399(1996)122:12(1123).

[10] O. Coussy, *Mechanics of Porous Continua*. 1995.

[11] M. Rita, E. Fairbairn, F. Ribeiro, H. Andrade, and H. Barbosa, "Optimization of mass concrete construction using a twofold parallel genetic algorithm," *Appl. Sci.*, 2018, doi: 10.3390/app8030399.

[12] A. G. Evsukoff, E. M. R. Fairbairn, É. F. Faria, M. M. Silvoso, and R. D. Toledo Filho, "Modeling adiabatic temperature rise during concrete hydration: A data mining approach," *Comput. Struct.*, vol. 84, no. 31–32, pp. 2351–2362, 2006, doi: 10.1016/j.compstruc.2006.08.049.

[13] I. A. Ferreira, “Modelagem numérica do acoplamento térmico-químico-mecânico no concreto jovem,” Universidade Federal do Rio de Janeiro, 1998.

[14] I. A. Ferreira, “Solução em paralelo de um modelo termo-químico-mecanico para concreto jovem,” Universidade Federal do Rio de Janeiro, 2008.

[15] M. M. Silvoso, “Otimização da Fase Construtiva de Estruturas de Concreto em Face dos Efeitos da Hidratação via Algoritmos Genéticos,” Universidade Federal do Rio de Janeiro, 2003.

[16] G. Valentim, “Estudo da fissuração térmica de blocos de contraforte da UHE Itaipu: Análise numérica termo-químico-mecanica,” Universidade Federal do Rio de Janeiro, 2020.

[17] M. Cervera, J. Oliver, and T. Prato, “Thermo-chemo-mechanical model for concrete. II: Damage and creep,” *J. Eng. Mech.*, 1999, doi: 10.1061/(asce)0733-9399(1999)125:9(1028).

[18] M. Cervera, R. Faria, J. Oliver, and T. Prato, “Numerical modelling of concrete curing, regarding hydration and temperature phenomena,” *Comput. Struct.*, 2002, doi: 10.1016/S0045-7949(02)00104-9.

[19] F. J. Ulm, J. M. Torrenti, B. Bissonette, and J. Marchand, “Modeling Concrete at an Early Age,” in *Mechanical Behavior of Concrete*, John Wiley & Sons, Inc, 2013, pp. 297–338.

[20] F. J. Ulm and O. Coussy, “Couplings in early-age concrete: From material modeling to structural design,” *Int. J. Solids Struct.*, vol. 35, no. 31–32, pp. 4295–4311, 1998, doi: 10.1016/S0020-7683(97)00317-X.

[21] S. P. C. Marques and G. J. Creus, *Computational viscoelasticity*. Springer International Publishing, 2012.

[22] N. Ottosen and M. Ristinmaa, *The Mechanics of Constitutive Modeling*. Elsevier Inc., 2005.

[23] J. T. Oden, *An Introduction to Mathematical Modeling: A Course in Mechanics*. John Wiley & Sons, Inc, 2011.

[24] Y. Başar and D. Weichert, *Nonlinear Continuum Mechanics of Solids*, 1st ed. Springer, 2000.

[25] C. Truesdell and E. H. Dill, *The Elements of Continuum Mechanics*. 1968.

[26] C. A. Truesdell, *A first course in Rational Continuum Mechanics*, 2nd ed. Academic Press, Inc, 1991.

[27] I. S. Liu, *Continuum Mechanics*, 1st ed. Springer, 2002.

[28] P. Haupt, *Continuum mechanics and theory of materials*, 2nd ed. Springer, 2002.

[29] F. M. Capaldi, *Continuum mechanics: Constitutive modeling of Structural and Biological materials*, 1st ed. Cambridge University Press, 2012.

[30] C. D. Coman, *Continuum Mechanics and Linear Elasticity: An Applied Mathematics introduction*, 1st ed. Springer, 2019.

[31] J. N. Reddy, *An introduction to Continuum Mechanics with applications*, 1st ed. Cambridge University Press, 2008.

[32] E. Byskov, *Elementary Continuum Mechanics for everyone: with applications to Structural Mechanics*, 1st ed. Springer, 2013.

[33] Y. I. Dimitrienko, *Nonlinear Continuum Mechanics and large inelastic deformations*, 1st ed. Springer, 2011.

[34] L. M. Kachanov, "Time of rupture process under creep conditions," *Isv. Akad. Nauk. SSR. Otd Tekh. Nauk.*, 1958.

[35] Y. N. Rabotnov, "Creep rupture," *Appl. Mech.*, pp. 342–349, 1969, doi: 10.1007/978-3-642-85640-2_26.

[36] D. R. Hayhurst, "Creep rupture under multi-axial states of stress," *J. Mech. Phys. Solids*, vol. 20, no. 6, pp. 381–390, 1972, doi: 10.1016/0022-5096(72)90015-4.

[37] F. Krajcinovic and G. U. Fonseka, "The Continuous Damage Theory of Brittle Materials, Part 1: General Theory," *J. Appl. Mech.*, vol. 48, no. 4, pp. 809–815, 1981, doi: 10.1115/1.3157739.

[38] F. Krajcinovic and G. U. Fonseka, “The Continuous Damage Theory of Brittle Materials, Part 2: Uniaxial and Plane Response Modes,” *J. Appl. Mech.*, vol. 48, no. 4, pp. 816–824, 1981, doi: 10.1115/1.3157740.

[39] F. A. Leckie and D. R. Hayhurst, “Creep rupture of structures,” *Proc. R. Soc.*, vol. 340, no. 1622, pp. 323–347, 1974, doi: 10.1098/rspa.1974.0155.

[40] J. Lemaitre and J.-L. Chaboche, *Mechanics of solid materials*. Cambridge University Press, 1990.

[41] J. Lemaitre, *A course on damage mechanics*, 2nd ed. Springer, 1996.

[42] J. Lemaitre and R. Desmorat, *Engineering Damage Mechanics: Ductile, Creep, Fatigue and Brittle Failures*, 1st ed. Springer, 2005.

[43] S. A. Murakami, *Continuum Damage Mechanics: A Continuum Mechanics approach to the analysis of damage and fracture*, 1st ed. Springer, 2012.

[44] M. Jirásek, “Damage and smeared crack models,” in *CISM International Centre for Mechanical Sciences, Courses and Lectures*, 2011.

[45] Z. P. Bažant and L. Cedolin, *Stability of structures: Elastic, inelastic, fracture and damage theories*, 1st ed. World Scientific Publishing Inc., 2010.

[46] D. Gross and T. Seelig, *Fracture Mechanics: with an introduction to Micromechanics*. Springer, 2018.

[47] G. Pijaudier-Cabot and Z. P. Bažant, “Nonlocal damage theory,” *J. Eng. Mech.*, vol. 113, no. 10, pp. 1512–1533, 1987, doi: 10.1061/(ASCE)0733-9399(1987)113:10(1512).

[48] M. Jirásek, “Nonlocal damage mechanics,” *Rev. Eur. génie Civ.*, vol. 11, no. 7–8, pp. 993–1021, 2007.

[49] J. Mazars, “Application de la mecanique de l’endommagement au comportement non lineaire et a la rupture du beton de structure,” Universite Pierre et Marie Curie, 1984.

[50] N. Santos, “Modelos de dano para concreto,” Universidade Federal do Rio de

Janeiro, 2015.

[51] A. Hilaire, F. Benboudjema, A. Darquennes, Y. Berthaud, and G. Nahas, “Modeling basic creep in concrete at early-age under compressive and tensile loading,” *Nucl. Eng. Des.*, vol. 269, pp. 222–230, 2014, doi: 10.1016/j.nucengdes.2013.08.034.